Dissertations   Theses and Dissertations

1992

Multinuclear Magnetic Resonance Study of Chlorine and Cesium Ion Distribution in Human Erythrocyte Suspensions

Lisa Wittenkeller
Loyola University Chicago

Lisa Wittenkeller

Loyola University Chicago

MULTINUCLEAR MAGNETIC RESONANCE STUDY OF CHLORIDE AND CESIUM ION DISTRIBUTION IN HUMAN ERYTHROCYTE SUSPENSIONS.

The protein involved in the regulation of Cl^- and Na^+ transport is defective in cystic fibrosis patients. This defective protein generates abnormal Cl^- transport across cell membranes. We investigated the effect of ionophores on Cl^- distribution in human erythrocyte suspensions by measuring the membrane potential using ^{19}F and ^{31}P NMR methods. Ionophores can elucidate ion transport and alter the permeability of cellular membranes to specific cations and shift the electrochemical gradient across the membrane. Two subclasses of ionophores exist: 1) neutral ionophores, such as valinomycin and nonactin, and 2) carboxylic or charged ionophores, such as monensin, lasalocid, and nigericin. Because of the formation of a positively charged cation-ionophore complex, the neutral ionophores are expected to have a stronger attraction for Cl^- and may alter the membrane potential. Of the ionophores tested, valinomycin and nonactin were found to induce the largest change in Cl^- distribution across human erythrocyte suspensions. In methanol, the $^{35}Cl^-$ NMR linewidth in the presence of valinomycin was twice as broad as those observed in the presence of carboxylic ionophores, suggesting that neutral ionophores induce Cl^- efflux in part via ion pairing.

In cell suspensions, the presence of shift reagents (SRs) in the suspension medium leads to transmembrane differences in chemical shifts that result in the resolution of intra- and extracellular $^{7}Li^{+}$, $^{23}Na^{+}$, $^{39}K^{+}$, and $^{87}Rb^{+}$ NMR resonances. In contrast, the chemical shifts of the two ^{133}Cs NMR resonances in Cs^{+}-loaded human erythrocyte and perfused rat heart suspensions are distinguishable without the incorporation of a SR in the suspension medium. At physiologically relevant red blood cell (RBC) concentrations, 2,3-diphosphoglycerate (DPG), of all the intracellular phosphates tested, caused the largest $^{133}Cs^{+}$ shift. The $^{133}Cs^{+}$ resonance in carbonmonoxygenated RBC lysate shifted downfield by approximately 2.0 ppm with increasing hemoglobin concentration, whereas as increase in the diamagnetic susceptibility of the sample induced by hemoglobin is expected to induce an upfield shift of 0.1 ppm. The $^{133}Cs^{+}$ resonance was shifted downfield with increasing concentrations of two unrelated proteins, carbonmonoxyhemoglobin and lysozyme. We concluded that, in the absence of SRs, the physical basis for the resolution of intra- and extracellular ^{133}Cs NMR resonances in Cs^{+}-loaded human RBC suspensions arises from Cs^{+} binding to intracellular phosphates, in particular DPG, and from the non-ideality of intracellular water induced by hemoglobin.

MULTINUCLEAR MAGNETIC RESONANCE STUDY OF CHLORIDE AND CESIUM ION DISTRIBUTION IN HUMAN ERYTHROCYTE SUSPENSIONS.

by

Lisa Wittenkeller

A Dissertation Submitted to the Faculty of the

Graduate School of Loyola University Chicago in

Partial Fulfillment of the Requirements of

the Degree of Doctor of Philosophy

May 1992

ACKNOWLEDGEMENTS

My sincere thanks to my family for helping me never to lose sight of my goal. Special thanks to my husband, Mark, for putting up with my many long hours and absence from my duties at home.

Finally, I am very grateful to God for all of these blessings.

To my husband Mark

TABLE OF CONTENTS

ix

LIST OF TABLES

LIST OF FIGURES

LIST OF ABBREVIATIONS

AAS	atomic absorption spectroscopy
acac	acetylacetonate
ADP	adenosine diphosphate
ATP	adenosine triphosphate
CD	circular dichroism
CF	cystic fibrosis
Cl^-	chloride ion
COHb	carbomonoxyhemoglobin
Cs^+	cesium ion
δ	NMR chemical shift
$\Delta\nu_{1/2}$	line width of NMR resonance at half height
DDC	Diethyldithiocarbamic acid
deoxyHb	deoxyhemoglobin
DIDS	4,4'-dinitrostilbene-2,2'disulfonic acid
DOTA	1,4,7,10-tetraazacyclododecane-N,N',N'',N'''-tetraacatate
DPA	dipicolinate
DPG	2,3-diphosphoglycerate
DTPA	diethylenetriamine pentaacetate
FT-IR	Fourier transform infrared
GABA	gamma aminobutyric acid

Hb	hemoglobin
HEPES	4-(2-hydroxyethyl)-1-piperazine ethanesulfonic acid
HP	hypophosphite
Ht	hematocrit
ISM	ion selective microelectrodes
Las	lasalocid
LUVs	large unilamellar vesicles
Mon	monensin
Nig	nigericin
NMR	nuclear magnetic resonance
Non	nonactin
NOTA	1,4,7-triazacylononane-N,N',N''-triacetate
η	viscosity
PC	phosphatidylcholine
P_i	inorganic phosphate
PBS	5 mM sodium phosphate buffer containing 150 mM NaCl
PPP	triphosphate
PVP-100	polyvinyl pyrrolidone
RBCs	red blood cells
ρ	rho, $[SR]/[M^+]$ ratio
SPQ	6-methoxy-N-(3-sulfopropyl)quinolium
SR	shift reagent
TFA	trifluoroacetic acid

TFM   trifluoroacetamide

TMS   tetramethylsilane

TTHA   triethylenetetraminehexaacetate

Val   valinomycin

CHAPTER I

INTRODUCTION

I.A1   Chloride Transport in Biological Systems

Chloride ion (Cl⁻) is one of the most abundant free anions in living cells. Quantification of intracellular chloride activity and the study of the mechanisms involved in regulation of intracellular Cl⁻ are of paramount importance in living cells for the following reasons: (a) chloride activity determines the Cl⁻ membrane potential; (b) transport mechanisms responsible for intracellular pH regulation are coupled to Cl⁻ activity; (c) chloride ion distribution is a major contributing factor towards regulation of cell volume; and (d) synaptic inhibition is dependent on intracellular Cl⁻ hemostasis.

In light of these varied functions, Cl⁻ transport in biological systems has been the subject of active investigation (1-7). Cl⁻ is transported across the cell membrane via three fundamentally different pathways: an electrically conductive transport pathway and two electroneutral pathways, Cl⁻ anion exchange and Cl⁻ cation cotransport (Figure I).

The contribution of each of these Cl⁻ transport pathways varies from system to system. Also, the role of Cl⁻ towards generating the resting membrane potential varies from system to system depending on whether Cl⁻ actively or passively distributes across the cell membrane.

Electrically conductive transport of Cl⁻ occurs when Cl⁻ moves across the membrane

Figure I.   Major Transport Pathways for Cl⁻ Across Cell Membranes.
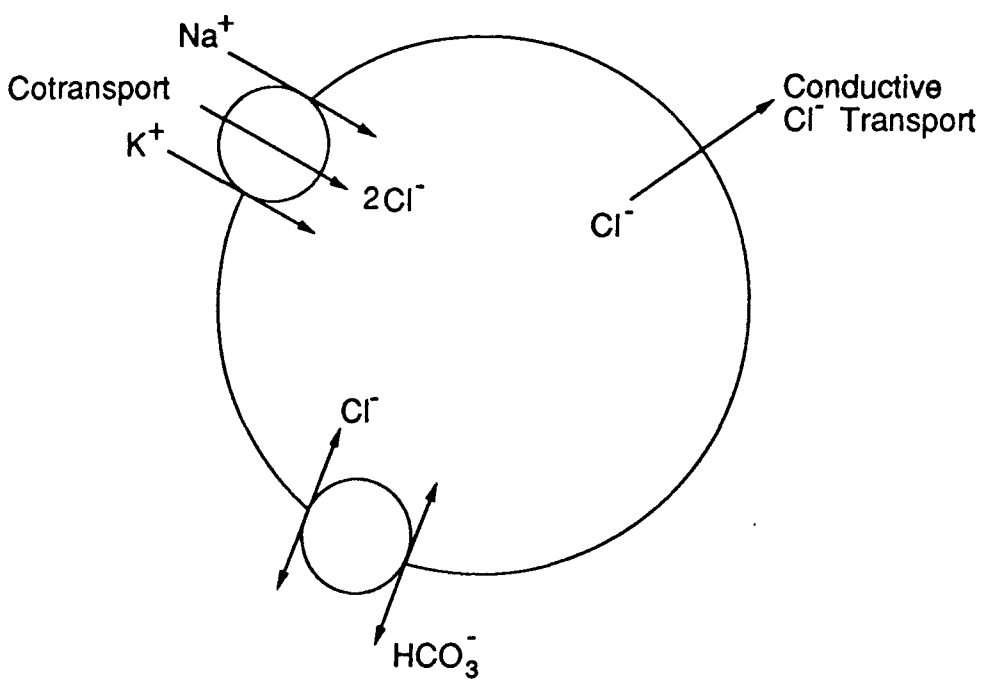
Cl⁻ - HCO₃⁻ Antiport Pathway
    Exchange by diffusion through
    band 3. (Inhibited by DIDs)
    pH regulated

and is not exchanged by another anion in the outer cell compartment. Changes in membrane potential occur with electrically conductive Cl^- transport. The hyperpolarization of post synaptic inhibitory neurons in response to gamma aminobutyric acid (GABA) is primarily due to increased Cl^- conductance (2). In these neurons, the electrochemical Cl^- gradient is inwardly directed so that the activation of Cl^- channels by GABA allow Cl^- to enter the cell and hyperpolarize the membrane. This hyperpolarization is believed to counteract the effect of other membrane-depolarizing neurotransmitters, such as glycine. Conductive Cl^- transport is also important in the function of the T tubule system of skeletal muscle. The large Cl^- conductance of the T-tubule effectively applies a partial voltage, thus preventing depolarization of the membrane by K^+ during the action potential.

Electroneutral Cl^- anion exchange pathway is by far the best characterized of all the chloride pathways (1). In red blood cells (RBCs), this exchanges Cl^- for HCO_3^-. This exchange occurs as RBCs pass through the microvasculature of the lungs and the peripheral circulation. The band-3 (or anion exchange) protein is the channel responsible for this transport pathway in RBCs and is inhibited by 4,4'-dinitrostilbene-2,2'disulfonic acid (DIDS). In addition, the electroneutral Cl^- anion exchange pathway appears to be involved in the regulation of cytoplasmic pH. This provides a mechanism by which the cell is able to respond to both acidification (3) and alkalization (4).

Electroneutral cotransport pathways for the coupled movement of Na^+, K^+, and Cl^- is observed in many cells. This pathway has been well characterized in cultured human fibroblasts (5-6). Cell volume regulation is considered to be an important function of this cotransport system (7). In Ehlrich cells exposed to hyperosmotic medium, experimental evidence suggested that the initial shrinkage followed by rapid increase back to the original

cell volume was due to the activation of the bumetanide-sensitive Na^+-Cl^- cotransport system with subsequent replacement of Na^+ by K^+ via the Na^+-K^+ pump (8). Presence of defective pathways of Cl^- transport have been observed in Duchenne muscular dystrophy fibroblasts (9), congenital myotonia (10), and in cystic fibrosis (CF) (11).

It has also been observed that ion carriers, such as ionophores, do effect the cation and anion distribution across cell membranes. A brief account of ionophore induced ion transport is discussed in section I.A.3.

I.A2   Abnormal Chloride Transport in Cystic Fibrosis

In recent years considerable progress has been made towards understanding the metabolic abnormality in CF (11-12). CF is an autosomal recessive disorder. It is the most lethal genetic disease in the Caucasian population, affecting 1 in 2,000 births (13). The median age of survival is in the twenties. Almost 95% of CF patients die of respiratory failure. The lung disease develops because thick, dehydrated mucus impairs airway mucociliary clearance and predisposes the patient to recurrent bronchial infections. CF airways show a particular tendency to infection with the bacterium *Pseudomonas aeruginosa*. The recurrent infections and pneumonia progressively destroy the lung and lead to respiratory failure. Abnormalities of sweat gland function were discovered early in the history of the disease and led to the classical clinical test for CF, an increased concentration of Cl^- in the sweat. Organs such as salivary glands, intestines, epididymis, and liver are also affected in CF. These clinical manifestations have been important in guiding investigators to perform basic research that has resulted in significant advances in two main areas: identification of the part of chromosome 7 which contains the CF gene, and observation of abnormal Cl^- transport

in epithelial cells.

The sweat glands, airways, and pancreas are the three organs involved in CF and each of these organs contain epithelium. In CF, each of these epithelia have decreased anion permeability (14). Quinton and Bijman (14) examined the ion transport properties of the sweat duct. They found that both *in vivo* and *in vitro* CF sweat ducts had a higher transepithelial electrical potential difference than normal ducts. When the lumen Cl^- concentration was reduced in normal ducts, lumen voltage became more negative suggesting that Cl^- transport is electrically conductive. In contrast, when the lumen Cl^- concentration was reduced in CF ducts, transepithelial voltage became more positive (15-16).

These studies suggest that CF sweat ducts have a decreased Cl^- permeability and that the increased transepithelial voltage results from an intact Na^+ absorptive mechanism in the presence of Cl^- impermeability. It has been demonstrated that the secretory coil of sweat gland also transports electrolytes abnormally (17). A defect in the cAMP-mediated regulation of Cl^- secretion was observed in the above mentioned study (17).

The clinical observation that CF airway secretions are thick and dehydrated led Knowles and coworkers (18) to study electrolyte transport in CF epithelium. They observed that *in vivo* the voltage across upper nasal and lower tracheal airway epithelial is higher in CF patients than in normal subjects. Subsequently, *in vivo* Cl^- substitution studies (19), the observation that transepithelial Cl^- fluxes are decreased in excised nasal polyps (20), indicated that CF airway epithelium is relatively impermeable to Cl^-.

The most recent advances have demonstrated that the CF protein is, most likely, a chloride ion channel rather than a pump (12). Based on structural similarities with a family of membrane pumps that bind ATP, it was assumed that the cAMP regulated CF protein was

an energy dependent pump. Experiments involving substituting a negative amino acid, aspartate or glutamate, for the positively charged lysine changed the function of the CF protein. Chloride ions, which are normally transported more easily than iodide ions, are transported more slowly after lysine substitution. The role of cAMP is now believed to be involved in opening the CF protein and not as a source of energy normally required to pump ions across the cell membrane. Studies of the Cl⁻ abnormality in CF have been performed using invasive techniques to monitor Cl⁻ transport in biological systems. A review of the methods used in the study of Cl⁻ transport is presented in section I.A5.

I.A3   Ionophore Mediated Chloride Transport Systems

Membrane phospholipids are composed of both polar head groups and nonpolar hydrocarbon chains. This bilayer composition is held together by noncovalent bonds and coulombic interactions, which allow for a high degree of flexibility with regards to cell membrane composition and dynamic properties (21).

Despite the high degree of flexibility, the membrane remains relatively impermeable to small ions. This is a result of the large amount of energy needed to transfer an ion from the aqueous phase into the hydrocarbon, apolar phase (21). This barrier is important in maintaining selectivity and regulation of ion permeability. With the aid of ionophores, the cell membrane permeability for metal cations is increased (22).

There are two classes of ionophores: 1) channel forming ionophores; and 2) carrier ionophores. A channel forming ionophore, such as gramicidin, spans the cell membrane and provides a hydrophilic channel through which the cations can pass. Two subclasses of carrier ionophores exist: 1) neutral ionophores, such as valinomycin (Val) and nonactin

(Non), and 2) carboxylic or charged ionophores, such as lasalocid (Las), nigericin (Nig), and monensin (Mon) (23). Carrier ionophores function by binding the ions prior to transport. Neutral ionophores do not contain any ionizable groups and therefore carry monovalent cations as charged complexes, with an overall charge of $+1$. Carboxylic ionophores contain ionizable groups and therefore transport cations as neutral complexes. The structures of the carrier ionophores used in this investigation are shown in Figure II.

The ionophores function by binding the cation and transporting it through the membrane. This is accomplished with the extremely flexible ionophore backbone, comprised of strategically placed oxygen atoms (24). The oxygens are capable of forming a ring or cavity into which a cation may fit. With the polar groups of the ionophores located towards the interior, the apolar hydrocarbon chains then line the exterior surface. This ability to change conformation explains the lipid solubility of the ionophore cation complex. The mechanism by which a cation is transported through the membrane with the assistance of an ionophore is shown in Figure III. The steps of the ion transport mechanism are: a) formation of a carrier-metal complex at one surface of the cell membrane; b) transport of the complex through the membrane; c) dissociation of the metal ion from the carrier and its release to the other cell compartment; and d) transport of the carrier back through the membrane (24).

Nuclear Magnetic Resonance (NMR) studies as well as X-ray crystallography, CD, and IR studies have determined not only the free metal ionophore structures but also the ion bound conformations (23-29). As shown in Figure IV, three different conformations of metal-free valinomycin exist in different solvents (23). These conformations are observed in solvents of varying polarity. The A conformation exists in nonpolar solvents, such as chloroform and hexane, with six intramolecular hydrogen bonds between the NH of valine

Figure II. Structures of Carrier Ionophores Used in this Study. At physiological pH, Val and Non are neutral while Nig, Las, and Mon are negatively charged.
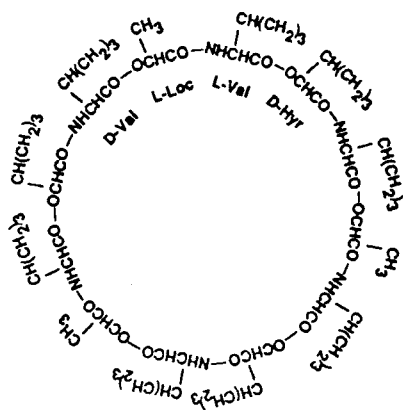
A. Valinomycin
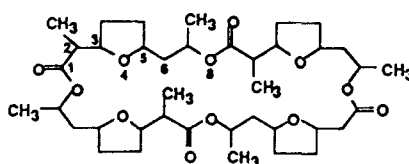
B. Nonactin
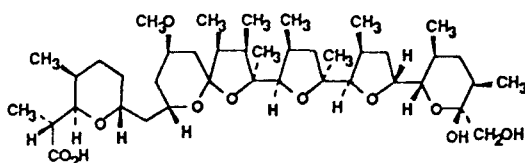
C. Nigericin
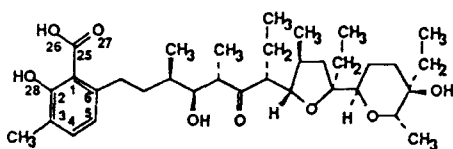
D. Lasalocid (X-537A)
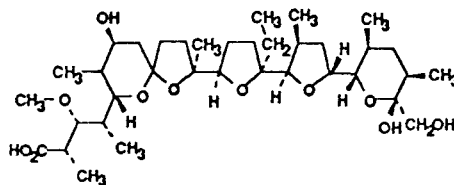
E. Monensin

Structures A and B are the neutral Ionophores
Structures C - E are the Carboxylic Ionophores

Figure III. Carrier Ionophore Mediated Cation Transport (adapted from reference 24). M is the cation being transported by the free ionophore I, k_{IM} is the rate of transport of the complex, K_I is the rate of transport of the free carrier, k_R is the rate of association between the carrier and the cation, and k_D is the rate of dissociation.

M + | I ←k_I— I | + M

k_R ↓   ↑ k_D

IM —k_{IM}→ IM
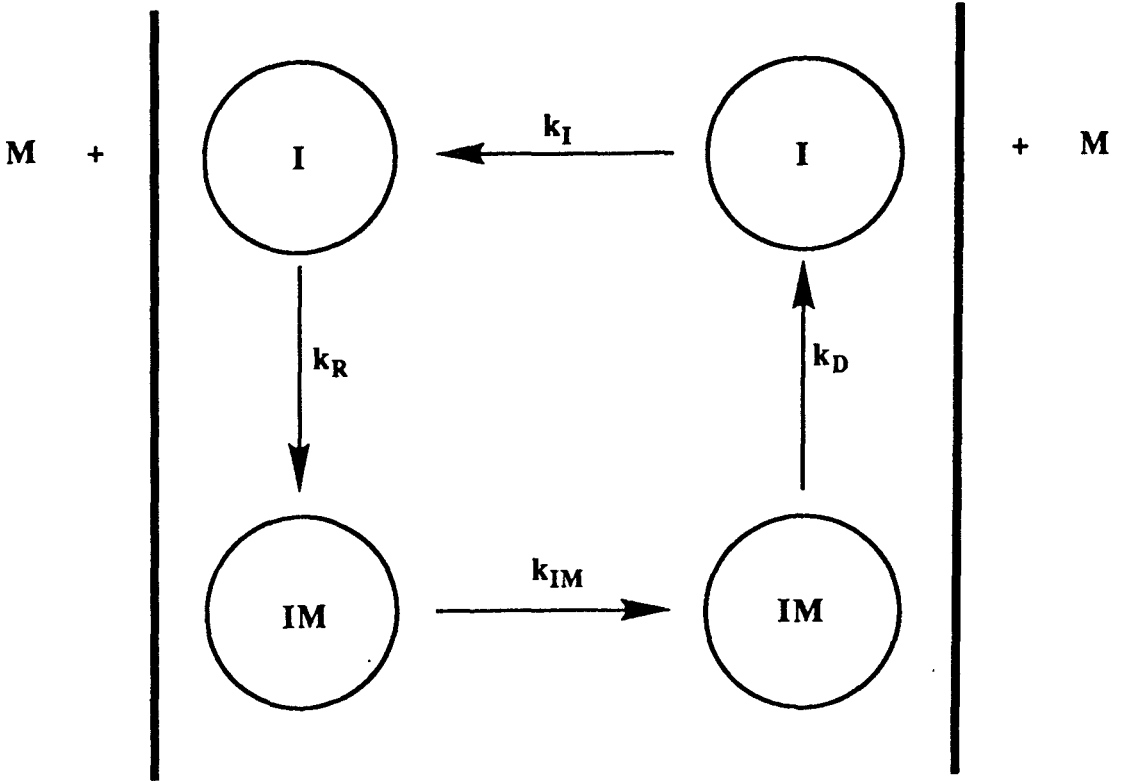
Figure IV. Metal Free Ionophore Conformations in various solvents (adapted from reference 23). A, B, and C are the solution conformations of valinomycin without the presence of a metal.

A ⇌ B ⇌ C
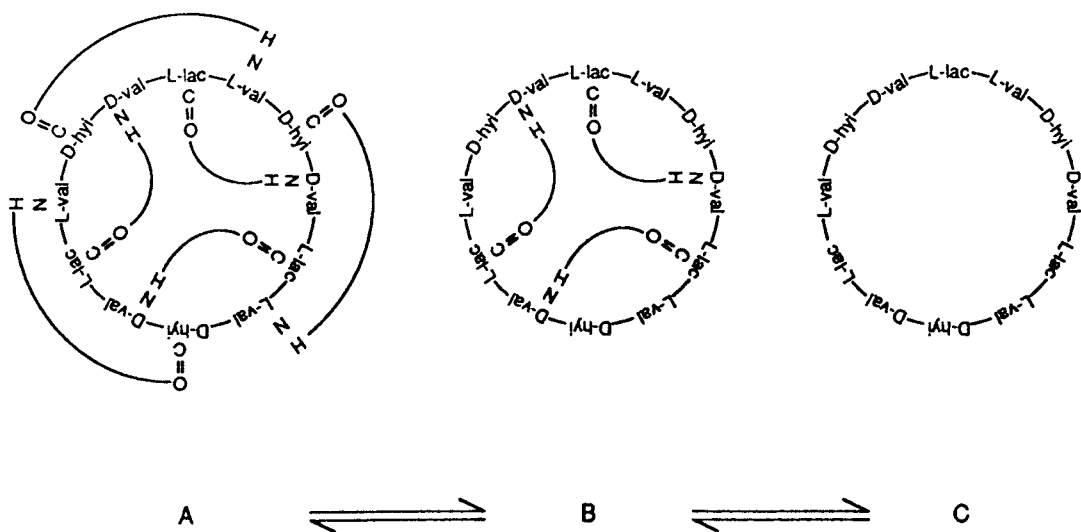
residues and the carbonyls of lactic acid. In solvents of medium polarity, such as 3:1 mixtures of DMSO and CCl_4, conformation B exists with only three NH and carbonyl hydrogen bonds. No hydrogen bonds exist for conformation C in highly polar solvents, such as methanol and DMSO. As the degree of solvent polarity increases, the flexibility of the ring increases. Solvent polarity also controls the relative populations of the three conformations.

Val is the most extensively documented ionophore, with the complete metal ion bound conformations available as well as the metal-free ionophore structures. From ^1H and ^{13}C NMR studies it was found that the mechanism by which ions enter the intramolecular cage of valinomycin involves several conformers (23-27, 29, 30). The carbonyls initially orient away from the interior allowing a free path for the ions to enter. The cation is then firmly trapped inside the ionophore cavity once the carbonyls reorient inwardly. The nonpolar, low dielectric environment of the membrane interior prevents release of the cation. It is only when the more polar membrane surface is reached that the cage opens, releasing the cation. These studies have revealed that all mobile carrier ionophores have a cyclic or quasi-cyclic structure capable of complexing ions directed towards the interior of the complex. For carboxylic ionophores, this requires head-to-tail H bonding in order to form a ring, since their basic structure has a linear backbone.

As a result of the cyclic conformation of the ionophore-cation complex a selectivity sequence exists for complex formation by ionophores. The selectivity sequence, shown in Table I, is based not only on the size ratio of the ionophore cavity to the radius of the cation, but also on the asymmetric ionophore charge distribution (24). Based on the selectivity sequences shown in Table I, the listed ionophores prefer monovalent cations over

Table I.   Ionophore Selectivity of Cations (adapted form reference 24)

Ionophore	Molecular Weight	Selectivity Sequence
I. Neutral Ionophores		
Valinomycin	1110	$Rb^+ > K^+ > Cs^+ > Ag^+ > Tl^+$ $>> NH_4^+ > Na^+ > Li^+$
Nonactin	736	$NH_4^+ > K^+ \approx Rb^+ > Cs^+ > Na^+$
II. Carboxylic Ionophores		
Monensin	670	$Na^+ >> K^+ > Rb^+ > Li^+ > Cs^+$
Nigericin	724	$K^+ > Rb^+ > Na^+ > Cs^+ >> Li^+$
Lasalocid	590	$Cs^+ > Rb^+ \approx K^+ > Na^+ > Li^+$; $Ba^{2+} > Sr^{2+} > Ca^{2+} > Mg^{2+}$

divalent cations when forming 1:1 complexes. However, ionophores such as A23187, have been shown to be more selective for divalent cations (23). The ionophores which complex with divalent cations form complexes of different stoichiometry based on the solvent used (23). The conformations of the divalent ionophores also differ in various solvents.

With all the information available on the structure and function of ionophores, there exists considerable ambiguity on the effect of ionophores on the membrane potential of biological systems (30). It was interpreted that transport of the positively charged neutral ionophore-cation complex out of the cell was accompanied by either Cl^- efflux through the anion transport band 3 protein, or proton exchange, thereby maintaining cell neutrality and not affecting the potential gradient (30). However, Hladlky and Rink (31) have clearly shown by fluorescence spectroscopy that Val does affect the membrane potential of RBCs. Alternatively, the positively charged neutral ionophore-cation complex could ion pair with a Cl^- and thus provide an additional transport pathway for anions.

I.A4   Ion Pairing

The concept of ion pairing pertains to two ions that are in the close vicinity of each other for a short time before their thermal motions tear them apart (32). There are several proposed models to represent the possible ion associations existing in solution (32-34). As shown in Figure V, three types of ion pairs exist, with the environment of the solvent and ions differing between each form. NMR spectroscopy has proved to be a valuable technique for differentiating between the types of ion pairs existing in solution (25-30). In particular, quadrupolar nuclei, such as $^{35}Cl^-$, have an electric field gradient which is very sensitive to the symmetric charge distribution around the observed nuclei (33,35). Changes in both chemical shift (δ) and line width ($\Delta\nu_{1/2}$) yield information on electron distribution about the nucleus of

Figure V. Types of Ion Pairs. M^+ and M^- represent cations and anions, respectively. C

differs from B in that a solvent molecule is not interposed between the cation and the anion.
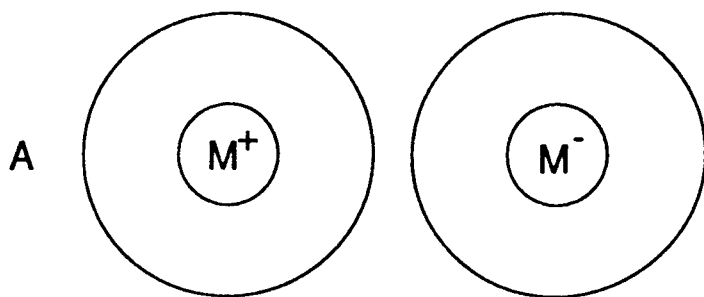
A — Solvated Ions
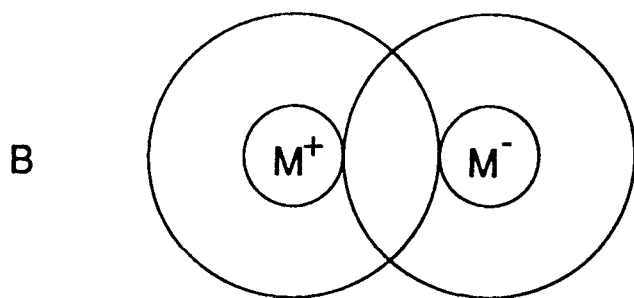
B — Solvent-separated Ion Pairs
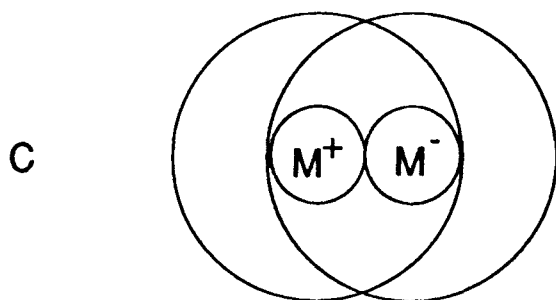
C — Contact Ion Pairs

interest. As a result of ion association a decrease in relaxation produces line broadening which is easily observed. The NMR line width is the only parameter which is able to distinguish between two of the possible ion associations, contact and solvent separated ion pairs (34). In the case of contact ion association the ^{35}Cl NMR line width increases compared to the solvent separated system (34).

FT-IR provides a complimentary approach to study ion pairing in solution. Formation of an ion pair can lead to changes in point group symmetry for perchlorate from T_d to C_{3v} or C_{2v} resulting in the appearance of new bands in the mid infra-red region (35). It is important to note that the time scale of the NMR and IR measurements are considerably different (35). For instance, for 10 MHz ^{35}Cl NMR spectroscopy the time scale is of the order of 10^{-7} s whereas for vibrational spectroscopy, it is of the order of 10^{-12} s. A consequence of the different observation times in the two techniques is that ion pair formation may be in fast exchange based on the NMR time scale and in slow exchange based on the IR time scale.

The electrostatic interactions of neutral ionophores with cations result in positively charged complexes which may ion pair with a counteranion, such as Cl^- or ClO_4^-. This ion pair association may provide an alternate transport pathway as mentioned in section IA.3. Val and alkali cations are known to ion pair with several paramagnetic anions, such as $CoBr_4^{2-}$ and $Co(SCN)_4^{2-}$ (36). No reports existed on ion pairing of ionophores with Cl^- or ClO_4^- prior to this study.

I.A5   Methods Used in the Study of Chloride Transport in Biological Systems

Cl^- transport and distribution in cell suspensions and perfused tissues have been

studied using radioactive tracers and ion selective microelectrodes. Recently, a halide sensitive fluorescent probe, 6-methoxy-N-(3-sulfopropyl)quinolium (SPQ), has been designed and successfully used to study chloride transport in cell suspensions (37-38). In this section, each of these techniques is reviewed.

Ion-selective microelectrodes (ISMs) are the most widely used devices for measuring the activity of chloride. Both steady state as well as changes in activity of chloride can be obtained by this technique. This technique also allows for measurement of Cl^- fluxes across plasma membrane of individual cells. ISMs measure the activity and not the concentration of Cl^- ions. It is possible to estimate the free intracellular ion concentration by dividing the measured activity by its intracellular activity coefficient (39). ISMs have good time resolution for studying Cl^- transport and permit continuous measurements of chloride activity (39-40). Despite these advantages, ISMs do have several drawbacks. The method is invasive and requires cells to be penetrated with two microelectrodes (41-42). This requires not only electrophysiological skill but also a cell that allows such impalement without suffering irreversible damage. Lack of perfect selectivity and inability to measure unidirectional fluxes are also additional drawbacks of ISMs.

The most common radioisotope used to study Cl^- transport in cells is ^{36}Cl. ^{36}Cl decays by emitting a ß (electron) particle to become the inert gas, argon. The energy of the emitted particle is 0.709 MeV and can be easily measured by scintillation spectroscopy. Theoretically, the highest attainable specific activity is 1.17 Ci/mole. In practice one gets about 0.3 Ci/mole. In order to use ^{36}Cl to monitor Cl^- fluxes, the flux must be high. This tracer method depends on several independent measurements. Its precision and accuracy are rather poor (43).

In recent years, Verkamn and his coworkers (37-38, 44-46) introduced SPQ, a fluorescent compound sensitive to Cl^-. This indicator is apparently non-toxic and very sensitive to Cl^- (38,46). It does not act as a Cl^- ionophore or Cl^- buffer (38, 44-45). However, the SPQ method has several limitations for the study of Cl^- transport in cells. SPQ leaks rapidly out of cells and the absolute signal depends on dye concentration. The leakage rate appears to depend on cell type and SPQ loading procedure (38,46). Another major limitation is the inability to make fluorescent ratio measurements and the lack of a second reference wavelength makes it difficult to determine accurately cell Cl^- activity if significant SPQ leakage occurs. The peak excitation of SPQ occurs at 350 nm, which is in the same range as that of the autofluorescence wavelength of most cells. Finally, a significant fall in the sensitivity of the dye to changes in the Cl^- activity occurs inside cells. It is reported that the quenching constant falls from 118 M^{-1} to 12 M^{-1} in rabbit proximal tubules (38) and 13 M^{-1} inside epithelial cells (46). This has been attributed to SPQ quenching by intracellular anions. This clearly indicates that intracellular sensitivity of this indicator must be evaluated and intracellular calibration performed for each cell type.

NMR spectroscopy provides a non-invasive method for monitoring ions in biological systems. The availability of multinuclear NMR spectrometers has made it possible to obtain spectra of biologically important cations like Na^+, K^+, Ca^{+2}, Mg^{+2}, etc (33). The intra- and extracellular resonances of cations in RBCs and tissues have been resolved with the use of aqueous shift regents (SRs) (47-57). Most SRs are negatively charged. Due to the bilayer nature of cell membranes, SRs are not soluble in the lipophilic membrane interior and they are repelled by the negatively charged head groups of phospholipids. Thus, SRs remain in the extracellular compartment during NMR experiments conducted on cell suspensions.

Through the use of SRs the extracellular resonance is shifted away from the intracellular resonance allowing the simultaneous observation of the two pools of metal ions. Information on metal cation transport and distribution in cell suspensions, and enzymatic activity is then easily obtained by metal NMR spectroscopy in the presence of SRs (51-53).

The presence of SRs in the suspension medium leads to transmembrane differences in chemical shifts resulting in resolution of intra- and extracellular $^7Li^+$, $^{23}Na^+$, $^{39}K^+$, and $^{87}Rb^+$ NMR resonances in cell suspensions (47-56). In the absence of shift reagents, transmembrane differences in relaxation times provide an alternative means of distinguishing intra- and extracellular pools of Li^+ and K^+ ions (57,58).

In contrast to the vast amount of literature on ^7Li, ^{23}Na, and ^{39}K NMR applications to biological systems, very few published literature exists on the biological applications of ^{35}Cl NMR spectroscopy. Brauer and Sykes (1) have attempted to elucidate Cl^- transport in RBCs using ^{35}Cl NMR. They report that intracellular Cl^- is invisible by ^{35}Cl NMR spectroscopy because of Cl^- binding to hemoglobin in human erythrocytes. Only changes in the extracellular ^{35}Cl NMR signal were observable. This does not allow for the simultaneous visualization of both intra- and extracellular Cl^- ions. Only information on changes in the extracellular Cl^- levels could be monitored. Recently, the visibility of intracellular ^{35}Cl resonance in dog RBCs and kidney tubules has been investigated by Boulanger et al. (59). They reported that intracellular Cl^- is 40% visible in dog erythrocytes but invisible in dog renal tubules. Riddell et al. (60) reported a method by which ^{35}Cl NMR spectroscopy can be used to study chloride ion transport in vesicles suspensions. Their approach takes advantage of efficient relaxation of Cl^- by Mn^{2+} and does not involve the use of SRs. Bryden et al. (61) report on the SR properties of several lanthanide macrocycles with Cl^-. From their

report, DyNOTA (where NOTA = 1,4,7-triazaclycononance-N,N',N''-triacetate) gave the largest Cl⁻ shift (-10.22 ppm). There is however a substantial contact contribution to this observed shift (61). This means that the chloride ion is directly coordinating to the lanthanide ion. Contribution of contact shifts to the observed shifts complicates the use of a SR. To minimize contact shift contribution, SRs with an overall higher negative charge and having the paramagnetic centers protected by bulky ligands that prevented direct Cl⁻ binding were tried in this study. These features lessen Cl⁻ attraction by the SRs, reducing the contact contribution. However, the resulting shift was insufficient to separate intra- and extracellular Cl⁻. Cobalt (II) was also tested as a possible Cl⁻ SR (62). Shulman et al. (62) report separation of intra- and extracellular Cl⁻ in vesicles. This approach suffers from some serious limitations which are discussed in detail in section IV.2. It has yet to be shown that one can resolve intra- and extracellular Cl⁻ resonances in cells with or without SRs by ^{35}Cl NMR spectroscopy.

NMR is also able to provide information on Cl⁻ binding in membranes. The binding of sodium to the saliva of CF patients by ^{23}Na NMR has been reported (63). This information is not obtainable by the other aforementioned techniques. There is a limited number of NMR studies of the disorder found in CF patients. The emphasis of these applications is on structural characterization of sialyloligosaccharide units from CF patients by ^{1}H and ^{13}C NMR spectroscopy (64-68). ^{35}Cl NMR has the potential of providing a direct way to monitor chloride binding and transport properties in cells of CF patients.

I.B1   Biological Importance of Cesium

The discovery of a convenient tool for Cs⁺ analysis comes at a time when much

interest in the biochemistry and physiology of Cs^+ in biological systems exists (69). The first area of interest is concerned with understanding the general properties of alkali metal ions in transport and enzyme activation. This typically involves using Cs^+ as a tracer to study K^+ transport and distribution *in vivo* because Cs^+ is considered to be physiologically similar to K^+. The second area of interest occurs in investigating the toxicological problems related to radioactive $^{137}Cs^+$ uptake. Radioactive $^{137}Cs^+$ has a biologically long half life and is a byproduct from nuclear explosions. Once generated it is passed quickly down the food chain and eventually settles in muscle and bone tissues. The third area of interest occurs in the application of Cs^+ to treat depression. Typically, Li_2CO_3 has been administered to treat depression. Cs^+ was found, however, to have a better absorption rate without some of the side effects associated with Li^+ salts. Since the evaluation of Cs^+ salts for their antidepressant activity by Messiah and coworkers (70-71), several studies have appeared on Cs^+ effects on neuromuscular systems (72), immune system (73), motor functions (74), and tumor growth (75). Pretreatment with CsCl was found to significantly counteract the chlorpromazine-induced decline in motility as well as increased spontaneous locomotor activity in mice (70). Pretreatment with CsCl was also found to produce a central antagonistic action on sodium pentobarbital induced sleep (71). The physiological similarity between Cs^+ and K^+ may indicate that Cs^+ can displace K^+ in some physiological processes. The use of Cs^+ to treat some forms of depression would then require careful monitoring of the K^+ levels to prevent possible toxicity associated with a K^+ deficiency (71). Studies investigating the effects of Cs^+ on the neuromuscular system found that Cs^+ is very photoelectrically active. The ability of Cs^+ to interfere in cellular functions and neural excitability resulting in alteration of tumor requirements and nerve impulse propagation may

be linked to the fact that Cs^+ is the most electropositive metal. In these studies, Cs^+ is generally administered in the chloride form because this is the least toxic source with an $L.D._{50}$ of 1,118 mg/kg (72). A comparison of Li^+, Rb^+, and Cs^+ uptake in mouse brains found that although Rb^+ had the highest uptake rate, Cs^+ was retained the longest. This is supported by the long biological half life for Cs^+ found in human studies. These findings suggest that treatment with Cs^+ salts may allow for short term drug free periods. Despite numerous reports on Cs^+, the interactions of Cs^+ with cell membranes and intracellular metabolites in human red blood cells (RBCs) and perfused tissues remain to be understood.

I.B2   Methods Used in the Study of the Cesium Ion

Intra- and extracellular $^{133}Cs^+$ NMR resonances in Cs^+-loaded cell suspensions exhibit a unique behavior. The chemical shifts of the two ^{133}Cs NMR resonances in Cs^+-loaded human erythrocyte suspensions and perfused rat heart are distinguishable without the incorporation of a SR in the suspension medium (76). Similar ^{133}Cs NMR observations were recently made with living plant tissue (77). On the other hand, with vesicular preparations triphosphate was required to separate the $^{133}Cs^+$ NMR resonances (78). The origin of the two ^{133}Cs NMR resolved resonances in Cs^+-loaded human erythrocyte suspensions in the absence of SR is not known (76).

Because of the large ionic radius of Cs^+, the NMR chemical shift (δ) range of $^{133}Cs^+$ is much larger relative to those of other alkali metal nuclei and is known to be extremely sensitive to chemical environment and is effected by counterions present, as well as temperature, and solvent composition (79). These effects arise from short range ion-solvent and ion-ion interactions. Iodide was found to have the largest effect on δ followed by Br^-,

Cl^-, and F^-. A similar trend is observed for the effect of counter ions on the δ in the crystal lattice. As the temperature is lowered the δ measured in different solvents becomes more paramagnetic. Once a temperature below 100 °C is reached, the shifts become independent of solvent (79). Of all alkali metals, Cs^+ was found to have the largest solvent dependent δ scale, varying by more than 100 ppm. Solvents with the lowest Gutmann donor numbers gave the largest downfield shifts. The ^{133}Cs nucleus has a nuclear spin of 7/2, a small quadrupole moment, and a relaxation rate approximately 200 times smaller than the other NMR detectable alkali metal nuclei (33). The Cs^+ ion is 100% visible by ^{133}Cs NMR spectroscopy (33). With a small quadrupolar moment, little distortion in the line shape of the Cs^+ NMR resonance is observed, enhancing the information obtainable by ^{133}Cs NMR spectroscopy. These factors make ^{133}Cs NMR spectroscopy an ideal technique for investigating Cs^+ distribution and transport in biological systems (76-78). Moreover, interesting information on rapid Cs^+ ion motion around DNA was recently obtained using multiple quantum ^{133}Cs NMR experiments of macroscopically oriented CsDNA (80).

Other methods used to study Cs^+ in biological systems include atomic absorption spectroscopy (AAS) and radioisotope labeling. The activity of Cs^+ as an antidepressant and its effect on certain neurological-psychiatric manifestations in rats has previously been studied by AAS (69). Experiments involved removal of the whole brain from rats previously administered CsCl. After homogenation in ice-cold perchloric acid, the supernatant was assayed for Cs^+ by AAS. Information on Cs^+ accumulation in the brain is obtainable without any information available on Cs^+ binding sites in the brain. Information on Cs^+ transport rates is not accurately determinable by this technique because it requires treating several animals CsCl for different time periods followed by a series of analytical procedures.

The radioactive ^{134}Cs has been used as a tracer to study the cation metabolism of human erythrocytes (81). From these radioisotope studies ^{86}Rb, ^{42}K, and ^{134}Cs were all found to enter into similar metabolic processes and concentrate within red cells to approximately the same extent. The exchange measured with ^{134}Cs as the tracer was much slower than for ^{86}Rb and ^{42}K as tracers. Radioisotope studies are hindered by the level of contamination, and the possibility of biological separation of this element by the system being studied in which the distribution of the radioisotope does not follow that of the substituted ion.

I.B3 Cesium Transport in Biological Systems

With the observation of intra- and extracellular Cs$^+$ resonances by ^{133}Cs NMR spectroscopy, the use of Cs$^+$ as a tracer for K$^+$ provides an ideal technique by which information on K$^+$ metabolism could be obtained. In systems deficient in K$^+$, Cs$^+$ is able to enter cells via the Na$^+$/K$^+$ ATPase (81). This membrane protein provides one of the major transport pathways for sodium and potassium. This pathway requires ATP to extrude sodium from the cell while simultaneously accumulating potassium. The rate of Cs$^+$ uptake is approximately 1/3 that of K$^+$ and can be reduced by a factor of 2 upon addition of ouabain, an inhibitor of Na$^+$/K$^+$ ATPase (76). The concentration of Cs$^+$ required to activate the Na$^+$/K$^+$ ATPase varies from system to system. In the presence of K$^+$, high concentrations of Cs$^+$ are required for Cs$^+$ transport. Once transported, Cs$^+$ deposits in the muscle and bone tissue. Despite the fact that Rb$^+$ is a better substitute for K$^+$, the NMR receptivity of ^{87}Rb is poor. Thus, the simultaneous observation of both intra- and extracellular ^{133}Cs$^+$ resonances without incorporation of a SR makes using Cs$^+$ a better substitute for K$^+$ transport studies.

CHAPTER II

STATEMENT OF THE PROBLEM

The primary goals of this project are to study ion pairing and distribution of Cl^- in human RBCs suspensions containing ionophores using noninvasive NMR techniques, and to investigate the origin of the two $^{133}Cs^+$ NMR resonances in the absence of SR in Cs^+-loaded human RBC suspensions.

Several studies have shown that an abnormal Cl^- transport exists in CF patients due to a defective protein coded by chromosome seven (82). The transport of Cl^- across cell membranes is important in cellular regulation, absorptive and secretory processes (37). However the conventional methods of measuring Cl^- transport, namely patch clamp, microelectrodes, and ^{36}Cl tracer techniques, are restricted by their sensitivity, time resolution, and applicability. Inefficient cell loading of SPQ severely limits the fluorescent method (38). ^{35}Cl NMR spectroscopy provides a non-invasive approach to study Cl^- ion pairing and distribution in RBCs.

Several studies have appeared on the biological effects of Cs^+ in RBCs and perfused tissues (76). Cs^+ has been shown to affect neuromuscular systems, immune systems, motor functions, and tumor growth (69-75). Current methods of studying Cs^+ in biochemical systems include: AAS and the use of radioisotopes. The discovery of a convenient tool for Cs^+ analysis which provides information on Cs^+ transport and binding would further enhance our understanding on the role of Cs^+ in biological systems. Intra- and extracellular ^{133}Cs NMR resonances in Cs^+ loaded cell suspensions exhibit an unique behavior (76). It is the

simultaneous visualization of the two Cs^+ pools in the absence of shift reagents that makes ^{133}Cs NMR spectroscopy an ideal technique to investigate the role of Cs^+ in biological systems. Brix et al. (83) have shown that chloride binding to Hb is stronger than that of DPG to Hb. Moreover, they have also shown that chloride shifts affect oxygen binding to Hb in RBCs (83). Theoretical analysis has shown that binding of metal ions to Hb or DPG affects oxygenation in RBCs (83). Cl^- and Cs^+ appear to have a similar effect on the uptake of O_2 in RBCs (83). We hypothesize that cesium toxicity could arise from its binding to Hb or DPG thereby affecting oxygenation in RBCs.

The two nuclei ($^{35}Cl^-$ and $^{133}Cs^+$) have interesting NMR behavior. $^{35}Cl^-$ is in fast exchange on the NMR time scale, while $^{133}Cs^+$ is in slow exchange. This interesting property combined with the above observations on the effects of Cl^- and Cs^+ in RBCs prompted our detailed investigation of these two ions in biological systems using NMR.

Specific experiments were designed to research each of the following specific aims:

II.1   Characterization of Lanthanide SRs for Monitoring Cl^- Transport and Distribution in Human RBCs by ^{35}Cl NMR Spectroscopy.

In an attempt to directly obtain Cl^- concentrations, I set out to discriminate the intra- and extracellular resonances of Cl^- across the membrane using lanthanide SRs and ^{35}Cl NMR spectroscopy. I have characterized the Dy^{3+} complexes of TTHA, PPP, DPA, NOTA, DOTA, and DTPA in order to obtain a suitable SR that produces $^{35}Cl^-$ shifts large enough to discriminate between intra- and extracellular signals and yet remain membrane impermeable in cell suspensions.

II.2   Investigation of Cl⁻ and ClO₄⁻ Ion Pairing in the Two Subclasses of Ionophores.

In order to investigate ion pairing of metal ion-ionophores with Cl^- and ClO_4^-, the ion pairing ability of neutral and carboxylic ionophores with Cl^- and ClO_4^- in different solvents with varying dielectric constants and donor numbers were studied. I hypothesize that neutral ionophores, and not carboxylic ionophores, change Cl^- distribution in RBCs via ion pairing mechanism. ^{19}F and ^{31}P NMR spectroscopies were used to quantitate Cl^- distribution ratios in RBC suspensions containing ionophores.

II.3   Physical Basis for the Resolution of Intra- and Extracellular Cs⁺ in RBCs by ¹³³Cs NMR Spectroscopy.

The factor(s) responsible for the observation of intra- and extracellular ^{133}Cs resonances in human RBCs by ^{133}Cs NMR spectroscopy were examined. Factors such as viscosity, magnetic susceptibility, and Cs^+ binding to RBC components as well as the membrane were examined. I hypothesize that the physical basis for the resolution of intra- and extracellular ^{133}Cs NMR resonances in Cs^+-loaded RBC suspensions is due to Cs^+ binding to intracellular phosphates, and to the non-ideality of intracellular water induced by hemoglobin. Factors responsible for Cs^+ toxicity in RBCs were also studied.

CHAPTER III

EXPERIMENTAL METHODS

III.1 Materials

III.1.1 Reagents

Sodium chloride (NaCl), cesium chloride (CsCl), potassium chloride (KCl), magnesium chloride (MgCl$_2$), calcium chloride (CaCl$_2$), cobalt (II) chloride (CoCl$_2$), nickel (II) chloride (NiCl$_2$), potassium perchlorate (KClO$_4$), lanthanide chloride salts (LnCl$_3$), potassium phosphate (KH$_2$PO$_4$) triethylenetetraamine hexaacetic acid (H$_6$TTHA), diethylene triamine pentaacetate (DTPA), dipicolinate (DPA), cobalt (II) acetylacetonate (Co(acac)$_2$), sodium triphosphate (Na$_5$PPP), glucose, tetramethylammonium hydroxide, sucrose, deuterium oxide (D$_2$O), 4,4'-dinitrostilbene-2,2'-disulfonic acid (DIDS), valinomycin, nonactin, nigericin, lasalocid, monensin, methanol, acetonitrile, nitromethane, dimethylsulfoxide (DMSO), hypophosphite (HP), trifluoroacetate (TFA), and trifluoroacetamide (TFM) were supplied by Aldrich Chemical Company (Milwaukee, WI). HEPES [4-(2-hydroxyethyl)-1-piperazineethanesulfonic acid], vitamin B$_{12}$, cobinamide dicyanide, adenosine triphosphate (ATP), adenosine diphophate (ADP), 2,3-diphosphoglycerate (DPG), polyvinyl pyrrolidone, n-octyl β-D-glucopyranoside, and L-α-phosphatidylcholine (PC) were obtained from Sigma Chemical Company (St Louis, Missouri). All chemicals were used as received except sodium triphosphate and the solvents which where further recrystallized or purified as described below.

32

III.1.2 Human Blood and Frog Specimens

Packed red blood cells (RBCs) were supplied by the Chicago Chapter of Life Source. Male Northern Grass Frogs were supplied by Kons Scientific (Germantown, Wisc). The protocols for experiments involving human blood and frogs were approved by the Institutional Review Board for the Protection of Human Subjects and the Institute for Animal Care and Use Committee (Lake Shore Campus).

III.2   Instrumentation

III.2.1 NMR Studies

^{7}Li, ^{13}C, ^{19}F, ^{23}Na, ^{31}P, ^{35}Cl, and ^{133}Cs measurements were made at 116.4, 75.4, 282.2, 79.4, 121.4, 29.5, and 39.4 MHz, respectively on a Varian VXR-300 NMR spectrometer. The instrument was equipped with a 10 mm multinuclear probe and a variable temperature unit. Some ^{19}F experiments were conducted on a General Electric GN-500 NMR spectrometer (Univ. of Texas at Dallas).

A standard single pulse sequence was employed to obtain the NMR spectra of all samples. Samples containing intact RBCs, ghosts, and vesicles were all run nonspinning. All NMR experiments were run under identical gain settings and absolute intensity conditions.

^{7}Li NMR spectra for testing ion pairing in ionophore solutions were obtained using a flip angle of 60° (14 μsec), an acquisition time of 0.97 sec, a 35 sec delay, a spectral width of 4500 Hz, and 25 transients. All ^{7}Li spectra were recorded at ambient temperature and referenced to 0.15 M LiCl.

^{13}C NMR spectra for the characterization of Cs$^+$-DPG interactions were obtained using

a flip angle of 45° (8.7 μsec), an acquisition time of 0.3 sec, a 2 sec delay, a spectral width of 13514 Hz, and 6000 transients. All ^{13}C spectra were recorded at ambient temperature and referenced to TMS.

^{19}F NMR spectra for determination of the Cl$^-$ distribution in RBCs were obtained using a flip angle of 90° (20.0 μsec), an acquisition time of 3.0 sec, a 30 sec delay, a spectral width of 100000 Hz, and 32 transients. All ^{19}F spectra were recorded at ambient temperature and referenced to TFA.

^{23}Na NMR spectra for testing LUVs for leakiness and ion pairing in ionophore solutions were obtained using a flip angle of 75° (20.0 μsec), an acquisition time of 0.5 sec, a spectral width of 10405 Hz, and 1000 transients. All ^{23}Na NMR spectra were recorded at ambient temperature and referenced to NaCl-D$_2$O.

^{31}P NMR spectra of ATP, ADP, DPG, and P$_i$ in RBCs and model systems were obtained using a flip angle of 45° (10 μsec), an acquisition time of 1.5 sec, a spectral width of 10000 Hz, and 4000 transients. All ^{31}P NMR spectra were recorded at 37°C for RBC samples and ambient temperature for model systems. All spectra were referenced relative to H$_3$PO$_4$. ^{31}P NMR spectra of HP in RBCs were obtained using a flip angle of 90° (11.5 μsec), an acquisition time of 1.0 sec, a spectral width of 10000 Hz, and 32 transients. Waltz decoupling was used at a high power of 75.

^{35}Cl NMR spectra of Cl$^-$ ionophore solutions were obtained using a flip angle of 45° (33 μsec), an acquisition time of 0.1 s, a spectral width of 8143 Hz, and 100000 transients. All ^{35}Cl NMR spectra were recorded at ambient temperature and referenced to KCl in D$_2$O. Line widths reported are corrected for any line broadening. Parameters similar to those used for acquiring the ^{35}Cl NMR spectra of Cl$^-$ ionophore solutions were also used for Cl$^-$ SR

experiments. Samples containing RBCs, LUVs, or muscle tissue were run nonspinning.

^{35}Cl NMR spectra of ClO_4^- ionophore solutions were obtained using a flip angle of 45°
(33 μsec), an acquisition time of 0.5 s, a spectral width of 5066 Hz, and 200000 transients,
with transmitter offsets of 3500 and 18700. All ^{35}Cl NMR spectra were recorded at ambient
temperature and referenced to $KClO_4$ in D_2O.

^{133}Cs NMR spectra of Cs^+ loaded RBCs and aqueous solutions were obtained using
a flip angle of 45° (16 μsec), an acquisition time of 1.0 sec, a spectral width of 8000 Hz, a
25 sec delay, and 1000 transients. With the exception of intact RBCs suspensions, the spectra
of all samples were recorded spinning. All ^{133}Cs NMR spectra were recorded at ambient
temperature, unless otherwise mentioned in figure legends. The reported paramagnetic shifts
were measured relative to samples that were free of SR. Downfield and upfield shifts were
defined as negative and positive, respectively.

Field-frequency locking on D_2O present in the aqueous media was used throughout.
No coaxial tube combinations were used, except for the experiments in which the contribution
of the non-ideality of intracellular water to the intracellular $^{133}Cs^+$ shift was investigated
(section IV. 6). In these experiments, the $^{133}Cs^+$ chemical shifts were referenced relative to
0.15 M CsCl placed in the bulb of a spherical bulb/cylindrical capillary (Wilmad Glass Co.,
Inc., Buena, NJ) supported in the outer 10 mm NMR tube with a vortex plug.

III.2.2 Vapor Pressure Osmometer

The osmolarity of the suspension medium used for all the RBC and vesicle
samples was adjusted with NaCl to 300 and 200 $\pm$ 5 mOsm, respectively, with a Wescor
Vapor Pressure Osmometer (Logar, Utah). The vesicles were prepared in 100 mM NaCl

resulting in an osmolarity of 200 mOsm.

III.2.3 Centrifuge

Blood processing was performed at 4°C using a Savant refrigerated centrifuge model RWC-825. Preparation of resealed RBC ghosts was carried out using either a Dupont model RC-5B refrigerated centrifuge, which was equipped with a Sorvall SS-34 rotor, or a Beckman J2-21, which was equipped with a JA-20 rotor.

III.2.4 Viscometer

The viscosity of the ionophore solutions was measured with a Brookfield Cone Plate Viscometer, equipped for low viscosity samples, using an 8° CP-40 cone, at 12 rpm. The viscosity of ATP, ADP, DPG, Pi, and Hb solutions was adjusted with either glycerol or polyvinyl pyrrolidone (PVP-100) to 5 cP to correspond to the viscosity inside RBCs (84).

III.2.5 UV/VIS Spectrometer

Hb concentrations were measured with an IBM UV-VIS double beam spectrometer, model 9420. The absorbance at 555 and 430 nm (extinction coefficients 12.5, 133 cm^{-1} mM^{-1}) were recorded for deoxyHb. The absorbance at 569 nm (extinction coefficient 13.4 cm^{-1} mM^{-1}) was recorded for COHb (85).

III.2.7 FT-IR Spectrometer

All FT-IR measurements were recorded on an Alpha Centauri FT-IR spectrometer located at Northwestern University, Chicago, Il.

III.3 Sample Preparation

III.3.1 Preparation of Shift Reagents

The shift reagent containing the ligand TTHA[6] was freshly prepared by *in situ*

methods previously described (50, 54, 57), with the exception that tetramethylammonium

hydroxide was used as a base. With this modified procedure, the shift reagent was in the

form of tetramethylammonium salt. This was done so that the bulky counter cation would be

less competitive with alkali and alkaline-earth metal cations being studied.

Tetramethylammonium Dy(III) triphosphate was prepared by the following method:

recrystallized Na_5PPP was passed down a cation-exchange Dowex-50 column loaded with

tetramethylammonium chloride. The tetramethylammonium triphosphate thus obtained was

recrystallized five times and was checked by ^{23}Na NMR and AAS for any residual sodium.

Sodium content of tetramethylammonium triphosphate was estimated to be less than 9% of

sodium present in Na_5PPP. The tetramethylammonium form of the shift reagent $Dy(PPP)_2^{7-}$

was obtained from the dysprosium chloride by an *in situ* reaction with tetramethylammonium

triphosphate (54).

NOTA was prepared by the following procedure (87): triazacyclononane (4.6 g) was

dissolved in acetonitrile and K_2CO_3 (15 g) while mixing at room temperature.

Chloroacetonitrile (8.15 g) dissolved in 60 mL CH_3CN was then added dropwise to the

triazacyclononane solution with vigorous stirring. The reaction was monitored by TLC (10%

methanol in $CHCl_3$) until a single spot of the trisubstituted amine prevails. The K_2CO_3 was

filtered off and washed with CH_3CN. The solution was then concentrated to half original

volume and then slowly titrated with ethanol until crystals form. It was allowed to stand

overnight. The crystals were collected, washed with ethanol, and allowed to air dry. Analysis was performed by Desert Analytics (Tucson, Az). The sample was reported to contain 41.58% C, 6.58% H, and 12.50% N. Theoretical calculations based on a total molecular weight of 303 yields 47.52% C, 6.93% H, and 13.86% N.

DOTA was a gift from Professor Carlos F.G.C. Geraldes (University of Coimbra, Portugal).

Dy(III)NOTA and Dy(III)DOTA were prepared by methods previously described (61, 88). In brief, solutions of either DyNOTA or DyDOTA were prepared in water with a 1:1 metal-to-ligand ratio by mixing appropriate aliquots from stock solutions of lanthanide chlorides and DOTA or NOTA. Each mixture was then heated and the pH readjusted to 7.5.

The HEPES buffer was adjusted to the physiologic pH range with tetramethylammonium chloride and used at a 5 mM concentration in all samples to maintain the pH.

III.3.2 Purification of Solvents

HPLC grade methanol was stored over 4Å Linde molecular sieves to remove any water. Solvent transfer was accomplished under a nitrogen atmosphere. Acetonitrile was purified as described in reference (89). In brief, acetonitrile was refluxed over anhydrous aluminum chloride prior to rapid distillation. Secondly, it was refluxed over alkaline permanganate prior to rapid distillation. Thirdly, it was refluxed over potassium bisulfate prior to rapid distillation. Finally, it was refluxed over calcium hydride prior to fractionation. DMSO was purified according to reference (90). In brief, DMSO was dried with 4Å Linde

molecular sieve and then distilled.

III.3.3 Preparation of Specific Buffers for Cs$^+$ in RBCs

To investigate the interaction of Cs$^+$ with each of the intracellular RBC components three buffers were prepared (see Table XIV). CsCl buffer A consisted of 10 mM CsCl, 140 mM NaCl, 5 mM glucose, and 5 mM HEPES, pH 7.4. CsCl buffer B consisted of 10 mM CsCl, 5 mM NaCl, 140 mM KCl, 1 mM CaCl$_2$, 2.4 μM MgCl$_2$, 5 mM glucose, and 5 mM HEPES, pH 7.4. This buffer contains the intracellular physiologic cation concentrations. CsCl buffer C was similar in composition to buffer B with the addition of PVP-100 to adjust the viscosity to 5 cP.

III.3.4 Preparation of Cs$^+$-Loaded RBCs

Freshly packed RBCs were washed three times by centrifugation at 2000 g for 4 min, with an isotonic buffer containing 150 mM NaCl and 5 mM sodium phosphate, pH 8 (5PBS) removing the buffy coat by aspiration.

Cs$^+$ loading was accomplished by incubation of the washed, packed RBCs at 45% hematocrit and 37 °C from 1 to 12 hrs with 150 mM CsCl, 5 mM glucose, and 5 mM HEPES, pH 7.4. The intracellular Cs$^+$ concentrations varied from 0.59 to 15.0 mM, depending on the incubation time used. The Cs$^+$-loaded RBCs were then washed and resuspended at 27 to 93% hematocrits in the isotonic buffers as described in the figure legends. This is a modified procedure taken from reference 76 in which loading was accomplished in the NMR tube during the course of the experiment. Carbonmonoxygenated (or deoxygenated) cell suspensions were prepared by exposure of the RBCs samples to CO

(or N_2) for 10 (or 30) min in septum sealed NMR tubes.

III.3.5 Preparation of Unsealed RBC Membranes

The unsealed RBC membranes were prepared by washing packed RBCs at least three times by centrifugation at 2000 g for 4 min, with 5PBS at 4°C. The plasma and buffy coat were removed by aspiration. Cell lysis was accomplished in a hypotonic buffer as previously described (91). Briefly, one volume of washed RBCs was diluted four fold with 5 mM sodium phosphate buffer, pH 8 (5P8 buffer). The RBC unsealed membranes were isolated by lysing and washing RBCs several times (at least five times) in 5P8 buffer by centrifugation at 38,720g for 8 minutes at 4°C on either a Sorvall RC-5B or a Beckman J2-21 high speed centrifuge. To the white membrane fragments 10 mM CsCl was added. For Cs^+-membrane fragments containing DPG, 5.4 mM DPG was added. The membrane fragments were then suspended in the desired media prior to analysis.

III.3.6 Preparation of Lysates

CORBC lysates were prepared by first bubbling intact RBCs with carbonmonoxide as described in section III.3.4 and then repeated rapid freezing in an ethanol dry ice mixture and then thawing in a water bath at 37 °C (92). Once the cells were lysed the desired concentration of CsCl was added, yielding Cs^+ CORBC lysates.

III.3.7 Preparation of Hemoglobin

Deoxygenated hemoglobin (deoxyHb) stripped of DPG was isolated from packed RBCs which were lysed in two volumes of cold distilled water. Purification of Hb

was accomplished by passing the dialyzed hemolysate down a Sephadex A-50 column suspended in 0.05 M Trizma base, 1.0 mM KCN, adjusted to pH 8.5 with concentrated HCl (85). Elution of various hemoglobin fractions were obtained using a pH gradient. Fractions containing hemoglobin were bubbled with nitrogen for 30 min prior to analysis by UV/VIS at 550 and 430 nm to determine the concentration of deoxyHb (85). Samples containing deoxyHb were placed in septum sealed NMR tubes that were previously purged with nitrogen to remove any oxygen. Carbonmonoxygenated (or deoxygenated) cell suspensions were prepared by exposure of the RBCs samples to CO (or N_2) for 10 (or 30) min in septum sealed NMR tubes.

III.3.8 Preparation of Vesicles

Phosphatidylcholine large unilamellar vesicles (LUVs) were prepared by a detergent dialytic removal procedure (93). To briefly describe this method, 100 μl of the 10 mg/mL PC stock solution in $CHCl_3/CH_3CH_2OH$ was purged with N_2 gas to evaporate off the solvent. To an aqueous solution of 100 mM NaCl, n-octylglucopyranoside detergent was added while vortexing. The detergent solution was then added to the lipid pellet. The sample was then transferred into dialyzing tubing. Detergent removal was accomplished by dialyzing the sample twice against 2 L of 100 mM NaCl, which was previously purged with N_2 gas for 12 h. At the time of analysis the samples were taken out of the dialysis tubing and transferred into septum sealed NMR tubes which were previously purged with N_2 gas. The resulting vesicles are LUVs with an average diameter of 450 nm (93).

III.3.9 Preparation of Frog Muscle Tissue

The frog sartorius muscle was excised after decapitation. Once removed the muscle samples were stored in a buffer containing 10 mM sucrose and 10 mM HEPES at pH 7.5 until needed. They were then transferred to a modified Ringer solution, which contained 10 mM glucose, 10 mM HEPES, 119 mM Na^+, 3.5 mM K^+, 122.5 mM Cl^-, and the desired SR, as previously described (94). Osmolarity was adjusted to 300 mOsm with K_2SO_4.

III.3.10 Preparation of Ionophore Solutions

After solvent purification, 5 mM KCl and 5 mM $KClO_4$ stock solutions were prepared. Once the desired salt was dissolved in the solvent of choice, an aliquot of the stock solution was then added dropwise to the ionophore in powder form, vigorous stirring required. The final ionophore concentration was 5 mM. To prevent distortion in the shape of the NMR spectrum, it was necessary to ensure that complete solubility of the alkali salts and the ionophores was achieved.

III.4 Data Analysis

III.4.1 Membrane Potential in Human RBCs

The membrane potential in RBCs as measured by ^{19}F NMR spectroscopy was determined from the following equation:

$$E_m = RT/F*ln[(A_{TFAin}/A_{TFAout})*(A_{TFMout}/A_{TFMin})]$$

where R is the gas constant, T is the absolute temperature, F is Faraday's constant, and

values of TFA and TFM are obtained from the peak areas of the ^{19}F NMR resonance (95).

The membrane potential in RBCs as measured by ^{31}P NMR spectroscopy was determined from the following equations:

$$E_m = (RT/F)*\ln r(H_2PO_2^-) \qquad r(H_2PO_2^-) = (A_{in}/A_{out})(1 - Ht)/\alpha Ht$$

where the gravimetrically determined fractional water volume is defined as α. A_{in} and A_{out} correspond to the peak areas of intra- and extracellular HP, Ht is the hematocrit, and all other constants are as described above (96a).

III.4.2 Cs$^+$ Concentration by ^{133}Cs NMR Spectroscopy

The concentrations of intra- and extracellular Cs$^+$ were determined from the following equations (76):

$$[Cs]_{in} = \{A_{in}*[Cs]_o\}/\{A_o*Ht\}$$

$$[Cs]_{out} = \{A_{out}*[Cs]_o\}/\{A_o*(1 - Ht)\}$$

where A_{in} and A_{out} are the peak areas for intra- and extracellular Cs$^+$ resonances, respectively, Ht is the hematocrit, $[Cs]_o$ is the concentration of the standard Cs$^+$ solution, and A_o is the peak area of the signal from the standard Cs$^+$ solution.

III.4.3 Cs$^+$ Binding Constant to DPG

A plot of $\delta_{obs}/[Cs^+]$ vs δ_{obs}, at pH 7.4, gave a linear graph ($r^2 = 0.90$) and the association constant for Cs$^+$-DPG was calculated from the slope.

CHAPTER IV

RESULTS

The study of anion transport and distribution in human erythrocytes by non-invasive and non-destructive NMR spectroscopy has not been fully explored. In this study we have tried direct and indirect NMR methods to study chloride transport and distribution in RBCs suspensions.

Initial studies on ^{35}Cl NMR in vivo have been limited by difficulties with resolution and visibility. Previous attempts were made to separate the intra- and extracellular ^{35}Cl resonances using paramagnetic SRs in a non-systematic manner. In certain studies, the physiology of the system was significantly affected due to the free paramagnetic ion binding to the membrane. Addition of paramagnetic metal salts resulted in broadening and shifting of extracellular ^{35}Cl$^-$ resonance. However, the intracellular ^{35}Cl$^-$ resonance in human RBCS was shown to be too broad (>200 Hz) to be detected (1). Also, it is well known that Cl$^-$ exchange is too fast in several biological systems. In our study we conducted experiments in a systematic manner to study Cl$^-$ in human RBCs.

In this section, we present the results on (a) ^{35}Cl NMR studies on the effect of various ionophores on chloride and perchlorate ion pairing (b) attempts to resolve intra- and extracellular ^{35}Cl NMR resonances in red cells and model systems using paramagnetic shift reagents and, (c) indirect ^{19}F and ^{31}P NMR methods using chemical probes to measure chloride

distribution in RBCs and study the effect of various ionophores on chloride distribution in RBC suspensions.

IV.1 Characterization of Chloride and Perchlorate Ion Pairing

IV.1.1 Effect of Various Ionophores on Chloride Ion Pairing in Methanol

^{35}Cl NMR spectroscopy was used to measure the Cl$^-$ line widths for methanol solutions in the presence and absence of K$^+$ complexes of the two subclasses of ionophores. The data shown in Table II indicate a greater change in ^{35}Cl NMR line width for samples containing the neutral ionophore, Val. Figure VI shows typical ^{35}Cl NMR spectra of KCl in the presence of two different types of ionophore. A two fold increase in the ^{35}Cl NMR line width was observed for Val with respect to all the carboxylic ionophores. In order to compare the results from one solvent to the next, the line widths were corrected by dividing them by the solvent viscosity. The trend in Table II for $\Delta\nu_{1/2}/\eta$ continues to indicate a higher degree of ion pairing for Val compared to carboxylic ionophores (Nig, Mon, and Las).

IV.1.2 Effect of Solvent on Chloride and Perchlorate Ion Pairing

Table III lists the donor numbers and dielectric constants for several solvents. Solvents with high dielectric constants and/or donor numbers are expected to inhibit ion pairing due to the difficulty in removing the solvent molecules from K$^+$ or ionophores and replacing them by Cl$^-$. Tables IV-VIII list the changes in ^{35}Cl NMR line width in methanol, 85% acetone-15% D$_2$O, acetonitrile, and DMSO. These solvents were chosen based on their range in dielectric constants and donor numbers. Not all of the ionophores were soluble in each of the above solvents as indicated in each table. Overall, the ClO$_4^-$ salts were more

Table II. ^{35}Cl line widths for 5 mM KCl with ionophores in methanol[a].

Ionophore (5 mM)	n	$\Delta\nu_{\frac{1}{2}}$/Hz	$\Delta\nu_{\frac{1}{2}}/\eta$, Hz/cP
Nigericin	3	60.91 ± 9.47	110.74
Monensin	3	53.52 ± 3.96	100.98
Lasalocid	3	61.09 ± 3.71	103.54
Valinomycin	3	122.2 ± 3.39	200.32
Nonactin	not soluble		
KCl (alone)	3	30.5 ± 1.61	55.45

[a]Line broadening used in the Fourier transformation of 25 Hz was subtracted out. There was no change in chemical shift from sample to sample.

Figure VI. ^{35}Cl NMR Spectra of 5 mM KCl in methanol in the presence of (a) 5 mM Mon and (b) 5 mM Val.

A

B

20   10   0   -10   -20 PPM   -30
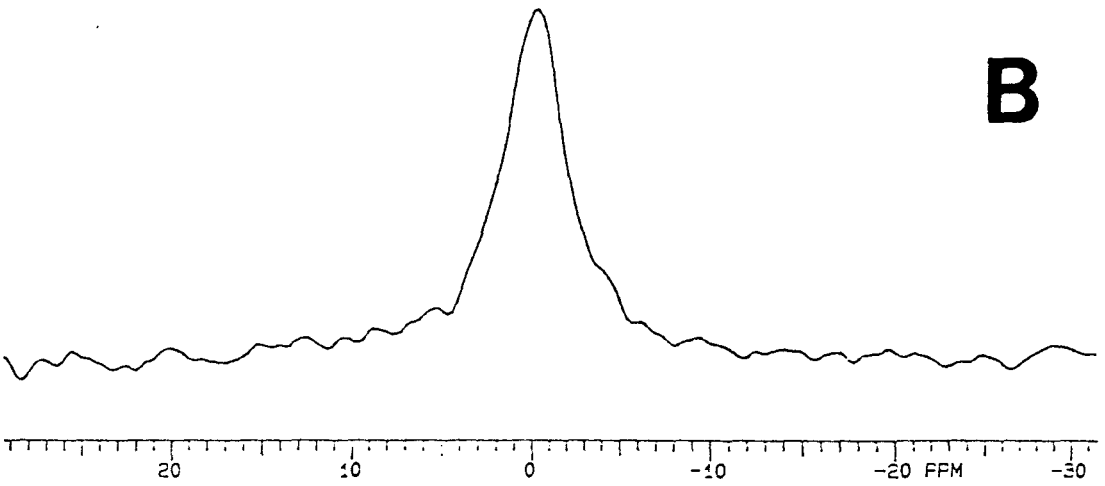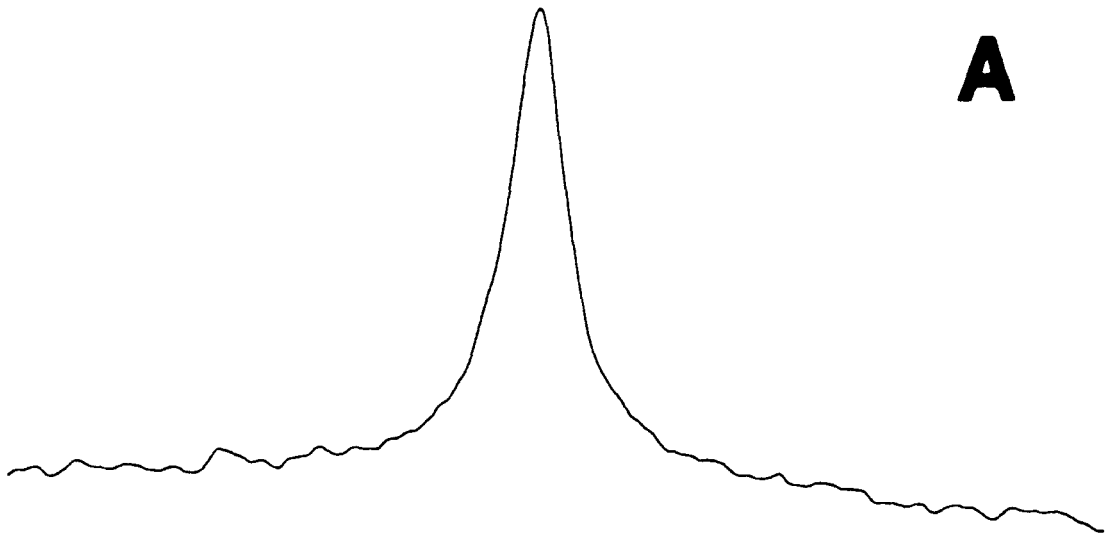
Table III. Solvent dielectric constants and donor numbers (35).

Solvent	Dielectric Constant	Donor Number
water	78.5	33.0
Dimethyl Sulfoxide	46.7	29.8
Acetonitrile	37.5	14.1
N,N-Dimethylformamide	36.7	26.6
Nitromethane	35.9	2.7
Methanol	32.7	25.7
Acetone	20.7	17.0
Pyridine	12.4	33.1
Tetrahydrofuran	7.6	20.0
Chloroform	4.8	4.0

Table IV. ^{35}Cl line widths for 5 mM KClO$_4$ with ionophores in methanol.[a]

Ionophore (5 mM)	n	$\Delta\nu_{1/2}$/Hz	$\Delta\nu_{1/2}/\eta$,Hz/cP
Nigericin	3	9.11 $\pm$ 4.76	14.23
Monensin	3	11.18 $\pm$ 2.16	19.61
Lasalocid	3	12.25 $\pm$ 0.76	23.56
Valinomycin	3	15.56 $\pm$ 1.06	28.29
Nonactin	not soluble		
KClO$_4$ (alone)	3	12.95 $\pm$ 0.22	22.72

[a] Line broadening used in the Fourier transformation of 5 Hz was subtracted out. There was no significant change in chemical shift from sample to sample.

Table V. ^{35}Cl line widths for 5 mM KCl with the ionophores in 85% acetone-15% D$_2$O. Referenced to Saturated KCl in D$_2$O.[a]

Ionophore (5 mM)	n	$\Delta\nu_{1/2}$/Hz	$\Delta\nu_{1/2}/\eta$,Hz/cP
Nigericin	3	73 $\pm$ 8.31	67.59
Monensin	not soluble		
Lasalocid	3	64 $\pm$ 2	50.39
Valinomycin	3	77.49 $\pm$ 7.99	78.27
Nonactin	3	80.40 $\pm$ 9.91	63.81
KCl (alone)	1	73.94	62.56

[a]Line broadening used in the Fourier transformation of 25 Hz was subtracted out. There was no significant change in chemical shift from sample to sample.

Table VI. ^{35}Cl line widths for 5 mM $KClO_4$ with ionophores in acetonitrile. Referenced to $KClO_4$-D_2O.[a]

Ionophore (5 mM)	n	$\Delta\nu_{1/2}$/Hz	$\Delta\nu_{1/2}/\eta$,Hz/cP
Nigericin	3	2.91 ± 1.22	8.10
Monensin	not soluble		
Lasalocid	3	2.48 ± 0.92	6.53
Valinomycin	3	5.04 ± 2.47	13.26
Nonactin	not soluble		
$KClO_4$ (alone)	3	3.50 ± 0.45	12.96

[a]Line broadening used in Fourier transformation of 5 Hz was subtracted out. There was no significant change in chemical shift from sample to sample.

Table VII. ^{35}Cl line widths for 5 mM KClO$_4$ with the ionophores in DMSO. Referenced to KClO$_4$-D$_2$O.[a]

Ionophore	n	$\Delta\nu_{1/2}$/Hz	$\Delta\nu_{1/2}/\eta$,Hz/cP
Nigericin	not soluble		
Monensin	not soluble		
Lasalocid	3	1.57 ± 0.83	0.77
Valinomycin	3	3.59 ± 1.25	2.87
Nonactin	3	7.43 ± 1.74	3.57
KClO$_4$ (alone)	3	6.23 ± 2.19	2.84

[a]Line broadening of 5 Hz used in Fourier transformation was subtracted out. There was no significant change in chemical shift form sample to sample.

soluble than the Cl^- salts. As shown in Tables II and IV-VIII, each of the line width readings are corrected for viscosity. After viscosity correction, the ^{35}Cl NMR line widths for ClO_4^- in the presence of Val are 16 - 50% larger than for Las, Nig, or Mon in methanol. The line broadening induced by Val in methanol was larger for Cl^- than for ClO_4^-. As shown in Table V, Cl^- in the presence of Val exhibits a slightly larger line width than in the presence of the other ionophores in 85% acetone-15% D_2O. Table VI lists the ^{35}Cl NMR line widths for ClO_4^- in acetonitrile. Val was the only neutral ionophore soluble in acetonitrile. A larger line width reading was also observed for Val in acetonitrile compared to the carboxylic ionophores. Table VII lists the line widths for ClO_4^- in DMSO. Both Val and Non have larger line widths than Las.

Figures VII and VIII show the effect of donor number on the ^{35}Cl NMR line widths for Cl^- and ClO_4^-, respectively, for each of the ionophores. As the donor number of a solvent increases the solvated ions more strongly feel the effect of the solvent and ion pairing is expected to be minimized. Val was the only ionophore to yield an increase in KCl line width with an increase in donor number (Figure VII). Val induces the largest ^{35}Cl line width for ClO_4^- over a range of donor numbers (Figure VIII). Figures IX and X show the effect of dielectric constant on the ^{35}Cl NMR line width for KCl and $KClO_4$, respectively, for each of the ionophores. Similar trends as shown in Figures VII and VIII are observed. Val and Non have the largest effect on KCl and $KClO_4$ line widths over a range of dielectric constants. Several other solvents were tried, such as pyridine, chloroform, and THF. The insolublity of the K^+-ionophore somplexes prevent ion pairing studies in these solvents.

55

Figure VII. ^{35}Cl NMR KCl Line Widths versus Donor Numbers for Different Ionophores with KCl in methanol (DN = 25.7) and acetone-D$_2$O (DN = 19.4). The plotted line widths are not viscosity corrected.

Donor Number vs Linewidth
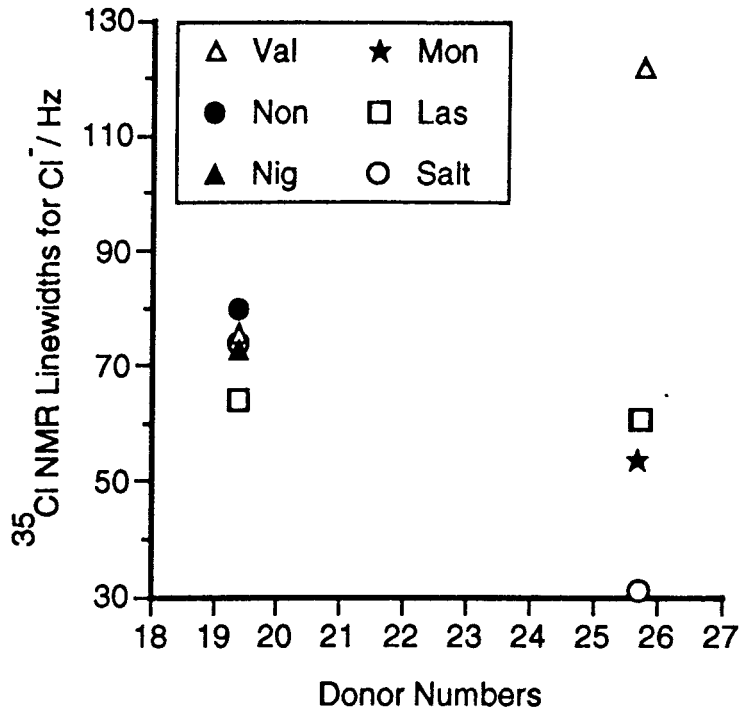
Figure VIII. ^{35}Cl NMR KClO$_4$ Line Widths versus Donor Numbers for Different Ionophores with KClO$_4$ in acetonitrile (DN = 14.1), methanol (DN = 25.7), and DMSO (DN = 29.8). The plotted line widths are not viscosity corrected.

Donor Number vs Linewidth
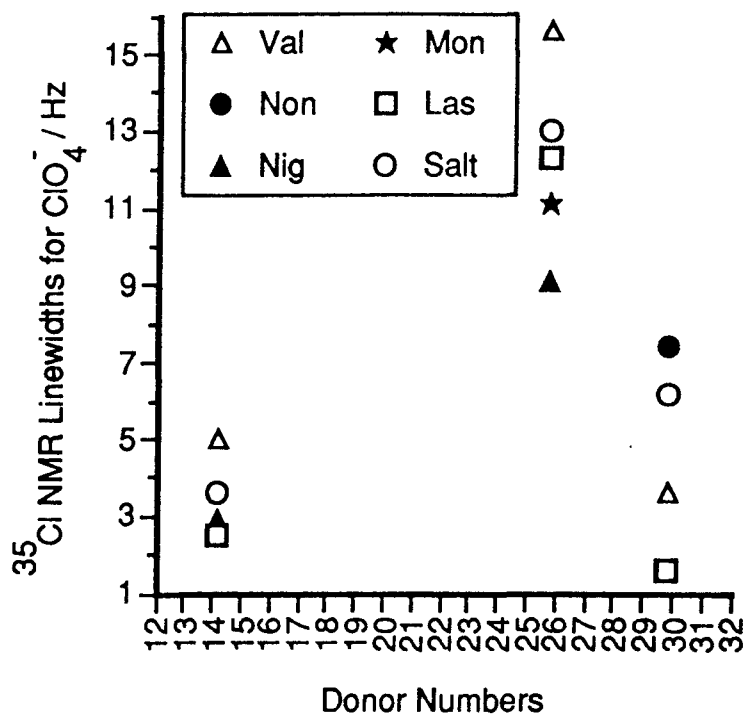
Figure IX. [35]Cl NMR KCl Line widths versus Dielectric Constants for Different Ionophores with KCl in methanol (DE = 32.7) and acetone-D$_2$O (DE = 29.4). The plotted line widths are not viscosity corrected.

Dielectric Constant vs Linewidth
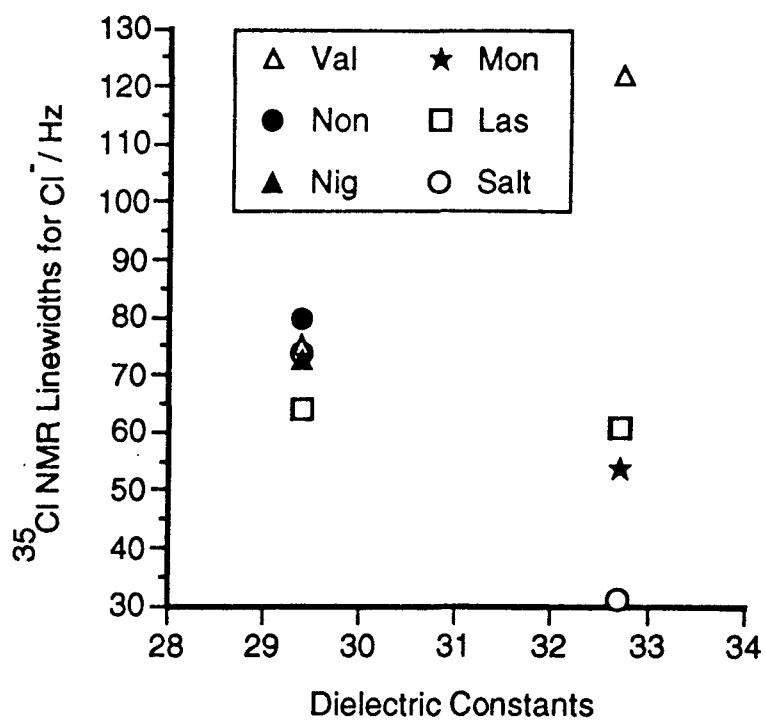
Figure X. ^{35}Cl NMR KClO$_4$ Line Widths versus Dielectric Constants for Different Ionophores with KClO$_4$ in acetonitrile (DE = 37.5), methanol (DE = 32.7), and DMSO (DE = 46.7). The plotted line widths are not viscosity corrected.

Dielectric Constant vs Linewidth
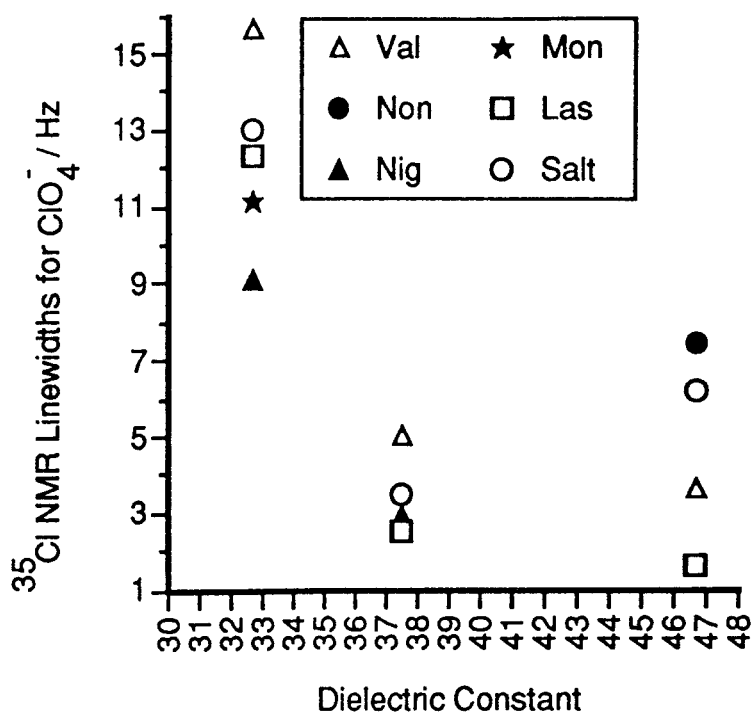
IV.1.3 Perchlorate Ion Pairing: FT-IR Results

For a given ionophore and solvent, the ^{35}Cl NMR line widths for Cl^- are broader than for ClO_4^- (Figures VII and VIII). FT-IR data were recorded for the ionophore samples containing perchlorate. The wavelength region from 1600-600 cm^{-1} was scanned. The wave length at 1130 cm^{-1} corresponds to the stretching frequency band ν_3. Coordination of $KClO_4$ splits this band into two new bands at 1150 and 1120 cm^{-1} (35). The symmetry changes from tetrahedral to C_{3v} or C_{2v} depending on whether perchlorate binds in a monodentate or bidentate fashion. Figures XI-XIII show the FT-IR spectra of (a) methanol, (b) $KClO_4$ in methanol, (c) 5 mM Val in methanol, (d) 5 mM Las in methanol, (e) 5 mM $KClO_4$ with 5 mM Val in methanol, and (f) 5 mM $KClO_4$ with 5 mM Las in methanol. All spectra were recorded in the absorbance mode. Figure XIV was obtained by a series of spectral additions and subtractions as follows, a + e - b - c for Val and a + f - b - d for Las. Using this series of spectral manipulations, only the absorbance due to a change in symmetry of the perchlorate remains. In Figure XIVg, the singlet at 1130 cm^{-1} has split into two bands as a result of the change in symmetry due to the coordination of the ClO_4^-. In Figure XIVh, a singlet remains indicating that the symmetry of the ClO_4^- has not changed.

IV.I.4 Effect of Cation on Ion Pairing

Table VIII lists the $^7Li^+$, $^{23}Na^+$, and $^{133}Cs^+$ chemical shifts and line widths for solutions containing LiCl, NaCl, or CsCl in the presence and absence of Val or Las. The corresponding ^{35}Cl NMR spectrum was also recorded for each (Table VIII). The largest effect was observed for samples containing CsCl with over a six fold increase in $^{133}Cs^+$ NMR line width for samples containing Val in place of Las. Of the LiCl samples those containing Val

Figure XI. FT-IR Spectra of (a) Methanol and (b) 5 mM KClO$_4$ in methanol.
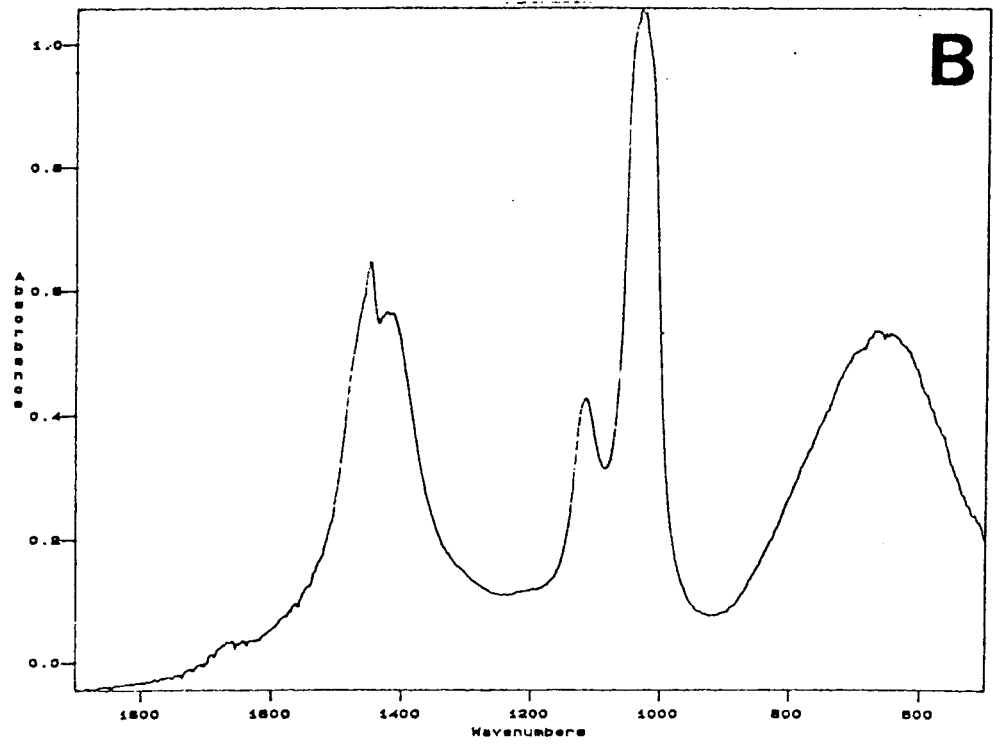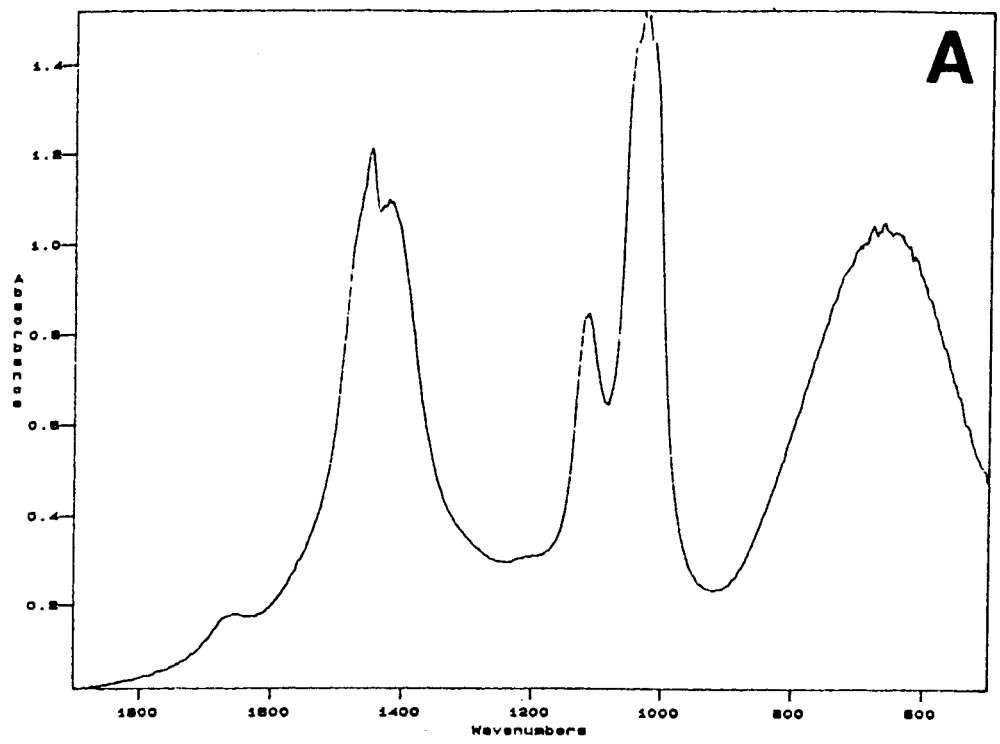
<u>Figure XII.</u> FT-IR Spectra of (c) 5 mM Val and (d) 5 mM Las in methanol.
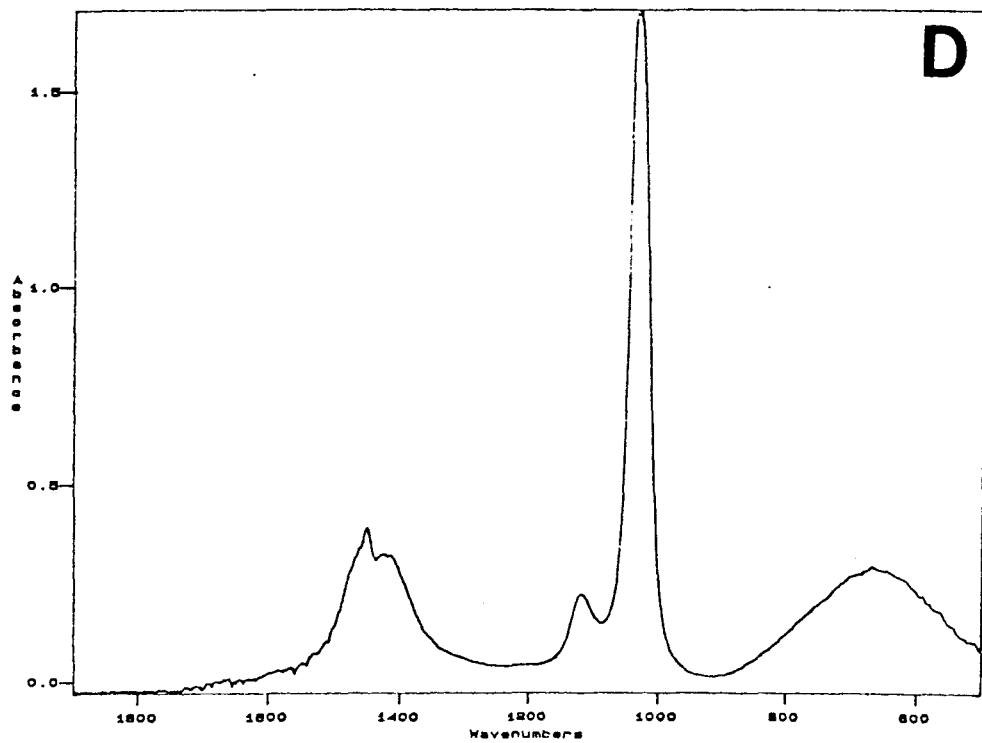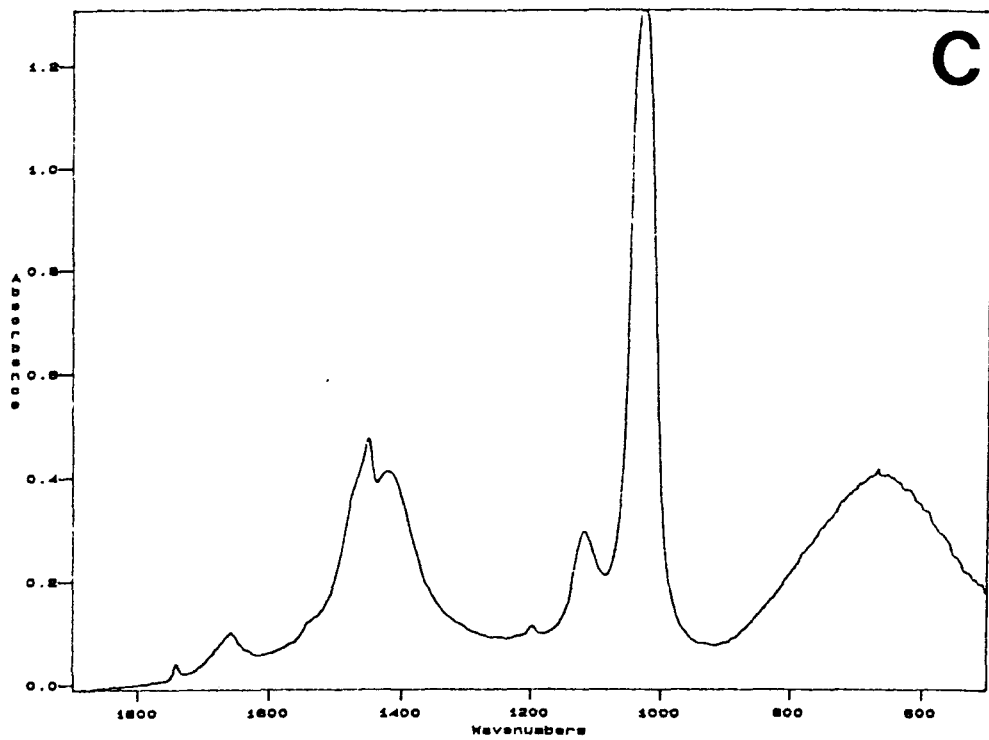
Figure XIII. FT-IR Spectra of 5 mM KClO$_4$ with (e) 5 mM Val and (f) 5 mM Las in methanol.
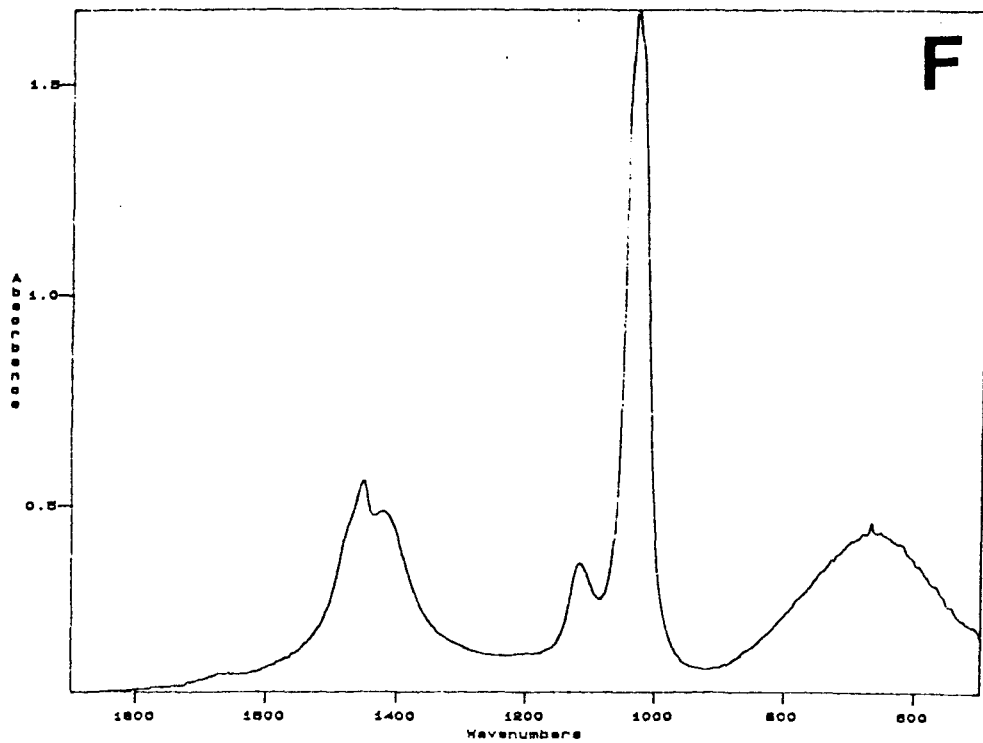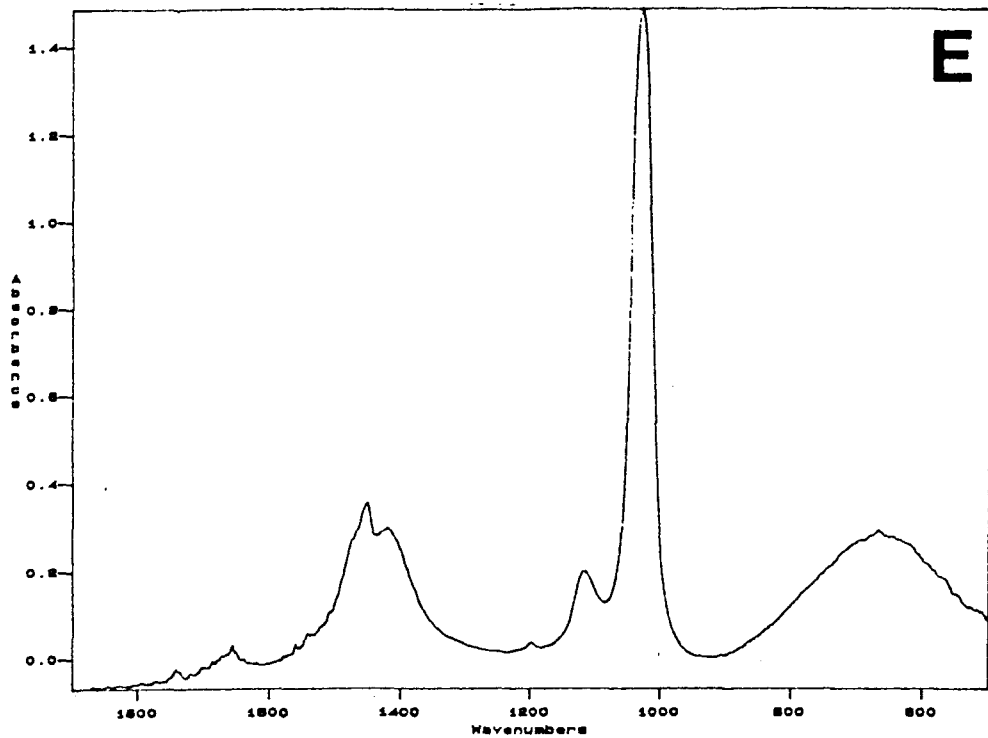
Figure XIV. FT-IR Resulting Spectra after addition and subtraction (g) Val and (h) Las.
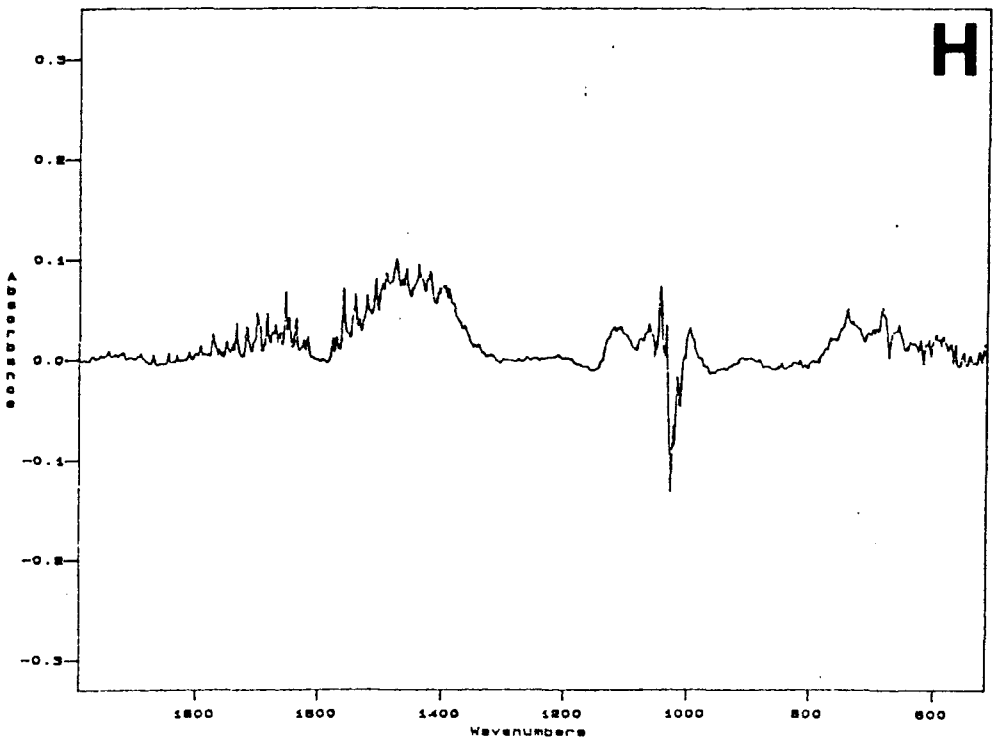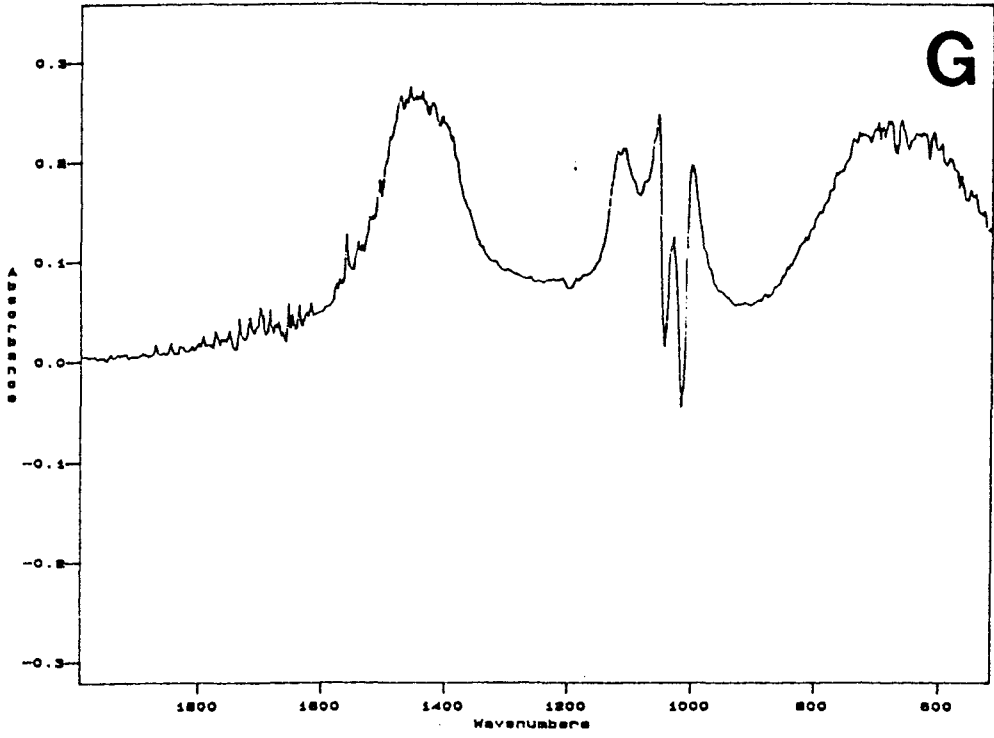
Table VIII. Effect of Alkali Metal Cations on Ion Pairing Ability of Ionophores in Methanol.

Sample[a]	Metal NMR Line Width/Hz	Chemical Shift[b]/ppm	^{35}Cl NMR Line Width[b]/Hz
CsCl	6.3	-42.0	97
CsCl + val	63.2	-12.4	117
CsCl + las	9.5	-14.7	97
NaCl	20.5	-2.6	91
NaCl + val	81.5	-2.9	114
NaCl + las	104	-3.2	94
LiCl	24.7	1.70	97
LiCl + val	53	1.72	98
LiCl + las	36	1.85	101

[a]Samples were prepared by dissolving each salt in methanol to a final concentration of 5 mM. Ionophores were added to the salt solutions to yield a final concentration of 5 mM. [b]Samples containing CsCl were referenced to 0.15 M CsCl-D_2O, those containing NaCl were referenced to 0.10 M NaCl-D_2O, and those containing LiCl were referenced to 0.15 M LiCl-D_2O. The ^{133}Cs$^+$, ^{23}Na$^+$, and ^{7}Li$^+$ NMR spectra were recorded twice and the average is reported. Errors in chemical shifts are less than 1.0 ppm and less than 1.0 Hz for line width measurements. All ^{35}Cl NMR spectra were recorded with an n = 1.

had $^7Li^+$ NMR line widths approximately 25% larger than those samples containing Las. For the NaCl samples however, Las was found to have a $^{23}Na^+$ NMR line width larger than Val. The ^{35}Cl NMR line widths for NaCl and CsCl were found to be larger for samples containing Val as opposed to Las. The extremely low selectivity for Li^+ by both Val and Las (Table I) is evident from the ^{35}Cl NMR line widths for LiCl in the presence of either Val or Las. The LiCl ^{35}Cl NMR line widths for Las and Val are approximately the same.

IV.I.5 Effect of pH on Ion Pairing

The effect of pH on the ^{35}Cl NMR line widths for samples containing Val or Mon in methanol was investigated. By lowering the pH, the carboxylic group of Mon was protonated. The ^{35}Cl NMR line width for Mon changed from 53.5 Hz (pH = 7.5) to 101 Hz (pH = 2.90). The ^{35}Cl NMR line width for Val changed from 122 Hz (pH = 7.6) to 111 Hz (pH = 2.91). In the case of Mon, the lowering of pH resulted in protonation and thereby formation of a neutral ionophore. Complexation with K^+ resulted in an ionophore-cation complex with an overall charge of +1. This in turn enhances the ability of the Mon-K^+ complex to ion pair with Cl^-. The reported values represent an average of two measurements.

IV.2 Cl^- Distribution in Biological Systems

IV.2.1 Shift Reagent Method

2.1.1 Lanthanide Shift Reagents

The efficacy of the dysprosium (III) complexes of ligands shown in Figure XV as shift reagents for $^{35}Cl^-$ NMR resonances was tested. In these experiments, the shift reagent concentration varied from 3 to 100 mM and the Cl^- concentration was 5 mM. The pH was held constant at 7.5. The $^{35}Cl^-$ shifts are plotted against the stoichiometric mole ratio of shift

Figure XV. Ligand Structures of Shift Reagents Used in this Study
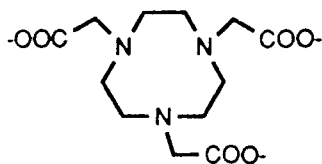
NOTA-1,4,7 Triazacyclononane-N, N^1, N^{11}-Triacetate
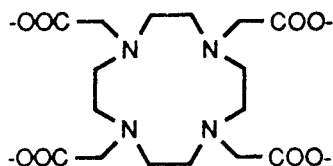
DOTA-1,4,7,10 Tetraazacyclododecane-N,N^1,N^{11}-Tetraacetate
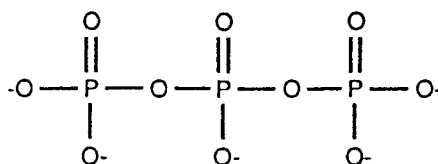
PPP-Tripolyphosphate
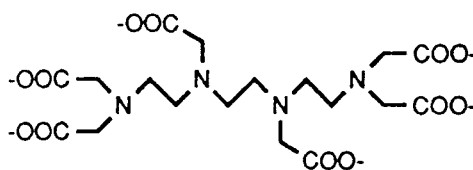
TTHA-Triethylenetetraaminehexaacetate
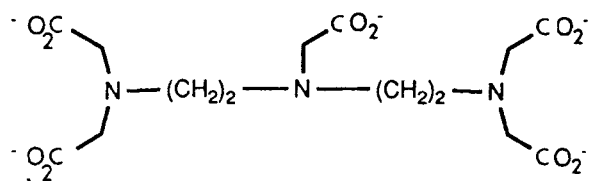
DTPA-Diethylenetriaminepentaacetate
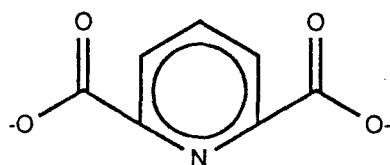
DPA-Dipicolinate

reagent to Cl⁻, ρ, in Figure XVI for Dy(PPP)$_2$$^{7-}$, Dy(TTHA)$^{3-}$, and Dy(NOTA). All shift

reagent induced downfield shifts from the NaCl reference. In the cases of Dy(PPP)$_2$$^{7-}$ and

Dy(TTHA)$^{3-}$, the ^{35}Cl⁻ shifts induced decrease as ρ increases, suggesting an increase in

electrostatic repulsion between the negative charge on the complex and the Cl⁻ ion. For

Dy(NOTA), the ^{35}Cl NMR chemical shift continues to increase with an increase in rho as a

result of the neutral charge of this SR and the lack of electrostatic repulsion with the Cl⁻. The

^{35}Cl⁻ shifts for Dy(DPA), Dy(DTPA)$^{2-}$, and Dy(DOTA)⁻ at a ρ = 0.5 were 3.5, 3.8, and

3.7 ppm. These shifts were not very different from those observed with Dy(NOTA) or

Dy(PPP)$_2$$^{7-}$. The ^{35}Cl shifts induced by other lanthanide complexes of TTHA were also

investigated and are shown in Table IX. Of the TTHA complexes, Dy(III) and Tb(III)

complexes of TTHA induced the largest ^{35}Cl⁻ shifts. The larger $\Delta\nu_{\frac{1}{2}}$ of the Tb(III) hinders

its use as a SR. The observed ^{35}Cl⁻ shift data for all the Ln(TTHA)$^{3-}$ were analyzed for

contact and pseudo contact contributions. The observed chemical shift can be analyzed by the

following equation for contact and pseudo contact contributions:

$$\delta = F(S_z) + G(C^D)$$

where F and G are ligand dependent parameters and S_z and C^D are lanthanide dependent

parameters (61). Table X shows the data in terms of the above parameters. The data shown

in Table X were plotted by two different methods (a) δ/C^D vs S_z/C^D and (b) δ/S_z vs C^D/S_z.

The absence of linearity in the plots (data not shown) failed to generate contact and pseudo

contact contributions.

Figure XVI. Rho Plots for Dy(TTHA)$^{3-}$, Dy(PPP)$_2$$^{7-}$, and Dy(NOTA)
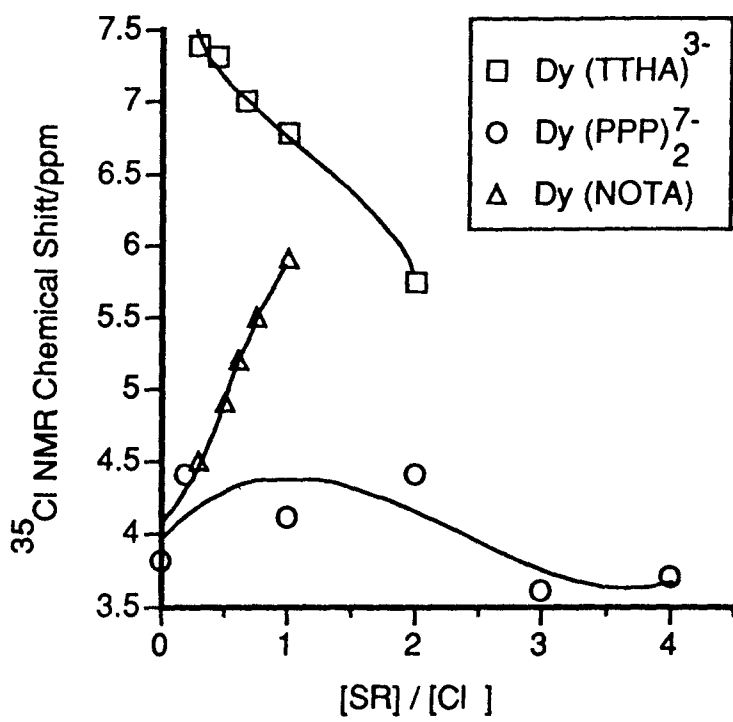
Table IX. ^{35}Cl NMR Chemical Shifts of Lanthanide TTHA Complexes. The SR concentration was 0.1 M and the Cl concentration was 0.5 M. Chemical shift was measured relative to 2.5 M NaCl-D_2O. The reported NMR parameters represent the average of measurments conducted on two separately perpared samples.

Lanthanide	Chemical Shift/ppm	Line Width/Hz
Lanthanum	0.7	67.2
Praseodymium	3.5	64.1
Neodymium	4.4	69.3
Samarium	3.2	68.2
Europium	4.0	62.3
Gadolinium	10.8	81.8
Terbium	21.4	94.7
Dysprosium	19.2	77.1
Holmium	16.9	69.7
Erbium	17.2	56.8
Thulium	7.5	46.8
Ytterbium	5.0	55.9
Lutetium	4.3	39.1

Table X. Pseudo Contact and Contact Contributions of Lanthanide TTHA Complexes, as Measured by ^{35}Cl Chemical Shifts.

TTHA Complexes of Lanthanides	δ^a	C^{Db}	S_z^b
La	0.000	-	-
Pr	1.999	-10.99	2.97
Nd	2.379	-4.15	4.49
Sm	0.175	-0.70	-0.063
Eu	1.774	4.05	-10.68
Gd	8.140	0	-31.50
Tb	24.721	-85.26	-31.50
Dy	16.086	-100	-28.55
Ho	16.121	-39.39	-22.63
Er	13.593	-32.41	-15.37
Tm	5.823	52.41 .	-8.21
Yb	3.124	21.54	-2.59

^{a}Shifts reported are corrected for diamagnetic contribution by subtracting the contribution of La from the reported chemical shifts. ^{b}Taken from reference 61.

2.1.2 Transition Metal Shift Reagents

Several transition metal complexes were also tested as possible Cl^- SRs. The $^{35}Cl^-$

shifts induced by Co(II) and Ni(II) solutions were measured. Figure XVII illustrates a plot

of $^{35}Cl^-$ shifts as a function of varying Co(II) or Ni(II) concentration. In general, the induced

shifts are larger as the concentration increases. The shifts induced by Co(II) are much larger

than those induced by Ni(II). It is evident from Figure XVII that Co(II) shift potency is 3-

5 times greater than that of Ni(II). The line widths at half height ($\Delta\nu_{\frac{1}{2}}$) are plotted as a

function of Co(II) and Ni(II) concentrations in Figure XVIII. $^{35}Cl^-$ resonances in the presence

of Ni(II) are much less broadened than in the presence of Co(II). However, based on shift

potencies and line width data it was decided to use Co(II) in the concentration range of 10-

20 mM for biological applications.

Table XI shows the data on $^{35}Cl^-$ chemical shifts and line widths obtained in the

presence of Co(acac)$_2$, vitamin B$_{12}$, and Cobinamide. The $^{35}Cl^-$ shifts induced by the above

complexes are much smaller than those obtained with free Co(II). Of the three complexes,

Co(acac)$_2$ at concentrations of 15-20 mM induces $^{35}Cl^-$ shifts which may be useful for

biological applications. The inorganic complexes of Co(II), CoEDTA, CoDTPA, and

CODPA, were also tested as possible $^{35}Cl^-$ SRs. Table XII shows the reagents tested and the

shifts obtained.

2.2 Application of SR Method to Detect Intra- and Extracellular Cl^- in Biological Systems

2.2.1 Vesicle Systems

Figure XIX depicts the discrimination of intra- and extracellular Cl^- in phospholipid

Figure XVII. ^{35}Cl NMR Chemical Shifts versus Concentration for Co(II) and Ni(II). The chloride form was used for each salt. The salt concentrations varied from 3 - 100 mM for each and [Cl$^-$] was 20 mM. The salts were prepared in 50 mM HEPES, pH 7.4. ^{35}Cl$^-$ NMR chemical shifts were referenced to 0.15 M NaCl in D$_2$O.
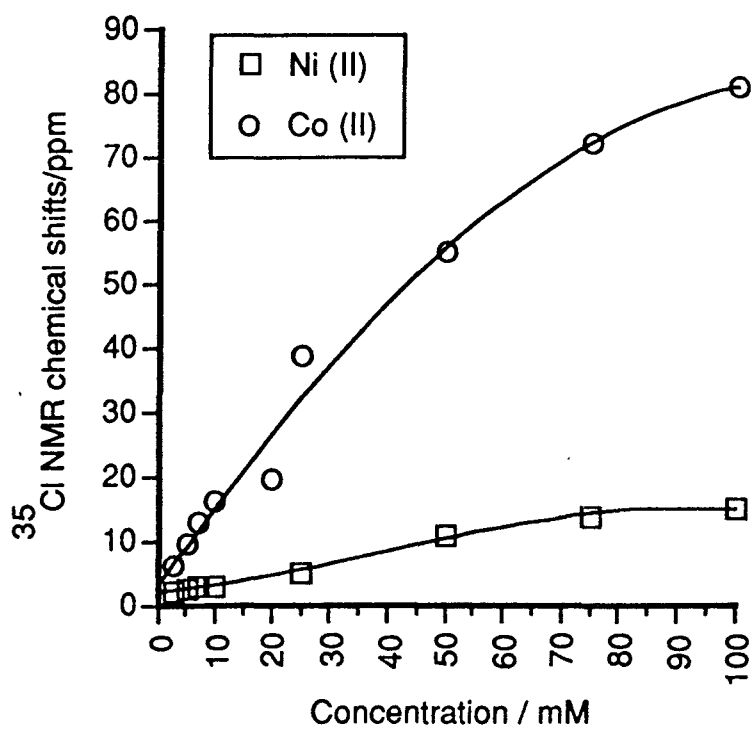
Figure XVIII. ^{35}Cl NMR Line Widths versus Concentration for Co(II) and Ni(II). Same experimental conditions as for Figure XVIII.
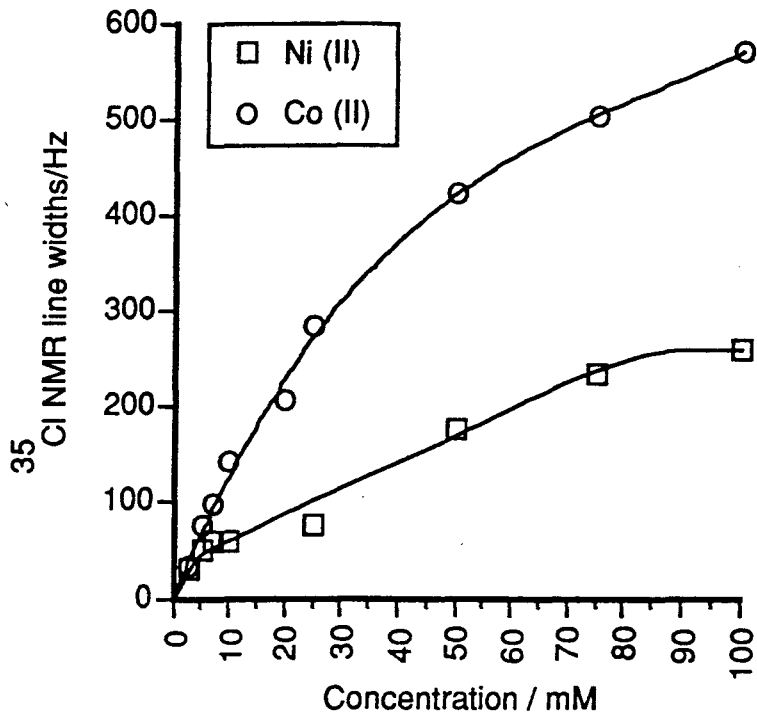
Table XI. ^{35}Cl Chemical Shifts and Line Widths in the Presence of Co(acac)$_2$, vitamin B$_{12}$, and Cobinamide.

Complexes	ρ^*	δ/ppm	$\Delta\nu_{1/2}$/Hz
10 mM CoCl$_2$	0.5	17.2	129
Co(acac)$_2$	0.05	0.81	36.87
	0.10	2.70	75.25
	0.15	4.83	102.60
	0.20	7.30	146.80
	0.25	8.90	171.40
vitamin B$_{12}$	0.30	4.10	16.00
	0.50	3.90	20.20
	0.60	5.00	28.00
	0.75	5.40	37.00
Cobinamide	0.30	3.10	21.00
	0.50	3.20	19.23
	0.60	3.50	25.04
	0.75	3.90	23.20
	1.00	4.00	32.42

* The chloride concentration was maintained at 100 mM for Co(acac)$_2$ and 20 mM for vitamin B$_{12}$ and cobinamide. The concentration of Co(acac)$_2$ ranged from 5-25 mM while the concentration of vitamin B$_{12}$ and cobinamide ranged from 6-20 mM.

Table XII. ^{35}Cl Chemical Shifts and Line Widths in the Presence of CoEDTA, CoDTPA, and CoDPA at Various Concentrations.

Complex	δ/ppm	$\Delta\nu_{1/2}$Hz
10 mM CoEDTA	2.44	38
10 mM CoDTPA	2.70	16
15 mM CoDTPA	5.13	19
20 mM CoDTPA	5.67	23
10 mM CoDPA	2.70	15
15 mM CoDPA	4.76	23
20 mM CoDPA	6.48	36

The reported data represents an average of two measurments. The Cl⁻ concentration was twice the SR concentration in each sample.

Figure XIX. ^{35}Cl NMR Spectra of (a) NaCl LUVs, (b) 20 mM CoCl$_2$, and (c) NaCl LUVs + 20 mM CoCl$_2$. The CoCl$_2$ suspension was prepared by adding 10 mM HEPES and glucose to adjust the final osmolarity to 200 mOsm.

C   NaCl LUVs +   0.15 M NaCl reference
    20 mM CoCl$_2$

B   20 mM CoCl$_2$ 0.15 M NaCl reference

A   NaCl LUVs   0.15 M NaCl reference

100   50   0   -50   -100 PPM
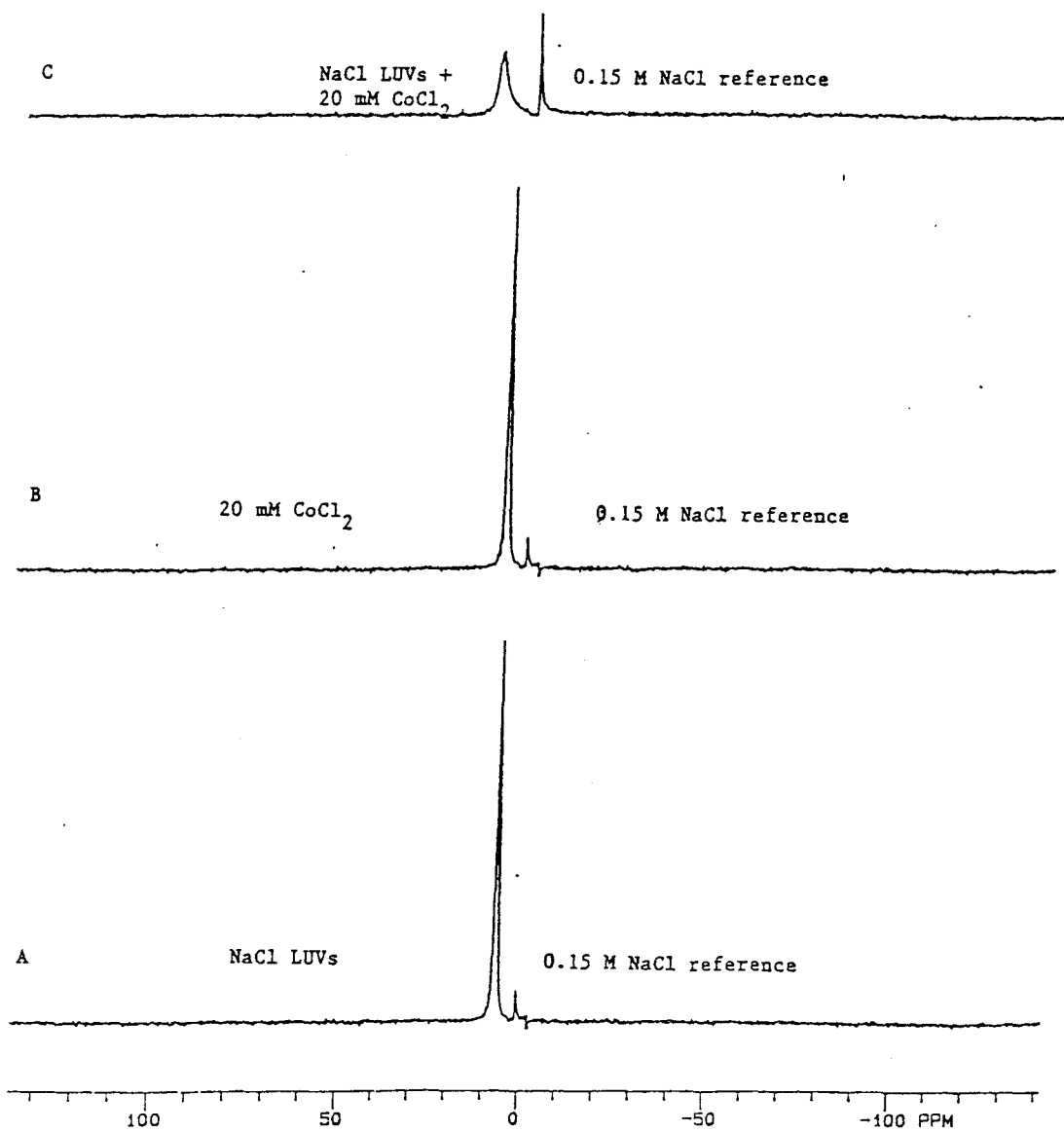
vesicles upon incorporation of 20 mM $CoCl_2$ in the suspension medium. The assignments of intra- and extracellular resonances were based on the sample replacement technique. This involved removing the vesicle sample from the NMR spectrometer, inserting the NaCl-D_2O reference, increasing the number of transients, and then resuming acquisition. The spectrum of the NaCl reference is added on top of the extracellular Cl^- resonance in the vesicle spectrum. The $CoCl_2$ peak shifts in the presence of the LUVs. It was also noticed that the vesicles themselves average a 4-5 ppm shift from the NaCl-D_2O reference.

As the Co(II) interacted with the membrane less Co(II) was available to shift the extracellular Cl^-. To further test this conclusion, LUVs were prepared in a 100 mM $NaNO_3$ dialyzing medium. If the $CoCl_2$ chemical shift decreased upon addition of the LUVs prepared in $NaNO_3$, then the decrease in shift could be attributed to a membrane interaction. This is because both NaCl and $NaNO_3$ LUVs have the same membrane composition. If on the other hand the decrease in chemical shift for the NaCl LUVs was due to saturation of the shift reagent caused by Cl^- leaking from the vesicle, the $NaNO_3$ LUVs should not have exhibited any decrease in chemical shift since these vesicles are Cl^- free.

It was found that the chemical shift decreased form 25.9 to 11.6 ppm in the presence of the $NaNO_3$ vesicles. This further supports the conclusion that Co^{2+} is interacting with the membrane. This interaction with the membrane renders the use of $CoCl_2$ an unacceptable SR. Although the $CoCl_2$ gave large enough shifts to discriminate the two Cl^- pools, its binding to the membrane renders it an undesirable choice. $Co(acac)_2$ was then tested as a possible [35]Cl NMR shift reagent.

From the rho plot, Table XI, 20 mM was chosen as the ideal concentration for $Co(acac)_2$ giving a shift of 7.3 ppm. The concentration of 25 mM gave a [35]Cl NMR shift of

8.9 ppm, but the line width was 171.4 Hz compared to 147 Hz for 20 mM Co(acac)$_2$. As the line width increases, the extracellular Cl$^-$ peak overlaps with the intracellular peak for shifts less than 10 ppm.

From Figure XX, the chemical shift of 20 mM Co(acac)$_2$ decreased from 37.9 to 27.1 ppm in the presence of the LUVs. The stability constant for Co(acac)$_2$ is 5.4 at 25 °C (97). A similar decrease was observed for Co(acac)$_2$ when added to vesicle prepared in NaNO$_3$. It was hoped that Co(II) would not interact with the membrane since it was complexed to the acetylacetonate ligand. The low stability constant of Co(acac)$_2$, however, allows for dissociation of the complex and binding of free Co^{2+} to the membrane.

Dy(NOTA) and Dy(TTHA)$^{3-}$ were also tested as ^{35}Cl$^-$ SRs to discriminate intra- and extracellular Cl$^-$ in vesicles. Dy(NOTA) at 19 mM exhibited a shoulder for the intracellular peak, whereas Dy(TTHA)$^{3-}$ did not show any signs of resolution for intra- and extracellular Cl$^-$ in vesicles. Thus, it was not possible using either Dy(NOTA) or Dy(TTHA)$^{3-}$ to clearly resolve intra- and extracellular Cl$^-$ resonances.

2.2.2   Frog Leg Muscle

Frog sartorius muscles were added to modified Ringer solutions containing 25 mM Dy(TTHA)$^{3-}$ and 122.5 mM Cl$^-$. Frog sartorius muscles exhibit high intracellular chloride concentrations. The ease of dissection and experimental procedures makes it a promising system for studying chloride distribution. In addition, sartorius muscle Cl$^-$ transport pathways are similar to those observed in human RBCs. However, reproducible separation of intra- and extracellular ^{35}Cl NMR resonances was not observed.

Figure XX. ^{35}Cl NMR Spectra of (a) NaCl LUVs, (b) 20 mM Co(acac)$_2$, and (c) NaCl LUVs + 20 mM Co(acac)$_2$.

C   NaCl LUVs + 20 mM Co(acac)$_2$

B   20 mM Co(acac)$_2$

A   NaCl LUVs

100   50   0   -50   -100 PPM
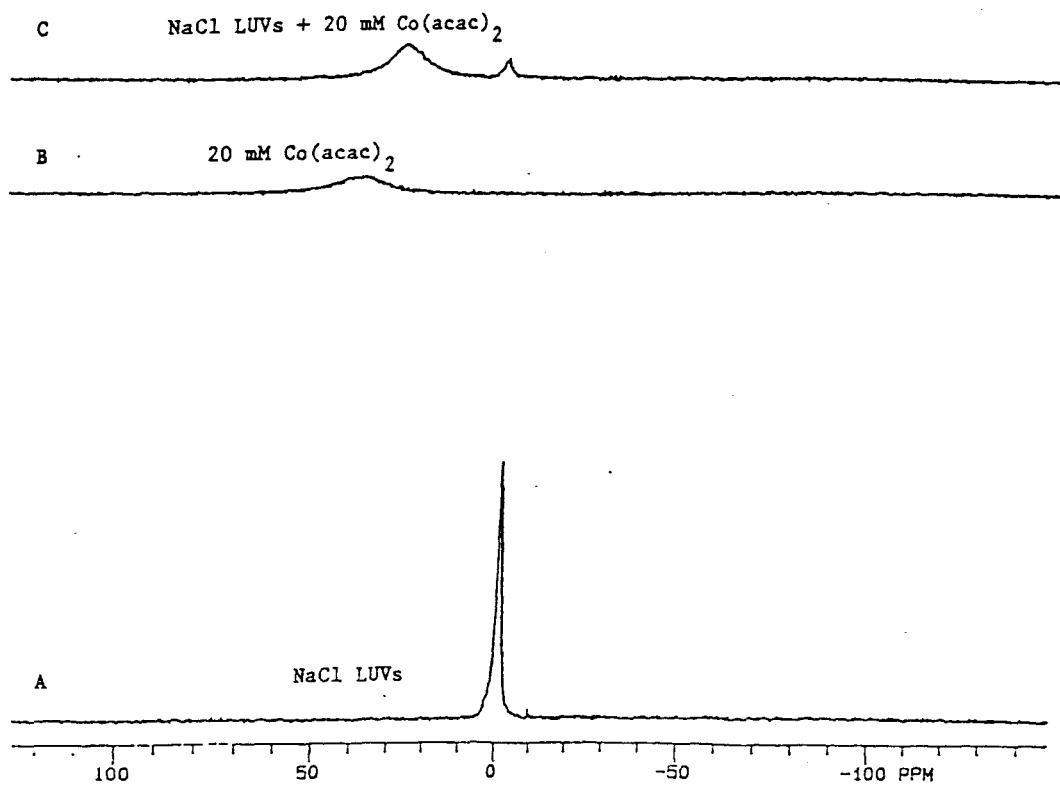
2.2.3 RBCs

After 3 washings in PBS buffer, intact RBCs were suspended directly into 20 mM CoCl$_2$. Discrimination between intra- and extracellular Cl$^-$ was not possible. Sykes *et al.* (1) had shown that intracellular Cl$^-$ in human RBCs is not visible by ^{35}Cl NMR spectroscopy due to the extreme broadening caused by the binding of Cl$^-$ to hemoglobin. Recently, Boulanger *et al.* (59) have reported observing 40% visibility of intracellular Cl$^-$ in dog erythrocytes. I was unable to observe intracellular Cl$^-$ in packed human RBCs. Recently, it was also reported that the enzyme superoxide dismutase in RBCs was responsible for broadening intracellular F$^-$ resonances (98). As reported by Scarpa *et al.* (98a) the contribution of paramagnetic Cu(II) in superoxide dismutase in RBCs towards ^{19}F NMR line broadening disappeared by incubating RBCs in 10^{-2} M diethyldithiocarbamate (DDC). Figure XXI displays the spectra of (a) DDC treated and (b) untreated packed RBCs at 95% Ht which were bubbled with CO. By bubbling with CO, diamagnetic CO-hemoglobin was formed which removed any paramagnetic line broadening. After washing both samples used in Figure XXI with isotonic NaNO$_3$ buffered to pH 7.4, the ^{35}Cl NMR spectra were obtained. No ^{35}Cl resonance was observed in either case suggesting that the ^{35}Cl resonance obtained in Figure XXI may be due to trapped Cl$^-$. Alternatively, fast Cl$^-$-NO$_3^-$ exchange may have depleted the intracellular Cl$^-$. The observation of intracellular Cl$^-$ resonance in human RBCs by ^{35}Cl NMR remains elusive.

IV.2.3 ^{19}F NMR Method

The direct determination of Cl$^-$ distribution in human RBC suspensions is not attainable by ^{35}Cl NMR spectroscopy because of the inability to distinguish between intra- and

Figure XXI. ^{35}Cl NMR spectra of (a) DDC treated and (b) untreated packed RBCs. Packed RBCs were incubated with 10^{-2} M DDC at 37°C for 1 hr.

A

B

60	40	20	0	-20	-40	-60	-80 PPM
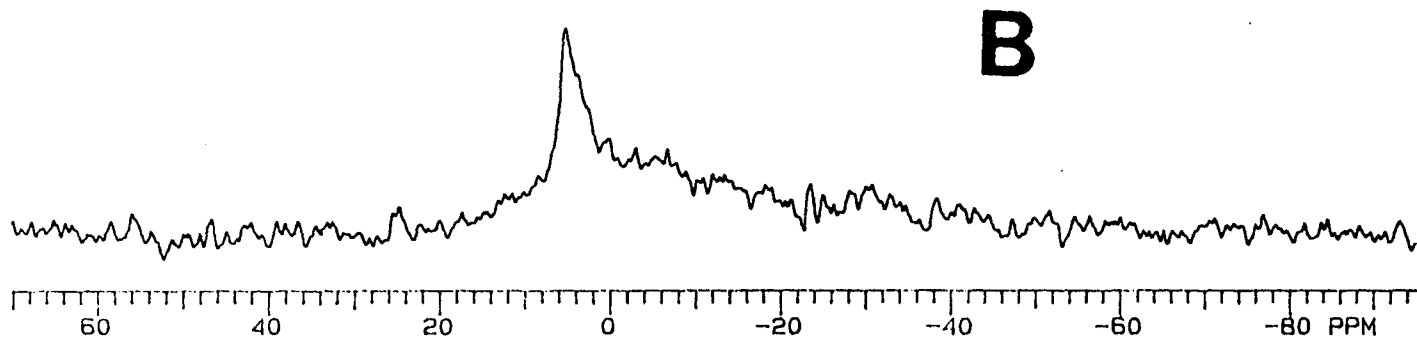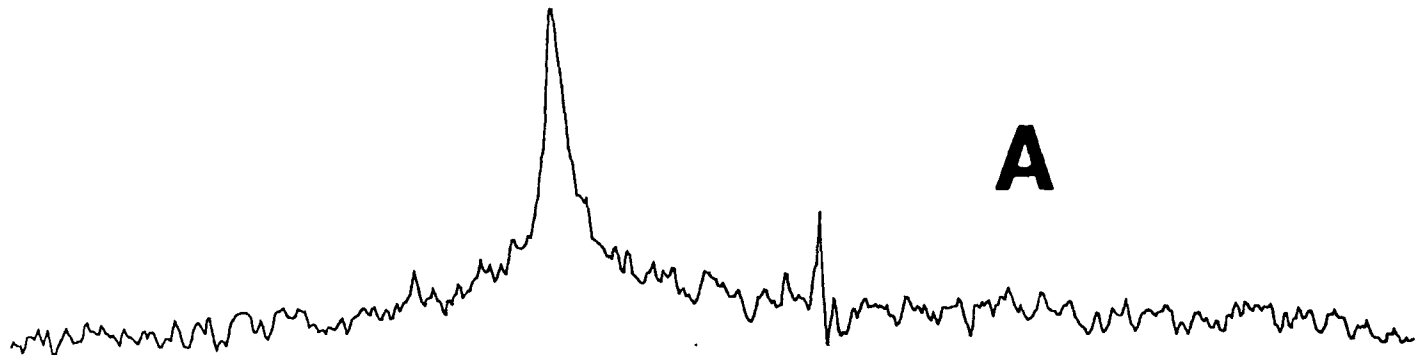
extracellular Cl^- resonances. The intracellular $^{35}Cl^-$ resonance in human RBC is subject to considerable line broadening due to Cl^- binding to hemoglobin (1). ^{19}F NMR spectroscopy, however, provides an indirect way to monitor Cl^- distribution in RBC suspensions (95). The TFA and TFM distribution ratios in RBC suspensions obtained from the ^{19}F NMR spectra were used to calculate the membrane potential (95). TFA probed Cl^- distribution whereas TFM measured cell volume changes induced by the ionophore. Because Cl^- distribution is a major determining factor of membrane potential in human RBC suspensions (95, 99), the steady state TFA distribution is a measure of RBC membrane potential.

Figure XXII shows typical ^{19}F NMR spectra for human RBC suspensions in the presence and absence of ionophores. The changes in TFA ratios with increasing ionophore concentrations are shown on Table XIII. The TFA ratio decreased from a value of 0.19 for RBC suspensions in the absence of ionophore to 0.11 for RBCs incubated with either 0.002 mM Val or 0.005 mM Non. Only at very high concentrations (>0.050 mM) of carboxylic ionophores did the TFA ratio changed appreciably. The TFM ratios shown on Table XIII indicate that the cell volume decreased with increasing ionophore concentration. Val and Non caused large decreases in cell volume whereas the carboxylic ionophores only induced cell volume changes at high ionophore concentration. Cell volume changes in the presence of increasing concentrations of Val are in agreement with those previously published (100). It is clear from Table XIII that the changes in TFA ratios are twice as great as changes in TFM ratios, indicating that the changes in E_m are not just due to volume changes.

The time dependence of Cl^- distribution was also monitored using ^{19}F NMR spectroscopy in the presence and absence of ionophores. No appreciable time dependence of Cl^- distribution was observed (data not shown). Cl^- distribution occurs too rapidly for the

Figure XXII. ^{19}F NMR spectra. (A) RBCs suspended at 45% Ht in 140 mM NaCl, 10 mM glucose, 2 mM TFA, 2 mM TFM, 10 mM HEPES, pH 7.4. (B) RBC suspension as in A with 0.005 mM Val. (C) RBC suspension as in A with 0.020 mM Mon.
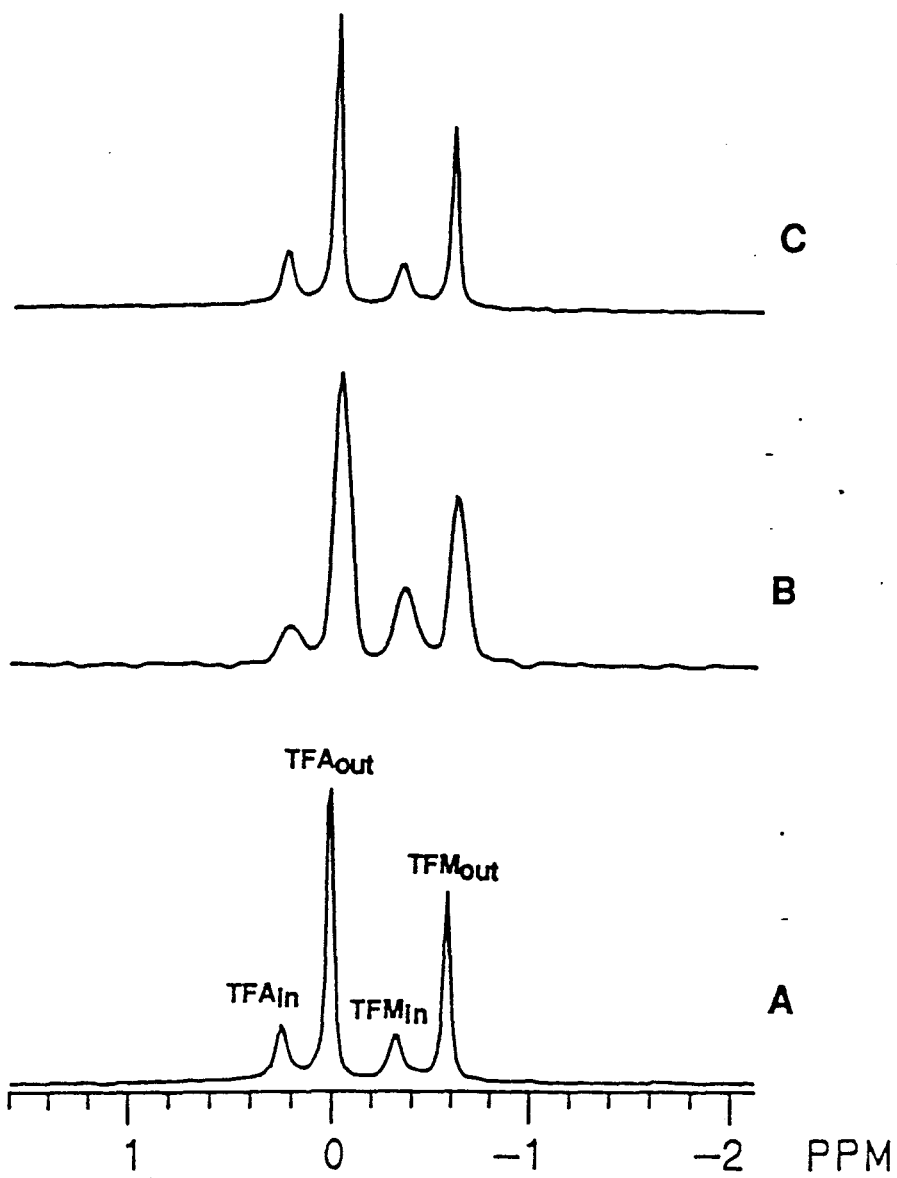
Table XIII. ^{19}F NMR Data of RBCs in the Presence and Absence of Ionophores[a]

Sample	TFA_{in}/TFA_{out}	TFM_{in}/TFM_{out}	E_m/mV
RBC control	0.19	0.27	-9.4
Val 0.001 mM	0.15	0.25	-12.9
0.002 mM	0.11	0.20	-16.2
0.005 mM	0.09	0.20	-21.2
Non 0.001 mM	0.17	0.26	-10.6
0.002 mM	0.14	0.24	-14.7
0.005 mM	0.11	0.22	-17.8
0.010 mM	0.09	0.20	-20.6
Mon 0.020 mM	0.17	0.25	-9.5
0.050 mM	0.16	0.25	-11.8
0.100 mM	0.14	0.24	-13.4
0.200 mM	0.13	0.24	-16.7
0.3000 mM	0.11	0.23	-18.6
Las 0.020 mM	0.18	0.26	-11.3
0.050	0.17	0.26	-11.3
0.100	0.17	0.26	-11.3
0.200	0.17	0.27	-11.8
Nig 0.020 mM	0.17	0.26	-9.9
0.050 mM	0.17	0.26	-10.8
0.200 mM	0.17	0.27	-11.7

[a]The reported NMR parameters are an average of 3 separately prepared samples. Variations in TFA and TFM ratios are less than 0.02 where as the errors for the E_m values were less than 0.5 mV.

NMR time scale (37). The steady-state TFA and TFM ratios were therefore used to calculate the membrane potentials, E_m, in the presence and absence of ionophores (Table XIII). The ^{31}P NMR HP indicator (96a) was also used to determine the E_m in human RBC suspended at 45% Ht in 140 mM NaCl, 10 mM glucose, 15 mM HP, and 10 mM HEPES, pH 7.4 in presence and absence of some ionophores. RBC suspensions in the absence of ionophores yielded E_m values of -9.6 mV ($n = 3$) with an average α value of 0.66. The addition of 0.001 mM Val yielded an E_m value of -14.1 mV with an $\alpha = 0.73$ ($n = 3$) whereas the addition of 0.02 mM Mon yielded an E_m value of -9.4 mV with an $\alpha = 0.64$ ($n = 3$). These E_m data are consistent with those shown in Table XIII. A decrease in the intracellular [Cl] concentration, measured with an Orion Cl$^-$ electrode (100b), was found in the presence of 0.005 mM Val but not with 0.100 mM Mon (data not shown). The Cl$^-$ electrode results indicate that the ionophore-induced Cl$^-$ transport is therefore independent of the method used for measuring Cl$^-$distribution.

To determine the mechanism of ionophore-induced Cl$^-$ transport, RBCs were treated with the RBC anion exchange inhibitor DIDS and the Cl$^-$ distribution was measured by ^{19}F NMR spectroscopy (95). RBCs were preequilibrated with 2 mM TFA and 2 mM TFM, and then incubated with 0.05 mM DIDS for 20 minutes prior to obtaining ^{19}F NMR spectra. We tested the activity of DIDS separately by incubating packed RBCs with 0.05 mM DIDS for 20 min prior to resuspension in the isotonic medium containing TFA and TFM; the influx of TFA measured by ^{19}F NMR in the presence of DIDS was much slower than in its absence, agreeing with the observations reported for the anion exchange inhibitor SITS (95). In the absence of ionophore the membrane potential measured by ^{19}F NMR (-9.4 mV, n=2) for DIDS treated RBCs did not change within one hour and was the same as for DIDS untreated

RBCs (Table XIII). The presence of 0.005 mM Val increased the Cl⁻ distribution ratio in DIDS-treated RBCs to -21.2 mV (n = 2) after one hour suggesting that the observed Cl⁻ transport is due to an ionophore-specific effect. DIDS-treated RBCs in the presence of 0.10 mM Mon, however, exhibited no appreciable change in membrane potential after one hour (E_m = -14.8 ; n = 2). The intracellular pH in RBCs did not change upon incubation with ionophores as revealed by ^{31}P NMR measurements (101). The intracellular pH was found to be 7.18 $\pm$ 0.04 before and after treating RBCs with ionophores. These results agree with those obtained by Hladky and Rink (31) for RBCs treated with Val using fluorescence spectroscopy. The mechanism of ionophore-induced Cl⁻ transport does not involve anion transport via the band 3 protein or H⁺ exchange across the human RBC membrane.

Riddell et al. (60) reported that Val had no significant effect on the rate of Cl⁻ transport across phosphatidyl choline vesicle membranes. They measured the rate of Cl⁻ transport in vesicle suspensions by monitoring the changes in the peak areas of the intravesicular ^{35}Cl NMR resonance; the extravesicular ^{35}Cl NMR signal was broadened by $MnCl_2$ present in the suspension medium (60). The effect of the presence of $MnCl_2$ on the membrane potential of human RBC was measured by ^{19}F NMR. Addition of 2.5 mM $MnCl_2$ to an RBC suspension pretreated with 2 mM TFA and 2 mM TFM gave a steady-state E_m value of +1.0 mV after 30 min. Addition of 0.001 mM Val to the $MnCl_2$-containing RBC suspension gave a steady-state E_m value of -9.9 mV, which is approximately the E_m value for an RBC suspension in the absence of $MnCl_2$ and Val. In contrast, the steady-state E_m value for a $MnCl_2$-free RBC suspension incubated with 0.001 mM Val was -12.9 mV.

IV.3   Resolution of Intra- and Extracellular ^{133}Cs NMR Resonances in the Presence and

Absence of SRs.

Figure XXIII shows the ^{133}Cs NMR spectra of Cs$^+$ loaded CORBCs suspended in a Cs$^+$ medium without SR (Figure XXIIIA), or containing Tm(DOTP)$^{5-}$ (Figure XXIIIB), Dy(TTHA)$^{3-}$ (Figure XXIIIC) or Dy(PPP)$_2^{7-}$ (Figure XXIIID). We made the assignment of intra- and extracellular ^{133}Cs resonances in SR-free RBC suspensions (Figure XXIIIA) by observing the changes in peak areas during Cs$^+$ loading, as previously reported (76). As shown in Figure XXIIIA, the intra- and extracellular ^{133}Cs$^+$ NMR resonances were resolved without the incorporation of a SR with the extracellular resonance being upfield. For the samples containing SR, we made peak assignments by centrifuging and separating the extracellular suspension from the Cs$^+$ loaded RBCs. The ^{133}Cs chemical shifts were recorded for the SR-containing media alone (no RBCs) and were approximately the same as for the extracellular resonance in the RBC suspension. Upon incorporation of either SR, Tm(DOTP)$^{5-}$(Figure XXIIIB), Dy(TTHA)$^{3-}$ (Figure XXIIIC) or Dy(PPP)$_2^{7-}$ (Figure XXIIID), in the Cs$^+$-containing suspension medium, the extracellular ^{133}Cs$^+$ NMR resonance was shifted downfield. The largest downfield shifts of the extracellular ^{133}Cs$^+$ resonance were observed in Cs$^+$-loaded RBC suspensions containing Tm(DOTP)$^{5-}$ in the medium.

Transmembrane Cs$^+$ distribution ratios were measured for Cs$^+$-loaded RBCs suspended in a Cs$^+$-containing medium at 37 °C over a 4 h period. We found that a steady-state transmembrane Cs$^+$ distribution was reached after 3 h of incubation time. The steady-state Cs$^+$ distribution ratio ([Cs$^+$]$_{in}$/[Cs$^+$]$_{out}$) across the RBC membrane was approximately the same (0.27 $\pm$ 0.01) in the presence and absence of Tm(DOTP)$^{5-}$ or Dy(TTHA)$^{3-}$. However, the Cs$^+$ distribution ratio observed in Dy(PPP)$_2^{7-}$-treated RBC suspensions (as is apparent from relative peal areas shown in Figure XXIIID) was significantly higher than those observed in

Figure XXIII. ^{133}Cs NMR spectra. (A) Cs$^+$-loaded CORBCs resuspended at 33% hematocrit in an isotonic medium containing 10 mM CsCl, 140 mM NaCl, 5 mM glucose, and 5 mM HEPES, pH 7.4. Initial concentrations were $[Cs^+]_{in}$ = 4.5 mM; $[Cs^+]_{out}$ = 5.1 mM. (B) Similar RBC suspension as in A at 40% hematocrit, except that 5.0 mM Tm(DOTP)$^{5-}$ replaced 25 mM NaCl in the medium. Initial concentrations were $[Cs^+]_{in}$ = 2.5 mM, $[Cs^+]_{out}$ = 5.3 mM. (C) Similar RBC suspension as in A at 33% hematocrit, except that 5.0 mM Dy(TTHA)$^{3-}$ replaced 15 mM NaCl in the medium. Initial concentrations were $[Cs^+]_{in}$ = 4.1 mM, $[Cs^+]_{out}$ = 7.9 mM. (D) Similar RBC suspension as in A at 45% hematocrit, except that 5.0 mM Dy(PPP)$_2^{7-}$ replaced 50 mM NaCl in the medium. Initial concentrations were $[Cs^+]_{in}$ = 6.1 mM, $[Cs^+]_{out}$ = 5.8 mM. Each spectrum was recorded in 1000 transients in a septum sealed NMR tube bubbled with moist CO gas. The symbols i and o denote intra- and extracellular ^{133}Cs$^+$ NMR resonances. The spectra are referenced relative to a sample of 0.15 M CsCl in D$_2$O which was measured separately.Cs$^+$-loaded RBCs suspended in Tm(DOTP)$^{5-}$ or Dy(TTHA)$^{3-}$-treated media or in SR-free medium.
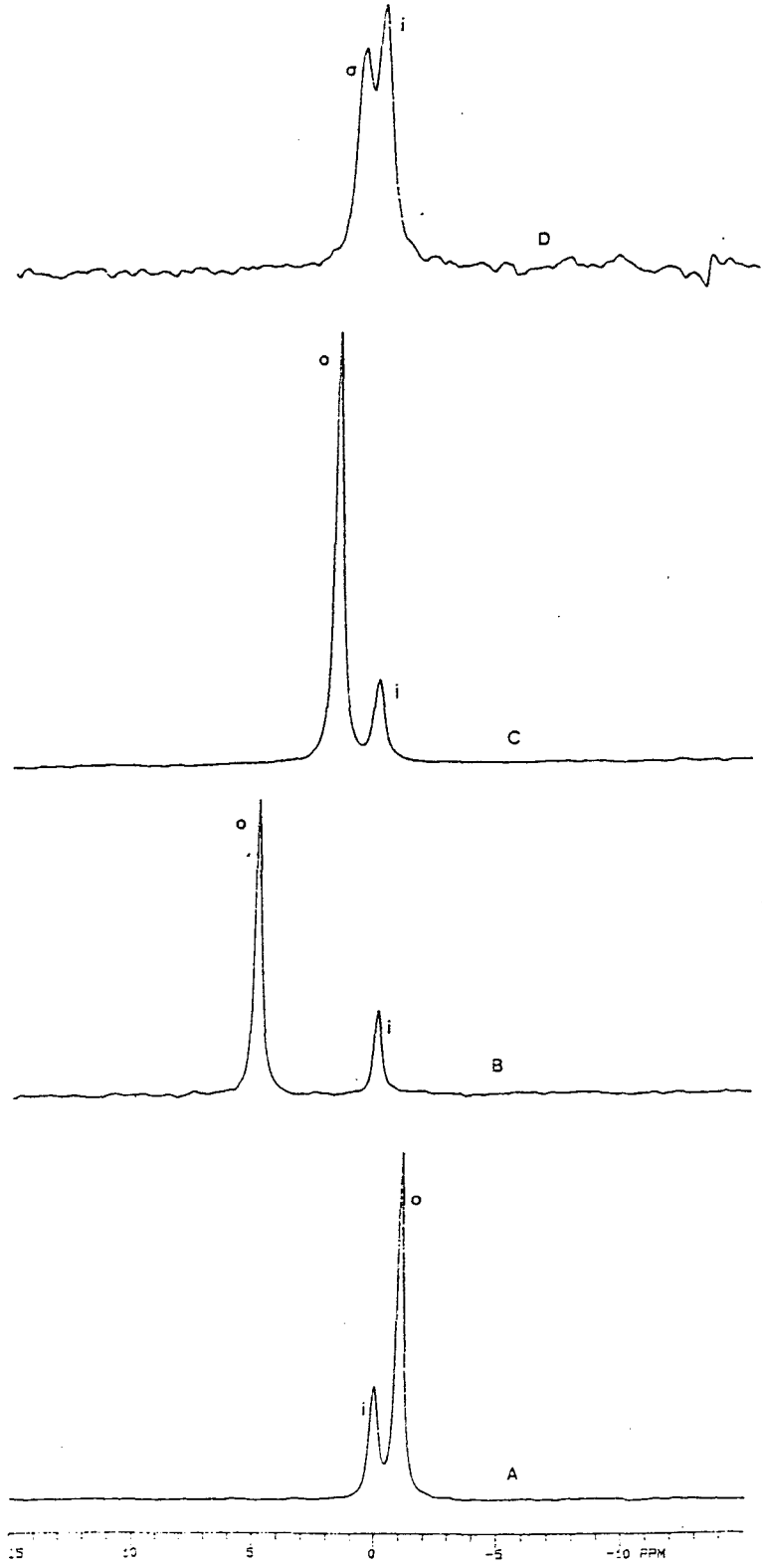
Cs$^+$-loaded RBCs suspended in Tm(DOPT)$^{5-}$- or Dy(TTHA)$^{3-}$-treated media, or in SR-free medium.

IV.4 Contribution of Cs$^+$ Binding to Intracellular Phosphates, Hemoglobin, and Cell Membrane To the Intracellular ^{133}Cs$^+$ Shift

We used three media to study the contribution of the intracellular RBC components at concentrations close to the physiologic values (102) to the intracellular ^{133}Cs$^+$ chemical shift (Table XIV). The composition of the media is indicated in the footnote to Table XIV. Buffer A had the same composition as did the suspension medium used in Figure XXIIIA. Buffer B contained competing intracellular cations, and buffer C, in addition to competing intracellular cations, had its viscosity adjusted with PVP-100 (103) to approximately 5 cP to mimic that of the intracellular RBC compartment (84). Table XIV shows that the chemical shift of the ^{133}Cs$^+$ NMR resonance was at least 0.8 ppm for physiologically relevant concentrations of DPG in buffer A. In contrast, the ^{133}Cs$^+$ NMR shifts in the presence of typical RBC concentrations of ATP, ADP, P$_i$, and COHb were approximately 57, 28, 27, and 28%, respectively, of those observed with DPG in buffer A.

To determine whether the large Cs$^+$-DPG shift was simply due to the high DPG concentration relative to that of other intracellular components, we also measured the ^{133}Cs NMR chemical shifts for each intracellular component at the same concentration (2 mM) in buffer A. The observed shifts were 0.46, 0.25, 0.75, 0.36, and 0.24 ppm for ATP, ADP, DPG, P$_i$, and COHb, respectively. These values were comparable to those measured in buffer A for each of the intracellular components at known physiological RBC concentrations (see Table XIV). The downfield shift of the ^{133}Cs$^+$ NMR resonance observed in the presence of

Table XIV. [133]Cs Chemical Shift Dependence on the Intracellular Components.

Sample	δ ([133]Cs)/ppm Buffer A[b]	Buffer B[c]	Buffer C[d]
2.0 mM ATP	0.46	0.43	0.46
0.2 mM ADP	0.23	0.23	0.33
5.4 mM DPG	0.81	0.81	0.83
1.0 mM P$_i$	0.22	0.27	0.27
2.7 mM COHb[e]	2.02	2.10	2.11

[a]Shifts are reported relative to a reference sample of 0.15 M CsCl in D$_2$O placed in a spinning 10 mm NMR tube and measured separately. The reported values represent an average of measurements conducted in three separately prepared samples. Errors are less than 0.05 ppm. [b]CsCl buffer A consisted of 10 mM CsCl, 140 mM NaCl, 5 mM glucose, and 5 mM HEPES, pH 7.4. The osmolarity was approx. 300 mosM. [c]CsCl buffer B consisted of 10 mM CsCl, 5 mM glucose, 5 mM HEPES, pH 7.4, 140 mM KCl, 5 mM NaCl, 2.4 mM MgCl$_2$, and 1 μM CaCl$_2$. [d]CsCl buffer C had the same composition as buffer B, except that the viscosity of this solution was adjusted to 5.6 cP with PVP-100. [e] Because of denaturation problems associated with Hb preparations at high concentration, the concentration of COHb used in this study was below the physiologic value in human RBC (4.8 - 5.4 mM) (102). However, for the COHb experiments we only used 5 mM CsCl in buffers A, B, and C. Thus, the concentration ratio of Cs^{+} to COHb is close to physiologic value in human RBC.

COHb at concentrations close to its normal range in human RBC (102) was larger than the downfield shift induced by DPG. However, the downfield shift induced by COHb is not due to specific Cs^+ binding to COHb (vide infra). In the presence of competing intracellular cations (buffer B) and with the solution viscosity adjusted to 5 cP (buffer C), the $^{133}Cs^+$ NMR chemical shifts in the presence of each intracellular RBC component was virtually unchanged relative to that observed in buffer A (Table XIV). Of all intracellular phosphates, DPG continued to induce the largest $^{133}Cs^+$ shift in the presence of competing cations within a physiologic viscosity range. When all of the intracellular components were present in buffer C, the shift observed was 0.99 ppm (n = 3). This is less than the calculated value, 4.00 ppm, obtained by addition of the shifts given separately by each RBC component. The shifts were not additive, presumably because there is competition between intracellular components for the Cs^+ ion.

Negatively charged phospholipids or amino acid side chains in RBC membrane proteins are also potential sites for Cs^+ interaction. The $^{133}Cs^+$ NMR parameters of 10 mM CsCl in the presence of unsealed RBC membranes suspended in buffer A (at 3 mg/ml protein concentration) were $\delta = 0.07$ ppm and $\Delta\nu_{1/2} = 8.3$ Hz (n = 3). Upon addition DPG to the same membrane samples, the $^{133}Cs^+$ NMR parameters were $\delta = 1.01$ ppm and $\Delta\nu_{1/2} = 15.3$ Hz (n = 3).

IV. 5 Contribution of Magnetic Susceptibility To the Intracellular $^{133}Cs^+$ Shift

^{31}P NMR spectra were recorded for Cs^+-free RBCs suspended in a Cs^+ free medium or for Cs^+-loaded RBCs in a Cs^+-containing medium (Table XV). Both deoxyRBC and CORBC suspensions were analyzed. As a further test of the magnetic field gradient effect

Table XV. Effects of Cs$^+$ loading, oxygenation, and SR on the chemical shifts and line widths of intracellular RBC ^{31}P NMR phosphate resonances.[a,b]

	DPG		P$_i$	ATP		
	3	2		γ	α	β
A. Cs$^+$-loaded deoxyRBCs						
δ/ppm	6.2	5.5	4.6	-2.9	-7.8	-16.9
$\Delta\nu_{1/2}$	42	28	19	42	48	137
B. Cs$^+$-free deoxyRBCs						
δ/ppm	5.9	5.2	4.3	-3.3	-8.1	-17.2
$\Delta\nu_{1/2}$	26	22	20	46	49	125
C. Cs$^+$-loaded CORBCs						
δ/ppm	5.7	4.9	4.2	-3.4	-8.3	-17.4
$\Delta\nu_{1/2}$	25	20	21	37	36	104
D. Cs$^+$-free CORBCs						
δ/ppm	5.6	4.8	4.2	-3.3	-8.3	-17.4
$\Delta\nu_{1/2}$	17	19	15	43	37	125
E. Cs$^+$-loaded deoxyRBCs in SR suspension						
δ/ppm	5.8	5.1	4.0	-3.6	-8.3	-17.7
$\Delta\nu_{1/2}$	36	36	35	51	55	126
F. Cs$^+$-loaded CORBCs in SR suspension						
δ/ppm	5.5	4.7	4.2	-3.5	-8.3	-18
$\Delta\nu_{1/2}$	56	120	37	56	55	150

[a]Samples A and C were suspended in the same medium as for Figure XXIIIA. Samples B and D were suspended in 150 mM NaCl, 5 mM glucose, and 5 mM HEPES, pH 7.4. Samples E and F were suspended in the same medium as for Figure XXIIIB. All suspension media contained 15% D_2O. RBCs were loaded with 150 mM CsCl for 3 hours. [b]Shifts are reported relative to a reference sample of phosphoric acid in D_2O, placed in a spinning 10 mm NMR tube and measured separately. The reported ^{31}P line widths represent the widths of the resonances at half-height (in Hz) after subtraction of 20 Hz used in line broadening. The reported NMR parameters represent the average of measurements conducted on two separately prepared samples. Errors in chemical shift and line width are less than 0.1 ppm and 1.0 Hz, respectively.

across the RBC membrane, we also examined Cs^+-loaded RBCs suspended in a medium containing 5.0 mM $DyTTHA^{3-}$. Deoxygenation of Cs^+-free or Cs^+-loaded RBC suspensions caused broadening and downfield shifts of the ^{31}P resonances of intracellular phosphates. These observations are in agreement with those previously reported (92, 104) and confirm the degree of oxygenation of the SR-free samples. Incorporation of 5.0 mM $Dy(TTHA)^{3-}$ in the medium of Cs^+-loaded RBC suspensions led to broadening and downfield shifts (relative to SR-free samples) of the ^{31}P NMR spectra of both deoxyRBC and CORBC suspensions. However, in suspensions containing SR the spectral changes were larger with CORBC than with deoxyRBC. These observations are consistent with those previously reported (92, 104) for RBC suspensions containing 3 mM $Dy(PPP)_2^{7-}$ and confirm the degree of oxygenation in SR-containing RBC suspensions. Cs^+ loading of deoxyRBC suspensions gave rise to broadened and slightly downfield shifted ^{31}P NMR spectra. In contrast, Cs^+ loading of CORBC suspensions led to virtually no changes in the line widths or chemical shifts of the ^{31}P NMR resonances.

The effect of the degree of oxygenation on the ^{133}Cs NMR spectra of the SR-free and SR-containing Cs^+-loaded RBC suspensions was also examined (Table XVI). As reported above for ^{31}P NMR spectra of RBC suspensions in SR-free media, deoxygenation also caused some broadening and small downfield shifts of the intra- and extracellular $^{133}Cs^+$ NMR resonances of Cs^+-loaded RBC suspensions in SR-free media. The presence of $Dy(TTHA)^{3-}$ in the suspension medium of deoxyRBCs induced an upfield shift and a sharpening of the intracellular $^{133}Cs^+$ resonance. In contrast, CORBCs gave rise to a broad and downshifted intracellular $^{133}Cs^+$ resonance in the presence of SR. Incorporation of $Dy(TTHA)^{3-}$ in the suspension media of either deoxy or CO Cs^+-loaded RBCs caused broadening and

Table XVI. [133]Cs NMR chemical shifts and line widths for Cs^{+}-loaded RBC suspensions in the presence and absence of 5 mM Dy(TTHA)$^{3-}$.[a,b]

	Cs$^+_{in}$		Cs$^+_{out}$	
	with SR	without SR	with SR	without SR
A. Cs[+]-loaded deoxyRBCs				
δ/ppm	2.1	2.3	3.8	1.1
$\Delta\nu_{1/2}$	10	10	4.9	3.9
B. Cs[+]-loaded CORBCs				
δ/ppm	2.1	1.9	3.7	1.3
$\Delta\nu_{1/2}$	13	9.5	10	7.1

[a]RBCs were loaded with 150 mM CsCl for 3 hours. [Cs$^+$]$_{in}$ = 2.5 mM. The SR-free samples were suspended in medium A (see Table XIV). The SR-treated samples were suspended in a medium similar to A, except that 5.0 mM Dy(TTHA)$^{3-}$ replaced 15 mM NaCl. Deoxy- and CORBC samples were prepared as described in Materials and Methods. [b]Chemical shifts are reported relative to a reference sample of 0.15 M CsCl in D$_2$O, placed in a spinning 10 mm NMR tube and measured separately. The reported [133]Cs$^+$ line widths represent the widths of the resonances at half-height (in Hz) after subtraction of 3.0 Hz used in line broadening. The reported NMR parameters represent the average of measurements conducted on two separately prepared samples. Errors in chemical shift and line width are less than 0.1 ppm and 1.0 Hz, respectively.

downshifting of the extracellular $^{133}Cs^+$ resonance, as reported above (Figure XXIII). In SR-free media, the chemical shift separation between intra- and extracellular $^{133}Cs^+$ NMR resonances from Cs^+-loaded RBCs was 1.2 and 0.6 ppm, respectively, in deoxyRBC and CORBC suspensions. In SR-treated media, the chemical shift separation was 1.7 and 1.6 ppm, respectively, in deoxyRBC and CORBC suspensions.

For further characterization of the volume and diamagnetic susceptibility contributions of hemoglobin toward the intracellular $^{133}Cs^+$ shift, we examined the effect of hemoglobin concentration on the ^{133}Cs NMR spectra by varying the hematocrit (Figure XXIV) or osmolarity (Figure XXV) in CORBC suspensions, or by diluting the CORBC lysates (Figure XXVI).

We varied the hematocrit (Ht) by changing the volume ratio of packed RBCs to suspension medium (buffer A). The chemical shifts of intra- and extracellular $^{133}Cs^+$ resonances were measured at different hematocrit values (Figure XXIV). The $^{133}Cs^+$ chemical shift of the suspension medium alone (Ht = 0) was 1.7 $\pm$ 0.1 ppm upfield from that extrapolated for packed cells (Ht = 100%). In carbonmonoxygenated RBC suspensions, as the hematocrit increased, the intracellular $^{133}Cs^+$ resonance and, to a lesser extent, the extracellular $^{133}Cs^+$ resonance were shifted downfield. The chemical shift separation between intra- and extracellular $^{133}Cs^+$ resonances in Cs^+-loaded CORBC suspensions increased slightly (by approximately 0.1 ppm) when the hematocrit increased from 25 to 95%. The intracellular Cs^+ concentration varied between 1.2 and 4.8 mM, whereas the extracellular Cs^+ concentration varied between 4.6 and 14.0 mM, when the Ht increased from 25 to 95%.

The chemical shifts of intra- and extracellular $^{133}Cs^+$ resonances were measured at different osmolarity values (Figure XXV). The osmolarity was increased by addition of

Figure XXIV. Dependence of intra- and extracellular $^{133}Cs^+$ NMR chemical shifts on hematocrit for Cs^+-loaded CORBCs suspended in buffer A (see Table XIV). The symbols ● and ○ represent the intra- and extracellular $^{133}Cs^+$ shifts, respectively, and the symbol ■ denotes the transmembrane chemical shift difference. The shifts were determined relative to a sample of 0.15 M CsCl in D_2O which was measured separately. A 2% correction was applied to the measured hematocrit to account for trapped suspension medium (105).
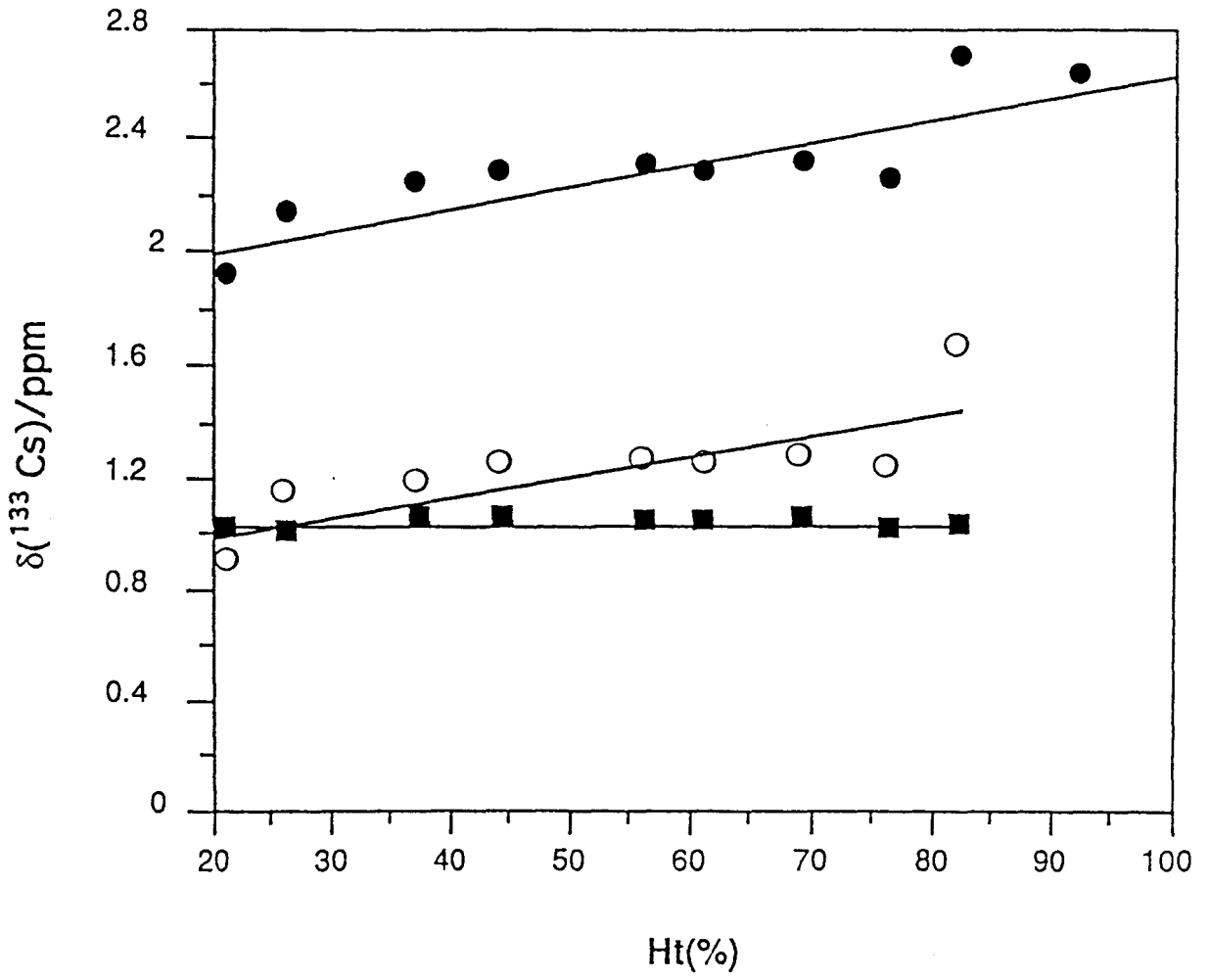
Figure XXV. Dependence of intra- and extracellular $^{133}Cs^+$ NMR chemical shifts on osmolarity for Cs^+-loaded CORBC suspensions. The osmotic pressure of the suspension medium was adjusted by addition of 0.3 mL of sucrose (ranging in concentration from 0 to 1000 mM) to 2.0 mL Cs^+-loaded CORBCs suspended in 0.6 mL of buffer A. The symbols ● and ○ represent the intra- and extracellular $^{133}Cs^+$ shifts, respectively, and the symbol ■ denotes the transmembrane chemical shift difference. The shifts were determined relative to a sample of 0.15 M CsCl in D_2O which was measured separately.
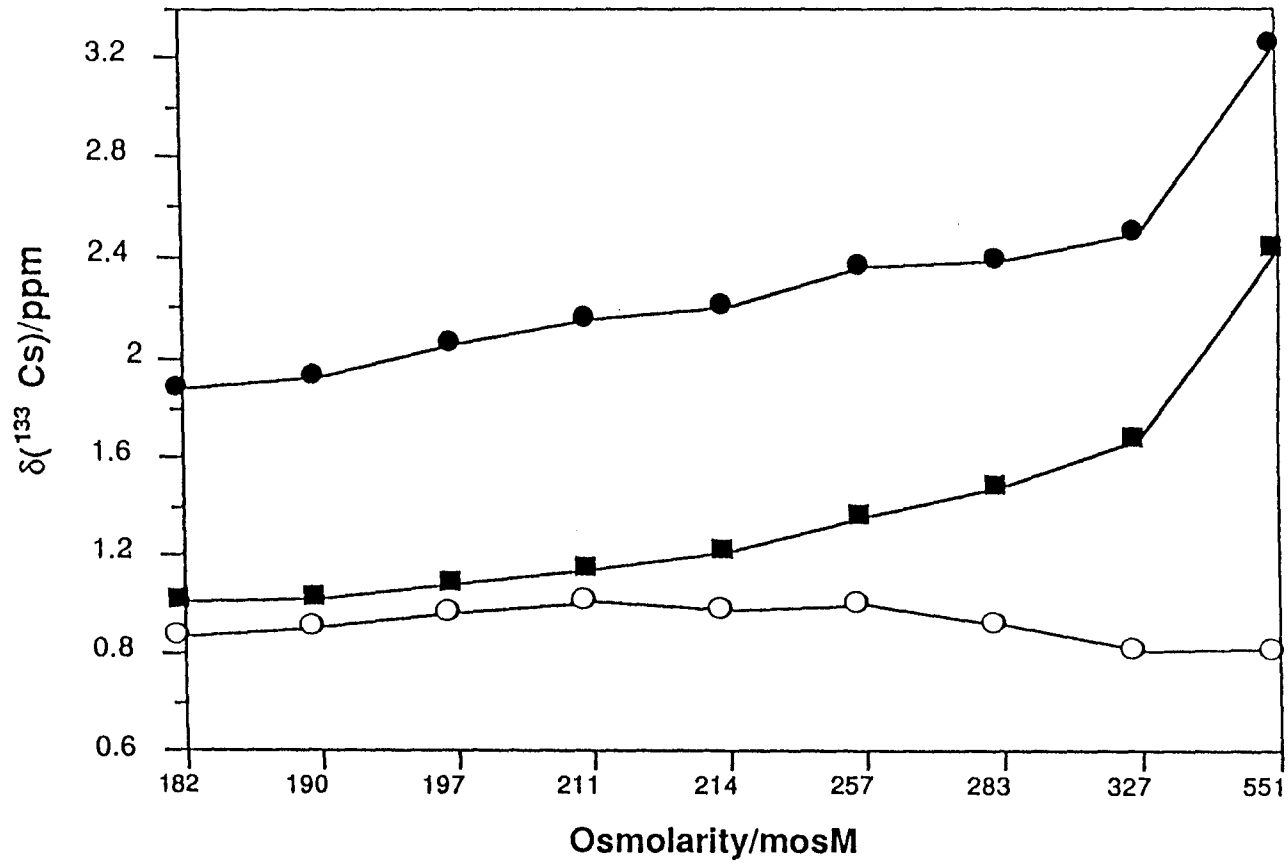
Figure XXVI. Dependence of the intracellular $^{133}Cs^+$ shift on CORBC lysate concentration. Concentrated CORBC lysates were prepared as described in Materials and Methods. The various lysate concentrations were obtained by addition of varying amounts of distilled water to concentrated RBC lysate. The CsCl concentrations ranged from 2.4 mM at a lysate concentration of 100% to 1.0 mM at a lysate concentration of 42%. The lysate concentration is given in units of %v/v, the percentage ratio of the initial volume of concentrated lysate and the volume of each sample after dilution. The reported $^{133}Cs^+$ shifts were measured relative to 0.15 M CsCl placed in the bulb of a spherical bulb/cylindrical capillary reference assembly.
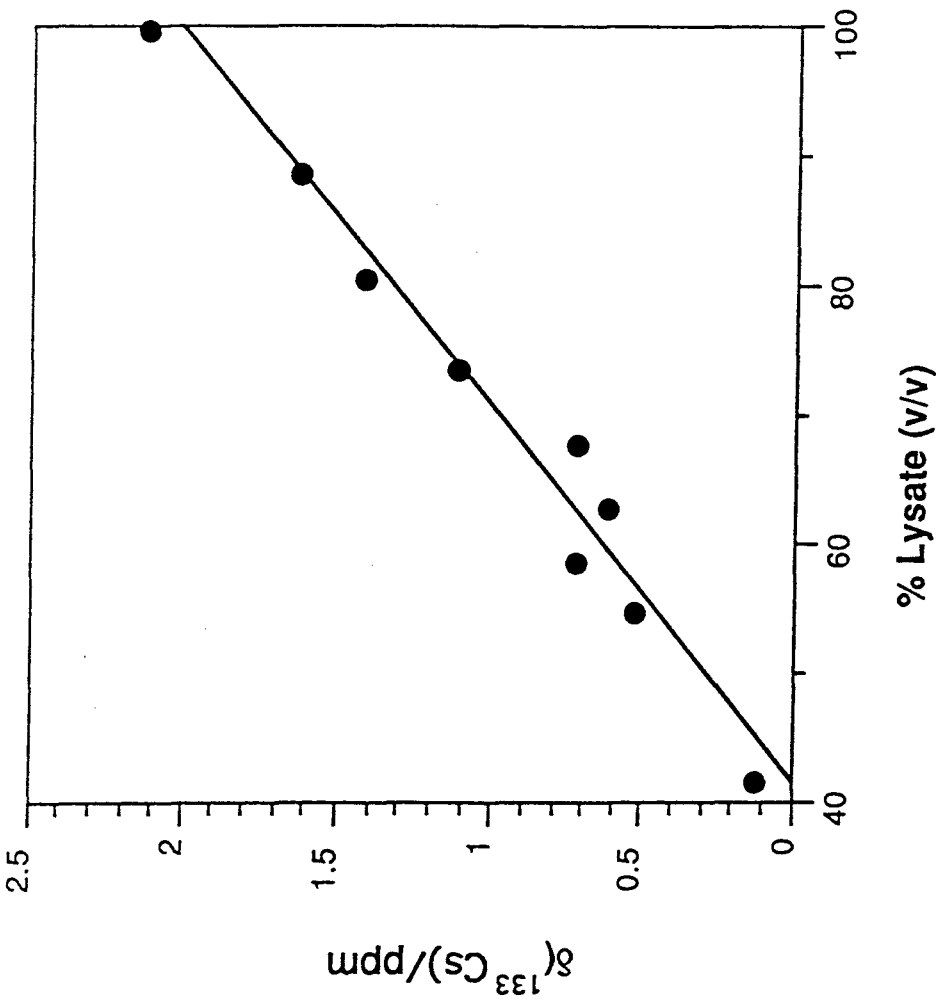
increasing amounts of the nonelectrolyte sucrose to the suspension medium. In CORBC suspensions, as the osmolarity increased, the intracellular $^{133}Cs^+$ resonance was shifted downfield, whereas the extracellular $^{133}Cs^+$ resonance was shifted slightly upfield. The chemical shift separation between intra- and extracellular $^{133}Cs^+$ resonances in Cs^+-loaded CORBC suspensions underwent an approximately two-fold increase as the osmolarity increased from 182 to 551 mosM. The intracellular Cs^+ concentration varied between 1.7 and 2.3 mM, whereas the extracellular Cs^+ concentration varied between 4.6 and 7.5 mM, when the osmolarity increased from 182 to 551 mosM.

IV.6   Contribution of Non-Ideality of Water To the Intracellular $^{133}Cs^+$ Shift

Concentrated RBC lysate bubbled with CO gas was diluted with distilled water to yield different COHb concentrations. Under these experimental conditions, the Cs^+/Hb concentration ratio was maintained constant. Figure XXVI shows the $^{133}Cs^+$ shift in RBC lysates when the chemical shift reference was 0.15 M CsCl placed in the bulb of a spherical bulb/cylindrical capillary reference assembly. Because of the spherical geometry of the reference assembly, the reference and sample solutions experience the same changes in magnetic field strength (106, 107). An increase in CORBC lysate concentration was accompanied by a 2.1 ppm downfield shift of the $^{133}Cs^+$ NMR resonance. The smaller downfield shift of the $^{133}Cs^+$ NMR resonance observed with increasing CORBC lysate concentration did not include the contribution from an increase in the diamagnetic susceptibility contribution of COHb. An increase in CORBC lysate concentration from 42 to 100% resulted in an increase of 7.7 Hz of the line width of the $^{133}Cs^+$ NMR resonance.

Figure XXVII shows the effect of increasing concentrations of COHb and lysozyme

Figure XXVII. Effect of varying concentrations of COHb (●) and lysozyme (○) on the chemical shifts (part A) and line widths (part B) of $^{133}Cs^+$ NMR resonances. The initial Cs^+ concentration was 10 mM. The COHb concentration is expressed in terms of tetramer concentration whereas the concentration of lysozyme is expressed in terms of monomer concentration. The protein samples were diluted by addition of varying amounts of distilled water. The reported chemical shifts were measured relative to 0.15 M CsCl placed in the bulb of a spherical bulb/cylindrical capillary reference tube assembly.
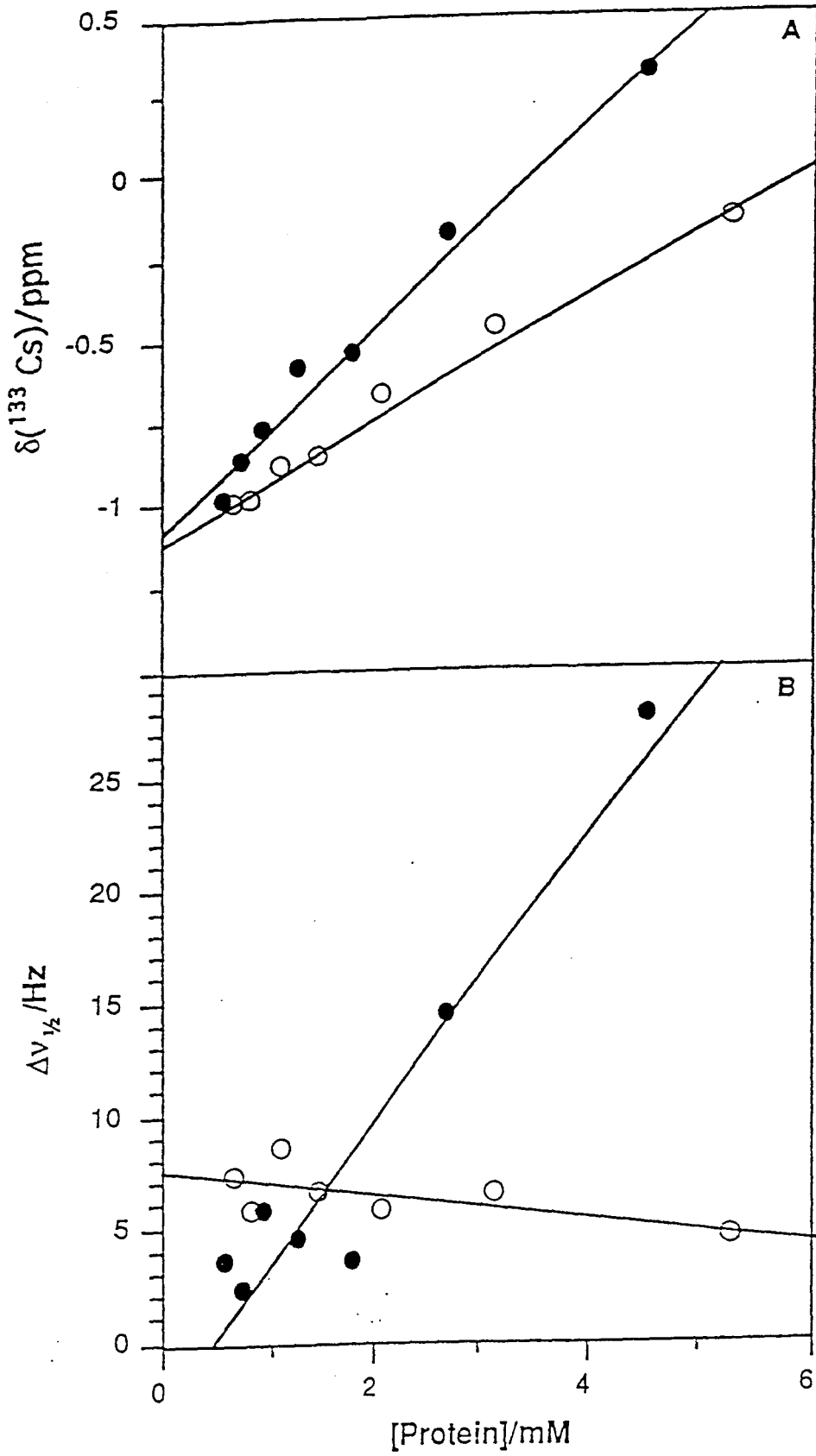
on the chemical shift and line width of the $^{133}Cs^+$ NMR resonance. Both lysozyme and COHb caused small downfield $^{133}Cs^+$ shifts, with the shifts induced by COHb being slightly larger. Whereas an increase in COHb concentration caused an increase from approximately 3.0 to 28 Hz in the line width of the $^{133}Cs^+$ NMR resonance, a similar increase in lysozyme concentration had a very small effect on the line width. An increase in protein concentration resulted in an increase in the diamagnetic susceptibility of the sample. However, because of the reference method employed, the observed downfield $^{133}Cs^+$ shifts measured in the presence of increasing COHb or lysozyme concentrations were due to a protein property independent of magnetic susceptibility. To ensure that the broadening of the $^{133}Cs^+$ signal induced by increasing concentrations of either COHb or lysozyme was not due to an increase in viscosity, we also measured the $^{133}Cs^+$ NMR parameters in PVP-100 samples which had the same viscosity as did the protein samples (Figure XXVIII). In contrast to COHb solutions, an increase in solution viscosity had no significant effect on the line width of the $^{133}Cs^+$ NMR resonance measured in PVP-100 solutions of varying concentrations. Unlike COHb or lysozyme, an increase in PVP-100 concentration did not lead to a downfield shift of the $^{133}Cs^+$ resonance.

IV.7   Cs$^+$ Binding to DPG

To characterize the interaction of Cs$^+$ with DPG, we obtained ^{31}P NMR and ^{13}C NMR spectra for DPG solutions in the presence and absence of Cs$^+$. The chemical shifts and line widths of ^{31}P and ^{13}C NMR spectra of DPG, in the presence and absence of competing ions at physiologically relevant concentrations, are given in Table XVII. ^{31}P peak assignments were made as previously reported (108, 109). ^{13}C peak assignments were based on standard chemical shifts for carboxylic, methylene, and methyne carbons. The chemical shifts of the

Figure XXVIII. Effect of varying the viscosity of solutions of PVP-100 on the chemical shifts (part A) and line widths of $^{133}Cs^+$ NMR resonances. The viscosity of the protein samples used in Figure XXVII was measured. Aqueous solutions containing PVP-100 (in varying concentrations) and CsCl (10 mM) were prepared that matched the viscosities of the protein samples. The reported chemical shifts were measured relative to 0.15 M CsCl placed in the bulb of a spherical bulb/cylindrical capillary reference tube assembly.
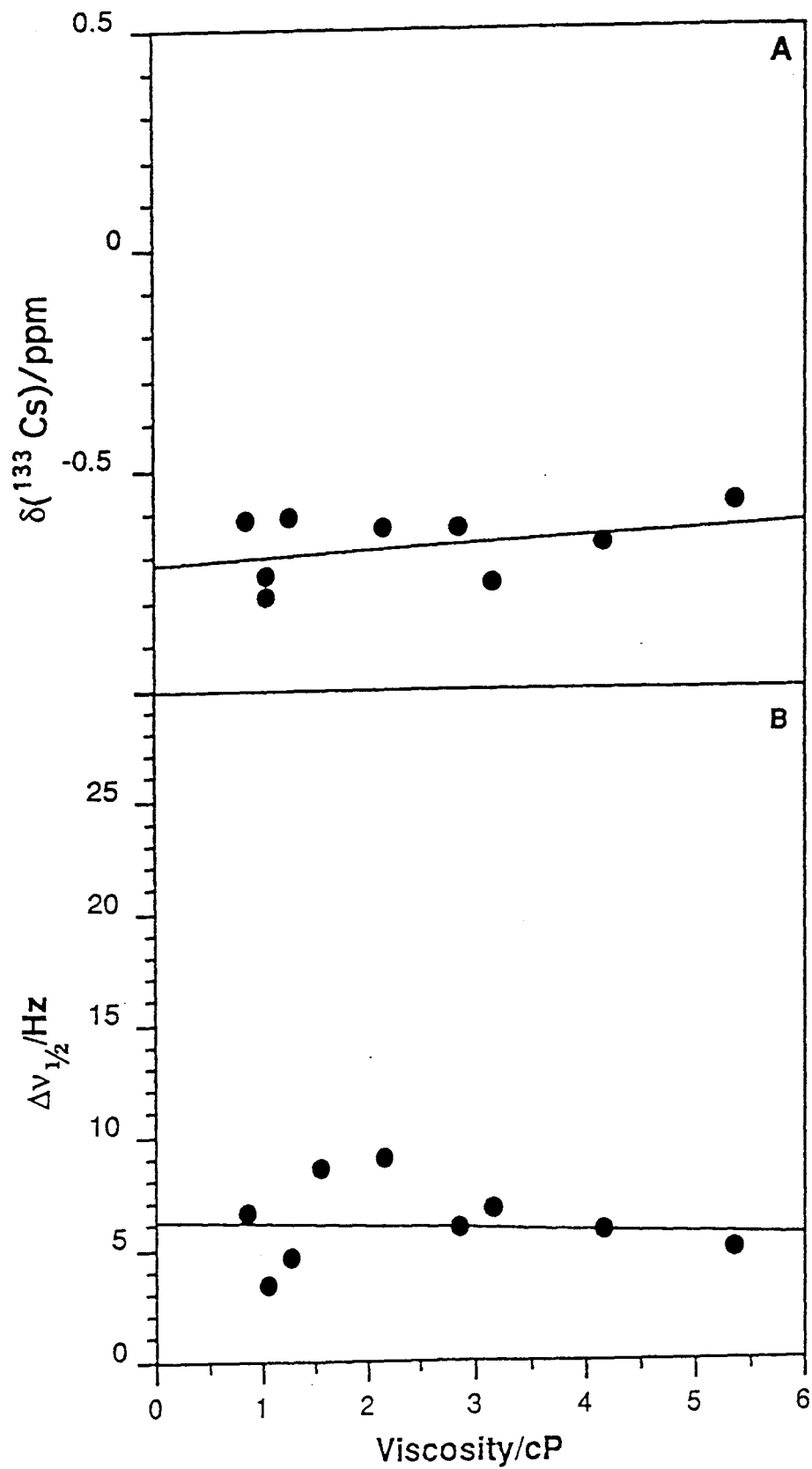
Table XVII. ^{31}P and ^{13}C NMR chemical shifts and line widths of DPG in the presence and absence of 10 mM Cs^+.[a]

	^{31}P NMR[b]			^{13}C NMR[b]		
Position	3	2		1	2	3
A. Medium A						
without Cs^+	5.5 (22)	4.6 (13)		179 (6)	75 (11)	67 (9)
with Cs^+	5.5 (38)	4.6 (43)		179 (12)	75 (20)	67 (18)
B. Medium B						
without Cs^+	5.6 (18)	4.6 (16)		179 (18)	75 (16)	67 (14)
with Cs^+	5.6 (30)	4.6 (29)		179 (24)	75 (29)	67 (15)

[a]Medium A consisted of 10 mM CsCl and 5.4 mM DPG. Medium B consisted of 10 mM CsCl, 5.4 mM DPG, 140 mM KCl, 5 mM NaCl, 2.4 mM $MgCl_2$, and 1 μM $CaCl_2$. We did not add HEPES and glucose to the solutions in order to simplify the ^{13}C NMR spectra. [b]Chemical shifts in ppm are followed by line widths in Hz in parentheses. ^{31}P chemical shifts are reported relative to a reference sample of 0.15 M CsCl in D_2O, placed in a spinning 10 mm NMR tube and measured separately. ^{13}C chemical shifts are reported relative to tetramethylsilane present in the sample. The reported ^{31}P and ^{13}C line widths represent the widths of the resonances at half-height (in Hz) after subtraction of 20 and 2.0 Hz,

respectively, used in line broadening. The reported NMR parameters are an average for three separately prepared samples. Errors in chemical shift and line width are less than 0.5 ppm and 1.0 Hz, respectively.

^{31}P and ^{13}C NMR resonances of DPG did not change upon addition of Cs^+ or competing ions. However, the line widths increased upon addition of Cs^+, but did so to a lesser extent in the presence of competing ions. Using ^{133}Cs NMR the Cs^+-DPG association constant was determined from plots of δ_{obs}/[Cs^+] vs. [Cs^+] (in mM) at pH 7.4 (Figure XXIX). The good linear fit (r^2 = 0.90) of the $^{133}Cs^+$ chemical shift data in the presence of DPG is consistent with a stoichiometry of 1:1 for the Cs^+-DPG complex. From the slope of the linear plot the dissociation constant was found to be K_D = 3.8 $\pm$ 0.2 mM at 23 °C.

Figure XXIX: Cs$^+$-DPG Dissociation Constant Determination
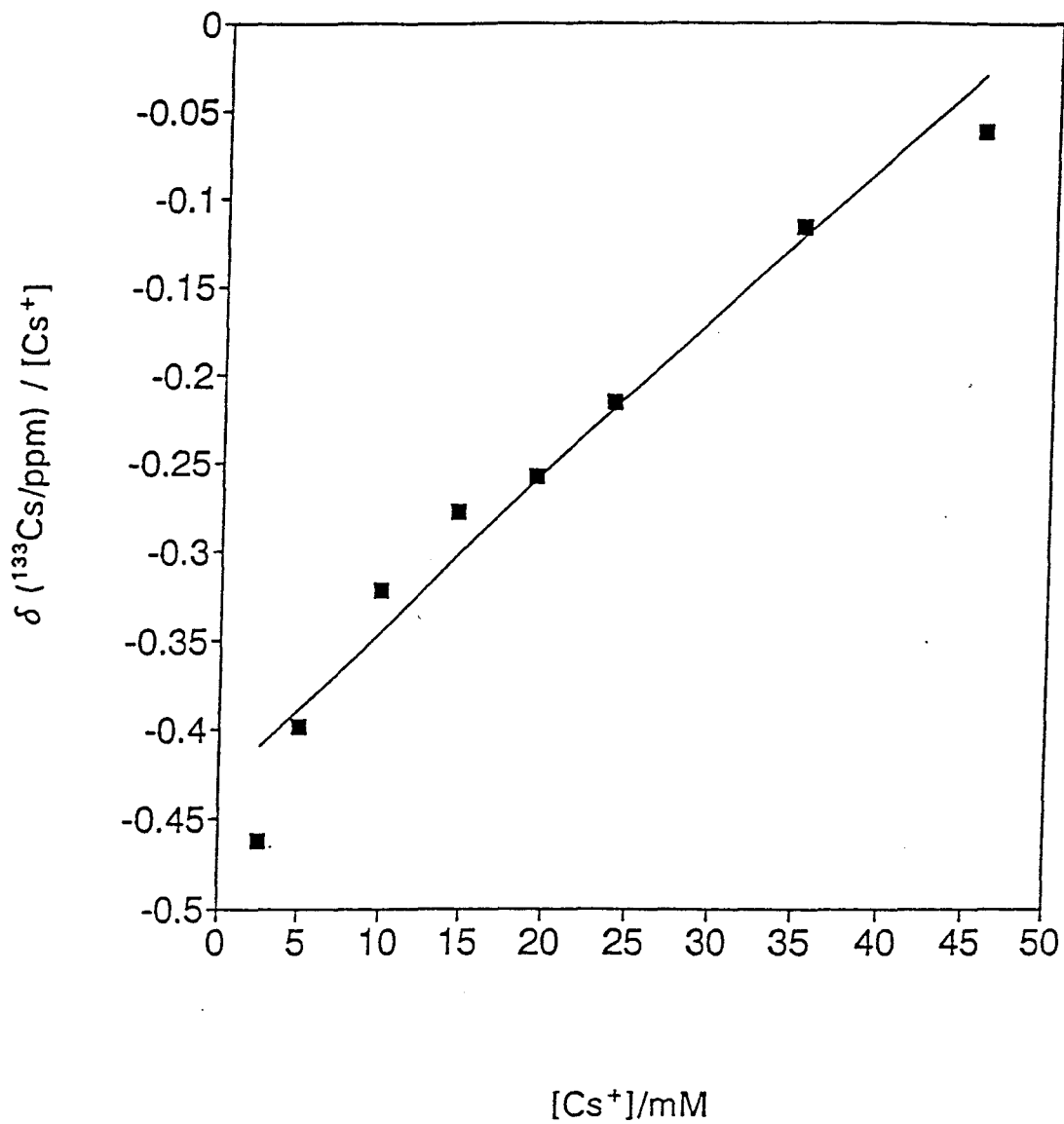
CHAPTER V

DISCUSSION

V.1   Multinuclear NMR Study of Cl⁻ in Biological Systems

In recent years attention has been increasingly focused on using ionophores to study

and understand the molecular basis of selective ion transport across biological membranes.

Several biophysical studies have been undertaken to elucidate the molecular mechanism by

which ionophores transport cations across membranes (23). Most studies up to date have

focused on cation ionophore interactions, but have neglected the role of anions. We have

focused on the ability of anions, in particular Cl⁻, to form ion pairs in ionophore solutions.

The effect of ion pairing induced by ionophores in several solvents systems was

examined for both Cl⁻ and ClO_4^-. A system in which ion pairing occurs is expected to have

an increase in the ^{35}Cl NMR line width, whereas if no ion pairing occurs the line width is

expected to remain similar to the reference sample (without any ionophore present) after

viscosity differences are taken into account. The following equation relates line width to T_2:

$$\Delta\nu_{1/2} = 1/\pi T_2 \tag{1}$$

where T_2 is the spin-spin relaxation time constant. In the case of extreme motional narrowing

the molecular tumbling is rapid on the NMR time scale, and the relaxation rate for a

quadrupolar nucleus is given by the expression (110)

131

$$\frac{1}{T_2} = \frac{1}{T_1} = \frac{3}{40} * \frac{2I+3}{I^2(2I-1)} * \{1+\frac{\eta^2}{3}\}\{\frac{eq_{zz}eQ}{\hbar}\}^2 * \tau c \qquad (2)$$

where T_1 is the longitudinal, or spin lattice relaxation time, eq_{zz} is the principle component of the electric field gradient tensor, and the correlation time τ_c is the time constant which describes the motional modulation of the quadrupolar interaction inducing nuclear relaxation. Fluctuations in electric field gradients in the coordination sphere of the chloride ion causes modulation of nuclear energy and hence affect relaxation properties. As the chloride ion pairs to the cation-ionophore complex T_2 decreases, the rate of tumbling $(1/T_2)$ increases, and consequently the ^{35}Cl NMR line width also increases. For solutions in which ion pairing does not occur T_2 is expected to remain unchanged.

The neutral ionophores (Val and Non), form an overall positive charge once they interact with the cation, K^+. It was hypothesized that the Cl^- and ClO_4^- counter anions would be attracted to the positive complex and ion pair. As shown in Tables II, IV-VIII, the ^{35}Cl NMR line widths of Cl^- and ClO_4^- do increase for the neutral ionophores for all solvents studied. The carboxylic ionophores (Las, Mon, and Nig) form an overall neutral complex when they interact with the cation, K^+. It was hypothesized that the Cl^- and ClO_4^- counter anions would not be attracted to the neutral complex. As shown in Tables II, IV-VIII, the ^{35}Cl NMR line widths of Cl^- and ClO_4^- in the presence of the negatively charged ionophores increase slightly compared to the control samples without ionophore present. We concluded that the neutral ionophores (Val and Non) do interact and ion pair with the Cl^- and ClO_4^- anion.

Solvents varying in donor number and dielectric constant were used in order to mimic

the range of polarities found in a biological membrane. As these parameters increase the degree of ion pairing is expected to decrease. A comparison of the various ionophores in the presence of KCl in methanol (DN = 25.7) and acetone-15% D_2O (DN = 19.4) result in ^{35}Cl NMR line widths which are slightly larger in acetone-15% D_2O, Figure VII. Because the donor numbers for methanol and acetone-15% D_2O are very similar, this is not surprising. A similar trend is observed when comparing the effect of dielectric constant on the ^{35}Cl NMR line width for ionophore samples containing KCl, Figure IX. According to Marcus (111a), a combination of a low dielectric constant of the solvent, that promotes the formation of ion pairs in general, and a low donor number of the solvent, that causes only weak solvation of the cation, favors the formation of contact ion pairs. It is reported for lithium salts (Cl⁻ or ClO_4^-) that the border between contact ion pair and non-formation results when the value of the product of DN*DE < 700 (111a). The product of DN*DE for methanol and acetone-15%D_2O are approximately 840 and 570, respectively. Based on the above argument, larger ^{35}Cl NMR line widths are predicted when acetone-15% D_2O is the solvent as shown in Tables II and V. A similar analysis for the ClO_4^- salts would predict that the largest ^{35}Cl NMR line widths would result when acetonitrile (DN*DE = 529) was the solvent, followed by methanol (DN*DE = 840), and lastly DMSO (DN*DE = 1392). As shown in Figures VIII and X, the largest ^{35}Cl NMR line widths were found in methanol. This study is limited by the changes in ion-solvent interactions when going from one solvent to another. These changes depend on factors other than DN and DE. It would have been helpful to include other solvents; however solubility problems existed.

FT-IR studies on Val in the presence of $KClO_4$ have been examined (96b). The amide I region which appears at 1659 cm⁻¹ has been assigned to the stretching vibration of amide

C=O groups involved in intramolecular H-bonds for Val in nonpolar solvents. A single ester carbonyl absorption is seen in chloroform. This band at 1754 cm^{-1} is characteristic of non H-bonded ester carbonyls. This band is also observed in other nonpolar solvents. Addition of KClO$_4$ to Val in CHCl$_3$, acetonitrile, carbontetrachloride, or cyclohexane results in a significant shift of both amide I and ester C=O absorption bands to lower wave lengths and a marked reduction in line width. It is known that complexation of cations to Val involve adjustments in the H-bonding network (96b). In solvents of high and medium polarity the IR spectrum of Val and KClO$_4$ was observed to be more complex. It was speculated that in high polarity solvents most intramolecular H-bonds are being broken and intermolecular H-bonds are being formed between the solvent and the ionophore. Hence, the FT-IR spectra were too complex to conclude any specific aspects of cation ionophore structure.

The change in symmetry of the perchlorate molecule from tetrahedral to C$_{3v}$ upon ion pair formation with Val is shown in figure XIVg by the splitting of the ν_3 stretching band at 1130 cm^{-1} into two bands (96b). For Las (Figure XIVh), however, the band remains unsplit indicating that the symmetry for the perchlorate molecule does not change. From the FT-IR data, K$^+$-Val appears to ion pair with ClO$_4^-$ while K$^+$-Las does not.

The effect of cation on Cl$^-$ ion pairing was examined. The selectivity of the ionophores for different cations is expected to vary from solvent to solvent. Within the same solvent, we found that Cs$^+$ and Li$^+$ interacted more strongly with Val than with Las but that Na$^+$ interacted more strongly with Las than with Val. With a radius of 1.69 Å, the Cs$^+$ ion fits snugly in the three dimensional cage like structure of Val (24). Las, on the other hand, is the smallest of the carboxylic ionophores with complexed ions sitting on rather than within the cage (24). The smaller sizes of Na$^+$ (r = 0.95 Å) and Li$^+$ (r = 0.60 Å) account for

the smaller changes in the $^{23}Na^+$ and $^7Li^+$ NMR line widths for samples containing Val compared to salt solutions alone. Based on the selectivity sequence in Table 1, ion pairing is better seen with tight metal ion binding, as with Na^+ and Cs^+, resulting in an increase in the ^{35}Cl NMR line width for samples containing Val as opposed to Las. The very low selectivity of both Val and Las for Li^+ yields very little difference in the ^{35}Cl NMR line widths.

The effect of pH on the ^{35}Cl NMR line widths of KCl in the presence of Val or Mon was also studied. By lowering the pH < 3, the carboxylic group on Mon was protonated (111b). The negative charge on Mon is lost and then interacting with K^+ an overall positively charged Mon-K^+ complex is formed. The protonated Mon-K^+ complex has the same overall charge as Val-K^+ complex and both are now expected to have similar ion pairing abilities resulting in an increase in the ^{35}Cl NMR line width. As mentioned in section IV.I.5, the ^{35}Cl NMR line width does increase for Mon from 54 Hz to 111 Hz. This indicates that the formation of an ionophore-cation with an overall charge of +1 results in an increase in the ^{35}Cl NMR line width independent of ionophore type.

The effect of ion pairing on the ^{13}C NMR spectrum of Val was also briefly examined. Addition of KCl produced only small changes in the chemical shifts and line widths of the ^{13}C NMR resonances which were attributed to cation binding (111c, 111d). This is not surprising if the cation-ionophore complex and Cl^- anion is pictured as two rotating spheres such that no specific interaction with the ionophore backbone results.

Lanthanide SRs have been successful in distinguishing between intra- and extracellular metal cation resonances in RBCs (47-57). In our efforts to obtain a possible $^{35}Cl^-$ SR, we investigated several complexes of Dy(III). Of the lanthanide SRs tested Dy(TTHA)$^{3-}$,

Dy(NOTA), and Dy(PPP)$_2^{7-}$ were the most promising. This selection was based on the data shown in Figure XVI and also on the relatively narrow line widths of ^{35}Cl$^-$ resonances observed in the presence of these complexes.

The ^{35}Cl$^-$ shifts decreased with increasing concentration of Dy(PPP)$_2^{7-}$ and Dy(TTHA)$^{3-}$. In these cases, the Cl$^-$ ion is being repelled by the highly negatively charged ligands and attracted by the positively charged lanthanide ion. Therefore, as the concentration of Dy(PPP)$_2^{7-}$ or Dy(TTHA)$^{3-}$ increases, the electrostatic repulsion increases between the negative charges on the ligand and the Cl$^-$, decreasing the observed ^{35}Cl$^-$ shifts.

The ^{35}Cl$^-$ shifts in Ln(TTHA)$^{3-}$ solutions do not appear to follow any pattern (Tables IX and X) which makes it difficult to obtain contact and pseudo contact contributions towards the observed shifts. Also, the possibility of a large bulk susceptibility contribution towards the observed ^{35}Cl$^-$ shifts in Ln(TTHA)$^{3-}$ solutions can not be ruled out (112). In order to obtain information on geometry, the SR-substrate adduct must maintain axial symmetry (51). The Ln(TTHA)$^{3-}$ SRs may violate this rule and thus information on contact and pseudo contact contributions can not be obtained directly from the analysis in section IV.2.1.1.

Dy(NOTA) has been shown by Bryden *et al.* (61) to induce large shifts in ^{35}Cl$^-$ NMR resonances. It was found however, that the shift induced by Dy(NOTA) was partially due to direct coordination of Cl$^-$ to Dy(III) (61). This may in turn affect the Cl$^-$ distribution across biological membranes, limiting the use of Dy(NOTA).

The paramagnetic shifts induced on the ^{35}Cl$^-$ resonance by transition metals Co(II) and Ni(II) are much smaller than those induced by paramagnetic lanthanides (Figure XVII). The line widths of ^{35}Cl resonance in the presence of Co(II) salts and complexes were much broader than those in the presence of Ni(II) salts tested in this study (Figure XVIII). The difference

between the paramagnetic shifts induced by lanthanides and transition metals are presumably due to the large influence of the f^7 electrons of lanthanides on the observed shift. Hence, the pseudo contact and contact shifts in the presence of lanthanides are much greater than those in the presence of transition metals. The data obtained on the shifts induced by Co(II) and Ni(II) clearly indicate that high concentration of these species are required to obtain optimal shifts in order to resolve intra- and extracellular $^{35}Cl^-$ resonances. Such high concentrations of transition metal species may result in severe impairment of physiologic functions.

Dy(TTHA)$^{3-}$, Dy(PPP)$_2^{7-}$, and Dy(NOTA) were tested for possible use as SRs in LUVs, frog leg muscle tissue, and intact RBCs. It was not possible to obtain separation between intra- and extracellular Cl$^-$ resonances in the above systems. It was observed that Cl$_{in}^-$ LUVs experienced a chemical shift without incorporation of a SR. This can be attributed to magnetic susceptibility. Any nuclei in a compartment senses an induced magnetic field. This induced field depends on the volume of the medium inside the component, shape of the compartment, its orientation relative to the applied field, and does not depend on the presence of any paramagnetic substances (112). In vesicle preparations there exists aggregation, non-uniformity of size, and possible fragmentation. These factors contribute to additional susceptibility, resulting in a change in chemical shift.

Several procedures including inhibition of Cl$^-$ channels with DIDS, reduction of paramagnetic centers in Hb and SOD, and lowering the sample temperature were attempted to slow down the known high rate of Cl$^-$ exchange in biological systems. It was hoped that these modifications would render the lanthanide SRs effective in separating the intra- and extracellular Cl$^-$ resonances. The lanthanide SRs were not found to directly bind to the membranes, making their use more physiologically useful. Despite all the attempted

procedures, the separation of intra- and extracellular resonances remains elusive.

The Cl⁻ has been shown to exchange rapidly across biological membranes (113). For slowly exchanging species $k << (\nu_A - \nu_B)$, where k is the first order rate constant describing the transport between two sites and ν_A and ν_B are the two resonances frequencies. For fast exchange $k >> (\nu_A - \nu_B)$. Based on an average ^{35}Cl⁻ NMR chemical shift of 5 ppm the separation between the two Cl⁻ pools is 150 s^{-1}. The magnitude for the rate of Cl⁻ influx in intestinal cells was reported to be in the order of 10^6 s^{-1} (114). From this it can be seen that $k >> (\nu_A - \nu_B)$ and thus, the Cl⁻ is in fast exchange on the NMR time scale and the two resonances for intra- and extracellular pools may not be easily distinguishable. In an attempt to obtain larger shifts as suggested by the above calculation, it was decided to try other non-lanthanide complexes for possible SRs. CoCl$_2$ solutions do cause larger ^{35}Cl⁻ shifts as reported by Shulman *et al.* (62). Upon addition of the SR containing extracellular suspension to LUVs the shift for the extracellular resonance was less than expected based on standard rho plots (Figure XVII). The decrease in chemical shift was believed to result from the binding of Co(II) to the negatively charged phospholipids in the vesicle membrane (Figure XIX). As the Co(II) interacted with the membrane less Co(II) was available to shift the extracellular Cl⁻. A similar decrease in ^{35}Cl⁻ chemical shift was also observed for Co(acac)$_2$ (Figure XX). It was hoped that the bulky acac ligand would prevent the Co(II) membrane interaction. The addition of NaCl LUVs to the Co(acac)$_2$ suspensions decreased the ^{35}Cl⁻ shift from 38 ppm to 27 ppm. The low stability of Co(acac)$_2$, logK $\approx$ 5 (97), allows for some Co(II) to exist freely in solution further reducing the amount of Co(II) available to interact with the extracellular Cl⁻.

As mentioned in the Chapter 1, intracellular Cl⁻ in human RBCs was reported to be

invisible due to binding with Hb (1). For this reason all SR experiments were conducted on

ghosts, muscle tissue, and vesicles. Recently, the paramagnetic Cu(II) center of Cu,Zn-

superoxide dismutase was found to strongly affect the F^- relaxation rates (98). The addition

of diethyldithiocarbamate (DDC) was found to reduce the paramagnetic Cu(II) center in

Cu,Zn-superoxide dismutase increasing both T_1 and T_2 of F^- in RBCs (98). The effect of

DDC treated RBCs on the visibility of intracellular $^{35}Cl^-$ was tested. DDC treated packed

RBC were prepared and the corresponding ^{35}Cl NMR spectrum recorded. The addition of

DDC failed to increase the visibility of intracellular Cl^-. After washing the DDC treated

RBCs (Figure XXI) with isotonic $NaNO_3$, the ^{35}Cl NMR spectrum was rerecorded. No ^{35}Cl

NMR resonance was observed indicating that the $^{35}Cl^-$ peak in Figure XXI for DDC-treated

RBCs may be due to trapped Cl^-.

In many systems, ionophores have been employed to alter the permeability of cellular

membranes to specific cations and shift the electrochemical gradient across the membrane

(115-117). Changes in phospholipid turnover have been observed after ionophore treatment

(100, 116, 118). The changes in chloride distribution, as a result of Cl^- efflux, and membrane

potential obtained in this study upon treating RBCs with various ionophores clearly indicate

the role of cation and anion distribution in maintaining cell membrane potential. Since the

transmembrane potential in the erythrocyte is dependent on the distribution of chloride and

potassium across the membrane under normal conditions, manipulations in cell volume and

ion distribution may either alter the distribution of chloride and potassium or alter the relative

permeabilities of chloride and potassium, resulting in hyperpolarization of the membrane (117,

119-122).

Our results indicate that Mn^{2+} and Val induce Cl^- transport across the cell membrane

in opposite directions. The presence of $MnCl_2$ in vesicle suspensions presumably masked the effect of Val on Cl^- transport (60).

In RBCs pretreated with DIDS, chloride transport via the Band 3 protein is inhibited (122-123). However, it has been shown that approximately one third of the transmembrane movement of chloride in erythrocytes is independent of the Band 3 (123). Hence, the TFA ratio changes observed in the presence of Val and DIDS in this study (Table XIII) clearly suggest that Val induces changes in chloride distribution which are independent of Cl^- transport via the band 3 protein. The changes in Cl^- distribution, as monitored by ^{19}F and ^{31}P NMR spectroscopy, induced by the addition of Val or Non to a human RBC suspension are presumably associated with Cl^- efflux by a pathway that involves ion pairing between Cl^- and K^+-Val or K^+-Non complexes. However, ionophore-induced Cl^- transport by other mechanisms, such as K^+-Cl^- cotransport or Cl^- leak, cannot be ruled out.

V.2   Multinuclear NMR Study of Cs^+ in Biological Systems

It is known that the resonances of monovalent alkali metal ions are shifted in the presence of lanthanide SRs (51-53, 124). The direction of the observed shifts for extracellular $^{133}Cs^+$ resonances in the presence of SRs is dependent on the angle of orientation of the Cs^+ with the principal axis of the lanthanide ion. It is clear from Figure XXIII that SRs are not needed for separation of the chemical shifts of intra- and extracellular $^{133}Cs^+$ NMR resonances in Cs^+-loaded RBC suspensions. The positions of the intra- and extracellular ^{133}Cs signals in the presence of SRs (Figures XXIIIB through XXIIID) were inverted relative to the positions when no shift reagent was used (Figure XXIIIA). The Cs^+ shifting properties of $Dy(PPP)_2^{7-}$ are unique in that for all other alkali metal ions, $Dy(PPP)_2^{7-}$ shifts the extracellular resonance

in the upfield direction (50, 54). However, Dy(TTHA)$^{3-}$ and Tm(DOTP)$^{5-}$ shift the extracellular Cs$^+$ resonance downfield, as for the other alkali metal cations (50, 54, 125). Moreover, the magnitude of the ^{133}Cs$^+$ shift induced by Dy(PPP)$_2^{7-}$ was considerably smaller than those caused by Dy(TTHA)$^{3-}$ and Tm(DOTP)$^{5-}$, at the same SR concentrations. In contrast, for other alkali and alkaline earth metal ions, the magnitude of the shifts induced by Dy(PPP)$_2^{7-}$ is considerably larger than those caused by Dy(TTHA)$^{3-}$, but only slightly larger than those induced by Tm(DOTP)$^{5-}$, at the same SR concentrations (50, 54, 125). The very large ^{133}Cs$^+$ shifts induced by Tm(DOTP)$^{5-}$ are presumably associated with the large size of the Cs$^+$ cation and its binding via four phosphonate oxygens close to the Tm^{3+} ion and near the cone axis.

The downfield ^{133}Cs$^+$ shift induced by Dy(PPP)$_2^{7-}$ is probably related to the large ionic radius of the Cs$^+$ cation and its location in the equatorial region formed by the dipolar cone angle around the effective magnetic axis of the SR (126). Addition of Na$^+$ to Cs$^+$/SR solution removed the Cs$^+$ ions from the Na$^+$ preferred sites and caused an increase in the downfield ^{133}Cs$^+$ shift. However, addition of Cs$^+$ to Na$^+$/SR solution caused a relatively large upfield ^{23}Na$^+$ shift, presumably because Cs$^+$ binds to both sides of the cone, with only some weak preference for the equatorial side. Thus, the Na$^+$/Cs$^+$ competition experiments indicate that Na$^+$ and Cs$^+$ have distinct binding sites on Dy(PPP)$_2^{7-}$, with Na$^+$ clearly preferring the axial portion outside the dipolar cone and binding strongly to the SR, whereas Cs$^+$ binds weakly to the equatorial portion inside the cone.

The steady-state transmembrane Cs$^+$ ratio ($[Cs^+]_{in}/[Cs^+]_{out}$) for Cs$^+$-loaded RBC suspensions measured in the presence of Dy(PPP)$_2^{7-}$ was higher than the ratios measured in its absence or in the presence of Dy(TTHA)$^{3-}$ or Tm(DOPT)$^{5-}$. More extracellular Na$^+$ ions

are presumably bound to $Dy(PPP)_2^{7-}$ because Na^+ ions are present at a 10-fold excess relative to extracellular Cs^+ ions. Moreover, the affinity of Na^+ ions for $Dy(PPP)_2^{7-}$ is probably stronger than that of Cs^+ ions because of the smaller ionic size of the Na^+ ions (54b, 127). The incorporation of $Dy(PPP)_2^{7-}$ in a Cs^+-loaded RBC suspension leads to more binding of Na^+ ions, which, in turn, may cause an efflux of intracellular Na^+ ions. The efflux of intracellular Na^+ ions is partially compensated by an influx of extracellular Cs^+ ions, leading to higher and lower values of transmembrane Cs^+ and Na^+ ratios, respectively, in Cs^+-loaded RBC suspensions in the presence of the triphosphate SR. The specific effect of $Dy(PPP)_2^{7-}$ on the Cs^+ distribution ratio is presumably due to the higher charge of this SR, because it was absent in the $Dy(TTHA)^{3-}$ containing RBC suspensions. This SR-specific effect on the Cs^+ distribution across the RBC membrane is in agreement with the higher and lower transmembrane Li^+ and Na^+ ratios, respectively, previously reported for Li^+-loaded RBC suspensions containing $Dy(PPP)_2^{7-}$ (57).

The contribution of each intracellular component (Table XIV) and of the RBC membrane toward the observed chemical shift of the intracellular ^{133}Cs NMR resonance in Cs^+-loaded CORBC suspensions was investigated. At concentrations close to physiologic values for ATP, ADP, DPG, and P_i, DPG gave the largest downfield $^{133}Cs^+$ shift of all the intracellular phosphates tested. We also measured the $^{133}Cs^+$ shifts for samples containing the same concentration (2.0 mM) of each intracellular phosphates and found that the interaction of Cs^+ with DPG was not due to an elevated DPG concentration relative to that of other intracellular phosphates in RBC. We also found evidence for a Cs^+-DPG interaction in the presence of competing cations and in samples whose viscosity was adjusted to that of the intracellular RBC compartment (Table XIV). In the absence of DPG, preparations of unsealed

RBC membranes gave no significant $^{133}Cs^+$ shifts or line broadening. It was concluded that the RBC membrane is not responsible for the downfield shift of the intracellular $^{133}Cs^+$ resonance observed in Cs^+-loaded RBC suspensions. The chemical shift of the $^{133}Cs^+$ resonance is known to be sensitive to the nature of the counteranion present in solution (79). The anion present at the highest concentration in RBCs is Cl^-. However, the Cl^- concentrations inside and outside RBCs are approximately the same and are unlikely to give be responsible for the observed resolution of ^{133}Cs NMR resonances in Cs^+-loaded RBC suspensions (Figure XXIIIA). In contrast, biological phosphates are present only in the intracellular compartment. It was therefore concluded that Cs^+ binding to intracellular phosphates, and to DPG in particular, contribute strongly to the appearance of two ^{133}Cs resonances in Cs^+-loaded RBC suspensions.

Magnetic susceptibility is known to be an important, albeit small, contributor to the observed chemical shifts of NMR resonances in biological samples. The effects of magnetic susceptibility on chemical shifts have sometimes been the cause of serious misinterpretation of data (92, 104, 107, 112, 128-133). Cell suspensions consist of two compartments, intra- and extracellular. If the intracellular compartment is spherical, the nuclei inside and outside the cells experience the same magnetic field, and thus there is no chemical shift difference between intra- and extracellular NMR resonances. For any nonsymmetric geometry, a chemical shift difference may be observed. The bulk magnetic susceptibility (BMS) contribution to the chemical shift depends on the volume susceptibility of the medium inside and outside the cells, the cell morphology, and the relative orientation of the sample with respect to the externally applied magnetic field (53, 112). When NMR experiments are carried out with superconducting magnets as in the case of this study, paramagnetic substances

have a positive susceptibility which generates a downfield shift, and diamagnetic substances have a negative susceptibility which generates an upfield shift (92, 104, 112). Because the direction and magnitude of the BMS shifts are dependent on the alignment of the magnetic moments of the individual nuclei with the applied magnetic field, the BMS shifts are of opposite sign in superconducting and in electromagnets (92, 104, 112). The effects of BMS can be changed in a sample by incorporation of a paramagnetic substance, such as a shift reagent, in the suspension medium (92, 104, 112).

In its deoxygenated form, Hb is paramagnetic (128-130), inducing a magnetic susceptibility difference between the intra- and extracellular compartments in deoxyRBC suspensions. The magnetic field gradient across the RBC membrane effects both broadening and downfield shifts of the ^{31}P resonances (92, 104). Upon incorporation of a SR in the suspension medium, the magnetic field gradient is decreased, and consequently the line widths sharpen and the chemical shifts move upfield (92, 104). In contrast to deoxyHb, COHb is diamagnetic (128-130). When a SR is incorporated in a CORBC suspension, a significant magnetic field gradient is generated across the cell membrane, causing broadening and downshifting of the ^{31}P NMR resonances. The magnetic susceptibility contribution of hemoglobin to the intracellular ^{31}P and ^{133}Cs$^+$ shifts was examined by comparing ^{31}P and ^{133}Cs NMR spectra of deoxyRBC and CORBC suspensions. Whereas deoxyRBC suspensions gave broad and downfield-shifted ^{31}P resonances for DPG and ATP, the corresponding resonances were sharp and were shifted upfield in CORBC suspensions (Table XV). The degree of oxygenation of Cs$^+$-free RBC suspensions as characterized by ^{31}P NMR parameters was in agreement with that previously reported (92, 104). The presence of 5 mM Dy(TTHA)$^{3-}$ in the suspension medium partially inverts the magnetic field gradient across the RBC membrane

in suspensions of Cs^+-loaded deoxyRBCs because the two compartments now feel a similar magnetic susceptibility. In contrast, incorporation of 5 mM $Dy(TTHA)^{3-}$ in the medium of Cs^+-loaded CORBCs leads to enhancement of the magnetic field gradient across the RBC membrane. Thus, magnetic susceptibility differences between the intra- and extracellular compartments are responsible for the chemical shift and line width changes observed in the ^{31}P NMR resonances of Cs^+-loaded RBC samples, as previously reported for SR-treated Cs^+-free RBC suspensions (92, 104).

Just like ^{31}P NMR resonances of intracellular phosphates, the intra- and extracellular $^{133}Cs^+$ NMR resonances of Cs^+-loaded RBC suspensions in the absence of SR were broadened and downshifted upon deoxygenation (Table XVI). Similarly to what was observed with ^{31}P NMR resonances, upon deoxygenation the presence of SR in the medium led to sharpening and an upfield shift of the intracellular $^{133}Cs^+$ NMR resonance. The chemical shift and line width changes observed for the intra- and extracellular $^{133}Cs^+$ NMR resonances that occurred upon deoxygenation or upon incorporation of SR in the medium were also small, but were not equal to those observed for ^{31}P NMR resonances of intracellular phosphates. The large effects of SR on the chemical shift and line width of the extracellular $^{133}Cs^+$ resonance are associated with the paramagnetism of the SR and are not due to magnetic susceptibility properties of the SR-treated samples. Unless a significant inhomogeneity component is present, magnetic susceptibility affects the resonance frequency of all nuclei equally. Thus, for a RBC suspension placed in a superconducting magnet, the magnetic susceptibility contribution toward the $^{133}Cs^+$ and ^{31}P shifts should be approximately the same. However, because inhomogeneity effects are present in blood samples (134), there may also be a contribution of the gyromagnetic ratios of ^{133}Cs and ^{31}P toward the observed BMS shift (112). At a constant

magnetic field, nuclei with a higher resonance frequency show stronger line broadening effects (104). It is therefore not surprising that broadening effects were less pronounced in ^{133}Cs than in ^{31}P resonances. The chemical shift separation between intra- and extracellular $^{133}Cs^+$ NMR resonances changed by not more than 0.6 ppm upon deoxygenation of Cs^+-loaded RBCs in the presence or absence of SR. Even when diamagnetic or paramagnetic susceptibility differences are present across the RBC membrane, as confirmed by ^{31}P NMR spectroscopy (92, 104), a clear separation between intra- and extracellular $^{133}Cs^+$ NMR resonances is observed in Cs^+-loaded RBC suspensions. If magnetic susceptibility effects alone were responsible for the resolution of ^{133}Cs NMR resonances in Cs^+-loaded CORBC suspensions, one would predict that intracellular ^{133}Cs NMR resonances would be shifted upfield from extracellular $^{133}Cs^+$ NMR resonances when recording the spectrum using a superconducting magnet (92, 104). Because the relative positions of the $^{133}Cs^+$ NMR resonances observed in Cs^+-loaded RBC suspensions are the opposite of those predicted, it was concluded that magnetic susceptibility effects are not responsible for the resolution of $^{133}Cs^+$ NMR resonances in human RBC suspensions.

In suspension medium alone or in packed cells, only one $^{133}Cs^+$ resonance was observed. However, the chemical shifts of the $^{133}Cs^+$ resonances observed either in suspension medium alone ($\delta_{out} = 1.0$ ppm; Ht = 0) or in packed cells ($\delta_{in} = 2.6$ ppm; Ht = 95%) differed significantly from those observed in Cs^+-loaded RBC suspensions of intermediate hematocrit (Figure XXIV). Dependence of ^{31}P chemical shifts on hematocrit was also observed for triethylphosphate, dimethyl methylphosphonate, and hypophosphite in oxygenated RBC suspensions (131). As the Ht increases, the diamagnetic susceptibility of the sample increases as a result of an increase in COHb concentration. An increase in diamagnetic

susceptibility with increasing Ht is associated with a decrease in BMS and, with a superconducting magnet, is expected to generate upfield shifts. However, downfield (as opposed to upfield) $^{133}Cs^+$ shifts of intra- and extracellular resonances were observed with increasing Ht (Figure XXIV). Clearly, an effect independent of magnetic susceptibility is responsible for the upfield $^{133}Cs^+$ shifts observed in Cs^+-loaded RBC suspensions. As the Ht decreases, the intracellular Cs^+ concentration also decreases, presumably because the rate of Cs^+ efflux from Cs^+-loaded RBCs is higher at low hematocrits. Thus, at high Ht values there is more interaction between Cs^+ and intracellular phosphates, leading to downfield $^{133}Cs^+$ shifts.

Theoretical calculations based on concentric cylindrical compartments with independent magnetic susceptibilities have predicted that the diamagnetic susceptibility of COHb should result in intracellular resonances that are 0.12 ppm upfield from extracellular resonances (92, 104). However, a recent calculation (131) that took into account the interdependence of the magnetic susceptibilities of the two cellular compartments has shown that the contribution of magnetic susceptibility effects toward the chemical shift separation between intra- and extracellular resonances in RBC suspensions is dependent on Ht and is less (0.06 ppm, Ht = 100%; 0.08 ppm; Ht = 0) than that previously predicted (0.12 ppm). The observed chemical shift separation between intra- and extracellular $^{133}Cs^+$ resonances in Cs^+-loaded RBC suspensions was weakly dependent on Ht, as expected (0.80 ppm, Ht = 1; 1.20 ppm, Ht = 0). However, the observed transmembrane chemical shift differences observed with $^{133}Cs^+$ resonances were much larger than those predicted. It was concluded that an effect independent of magnetic susceptibility is responsible for the clear resolution and the relative positions of the $^{133}Cs^+$ NMR resonances in Cs^+-loaded CORBC suspensions of intermediate

hematocrit.

An increase in osmolarity of the suspension medium leads to an efflux of intracellular water and a decrease in mean cell volume (132). The resulting increase in COHb concentration gives rise to an increase in the diamagnetic susceptibility of the sample with increasing osmolarity. An increase in diamagnetic susceptibility with increasing osmolarity is associated with a decrease in BMS and, with a superconducting magnet, is expected to lead to upfield shifts. However, a downfield (as opposed to upfield) $^{133}Cs^+$ shift, due to a magnetic susceptibility independent effect, of the intracellular resonances was observed with increasing osmolarity (Figure XXV). At low osmolarity values, partial cell lysis and a decrease in ionic strength may account in part for the magnitude of the $^{133}Cs^+$ shifts. The small upfield $^{133}Cs^+$ shift of the extracellular resonance with increasing osmolarity is presumably due to an increase in the BMS of the extracellular compartment, as previously reported for ^{31}P resonances of phosphoryl compounds in RBC suspensions (132). The chemical shift separation between intra- and extracellular $^{133}Cs^+$ resonances increased with osmolarity in Cs^+-loaded RBC suspensions. Similar increases in ^{31}P and ^{19}F NMR resonances were reported for phosphoryl compounds and difluorophosphate in RBC suspensions (107, 132). As the mean cell volume decreases with increasing osmolarity of the suspension medium, the intracellular concentrations of both biological phosphates and Cs^+ are increased. Since the concentration ratios of Cs^+ to biological phosphates are maintained at different mean cell volumes, the increasing downfield shifts of the intracellular $^{133}Cs^+$ resonance observed with increasing osmolarity are due not to Cs^+ interactions with biological phosphates, but to a magnetic susceptibility independent effect (vide infra). It was concluded that volume susceptibility is not responsible for the resolution and relative positions of the intra- and extracellular $^{133}Cs^+$ resonances

originating from Cs$^+$-loaded CORBCs that are suspended in media of varying osmolarity.

The high concentration of COHb present at high CORBC concentration should lead to an increase in the diamagnetic susceptibility of the sample. An increase in diamagnetic susceptibility with increasing RBC lysate concentration is associated with a decrease in BMS and, with a superconducting magnet, is expected to lead to small upfield shifts (0.12 ppm) (92, 131). Such small upfield ^{31}P NMR shifts were, in fact, observed for triethyl phosphate (131). Downfield ^{133}Cs$^+$ shifts were observed with increasing CORBC lysate concentration (Figure XXVI). The ^{133}Cs$^+$ NMR measured shifts in RBC lysate samples relative to 0.15 M CsCl placed in a spherical bulb are independent of changes in magnetic susceptibility of the RBC lysate sample (106, 107, 132). It was concluded that a magnetic susceptibility independent effect was responsible for the downfield ^{133}Cs$^+$ shifts observed in CORBC lysate samples. Precedents for magnetic susceptibility independent contributions towards ^{31}P and ^{19}F chemical shifts in CORBC lysate samples have also been reported for phosphoryl compounds and difluorophosphate (107, 131-133).

To determine the contribution of the non-ideality of water to the intracellular ^{133}Cs$^+$ shift, we measured ^{133}Cs$^+$ chemical shifts and line widths in the presence of increasing concentrations of COHb and lysozyme (Figure XXVII). To eliminate the diamagnetic susceptibility contribution in the protein samples, we measured the chemical shifts relative to CsCl placed in a spherical bulb/cylindrical capillary reference assembly. The finding that increasing concentrations of two unrelated proteins (COHb and lysozyme) caused similar downfield ^{133}Cs$^+$ shifts suggests that the observed intracellular ^{133}Cs$^+$ shifts in Cs$^+$-loaded RBCs are controlled by a general property of proteins and not by a specific property of Hb. Similar observations were reported for ^{31}P chemical shifts of phosphoryl compounds in the

presence of either COHb or lysozyme (133). The isoelectric point of hemoglobin is higher than that of lysozyme. At the neutral pH used in our experiments, COHb has a higher overall anionic charge than lysozyme. Nonspecific weak Cs^+ binding is therefore expected to be more important for COHb than for lysozyme. The general property of proteins responsible for the $^{133}Cs^+$ shifts is unlikely to be viscosity because the $^{133}Cs^+$ chemical shift changes measured in PVP-100 samples were significantly smaller than those measured in the presence of samples of COHb or lysozyme with the same viscosity (Figure XXVIII). The line widths of the $^{133}Cs^+$ resonances in the presence of COHb, lysozyme, or PVP-100 at the same viscosity were essentially the same, indicating that specific Cs^+ binding to COHb is not responsible for the observed downfield shifts of intracellular $^{133}Cs^+$ resonances in Cs^+-loaded CORBC suspensions.

In the extracellular compartment, the Cs^+ ion is coordinated to water ligands. In the intracellular compartment, however, hemoglobin is surrounded by ordered water of hydration. Thus, hemoglobin disrupts the hydrogen bonding network inside RBCs, leading to non-ideality of intracellular water. Intracellular Cs^+ presumably penetrates the ordered hydration phase of hemoglobin. The number of water ligands available for coordination to intracellular Cs^+ is smaller than to extracellular Cs^+. A decrease in electron shielding of intracellular Cs^+ should result in a downfield shift of the intracellular $^{133}Cs^+$ resonance, as observed. The downfield shifts of intracellular $^{133}Cs^+$ NMR resonances resemble the downfield shifts of ^{19}F NMR resonances of intracellular trifluoroacetate and difluorophosphate in RBC suspensions (95, 107). In contrast, the downfield shifts of intracellular $^{133}Cs^+$ are in the opposite direction of the upfield shifts of ^{31}P NMR resonances observed for intracellular phosphoryl compounds and difluorophosphate (107, 132, 133). Water coordinates to Cs^+ via oxygen atoms whereas

it coordinates to F via hydrogen atoms. In both cases hydrogen bonding results, however, in deshielding of the ^{133}Cs and ^{19}F nuclei. The dependence of the chemical shift of intracellular ^{133}Cs$^+$ on the non-ideality of water is consistent with the strong dependence of ^{133}Cs chemical shifts on the nature of the solvent (79).

Therefore, we conclude that the chemical shift separation of ^{133}Cs$^+$ NMR resonances in Cs$^+$-loaded RBC suspensions stems mostly from binding of Cs$^+$ to intracellular phosphates (in particular DPG) and, to a smaller extent, to the non-ideality of intracellular water and the magnetic susceptibility effects induced by hemoglobin.

The increase in the line widths of all ^{13}C and ^{31}P NMR resonances of DPG upon addition of Cs$^+$ is consistent with Cs$^+$ enhancement of the spin-spin relaxation times of the three ^{13}C and two ^{31}P resonances of DPG (Table XVII). Therefore, the interaction of the Cs$^+$ ion with DPG most likely involves the carboxylic group on carbon 1 and each of the phosphate groups on carbons 2 and 3 of DPG. The chemical shifts of the ^{13}C and ^{31}P NMR resonances of DPG did not change upon addition of Cs$^+$, presumably because the interaction with the carboxylate and phosphate groups of DPG occurs via the oxygen atoms and not directly with the reporter nuclei. From our ^{31}P and ^{133}Cs NMR results (Tables XIV and XVII), we conclude that Cs$^+$ interacts more strongly with DPG than with ADP or ATP. Cs$^+$ forms a 1:1 complex with DPG with a K_D of 3.8 mM (Figure XXIX). This Cs$^+$ interaction is unique because DPG is reported to bind Mg^{2+}, Zn^{2+}, and Al^{3+} more weakly than does either ADP or ATP, despite the presence of two basic phosphates (108, 135, 136). The stronger interaction of Cs$^+$, relative to Na$^+$ (137), with DPG may be related to the larger ionic size of Cs$^+$ and to the capacity of DPG to act as a tridentate ligand. We conclude from our ^{31}P and ^{13}C NMR data (a) that Cs$^+$ interacts with the phosphate and carboxylate groups of DPG,

and (b) that the competing ions decrease the observed Cs^+ interaction with DPG.

Comparison of ^{31}P NMR spectra of Cs^+-loaded and Cs^+-free RBC suspensions (Table XV) indicated that Cs^+ loading broadened and moved the ^{31}P resonances of DPG (and to a smaller extent the resonances of ATP and P_i) upfield in deoxyRBC, but not in CORBC suspensions. Deoxygenation did not cause any significant changes in the peak areas of the ^{31}P resonances of DPG in Cs^+-loaded or Cs^+-free RBC suspensions (data not shown). This lack of change in DPG levels upon deoxygenation is in agreement with previous reports (102a, 138). DPG binds more strongly to deoxyhemoglobin than to oxyhemoglobin (or its analogue, COHb) (102a, 109). Moreover, Mg^{2+} binds to DPG more strongly in CORBC than in deoxyRBC suspensions. Although less free DPG is available in deoxygenated RBC suspensions to bind Cs^+, DPG is not complexed as fully to Mg^{2+} (102a). Because the affinity of DPG for Mg^{2+} is higher than that for $Cs+$ (108), binding of Cs^+ to free intracellular DPG occurs most strongly in deoxyRBC suspensions. This may explain why the effect of Cs^+ loading in ^{31}P resonances of DPG is more noticeable in deoxyRBC than in CORBC suspensions (Table XV). Competition between Cs^+ and hemoglobin for DPG will have the result that smaller amounts of DPG are available to bind to deoxyHb, which, in turn, will result in an increase in the oxygen affinity of hemoglobin. The enhanced oxygen affinity of hemoglobin in the presence of Cs^+ may hinder the release of oxygen to tissues and may provide a mechanism for Cs^- toxicity.

BIBLIOGRAPHY

1.   Brauer M, Spread CY, Reibmeir R, and Sykes D (1985) ^{31}P and ^{35}Cl Nuclear Magnetic Resonance Measurements of Anion Transport in Human Erythrocytes. J. Biol. Chem. 260: 11643.

2.   Olsen RWM (1981) GABA Benzodiazepine Barbiturate Receptor Interaction. J. Neurochem. 37: 1.

3.   L'Allemain G, Paris S, and Poussegur J. (1985) Role of a Na^+-dependent Cl^-/HCO_3^- Exchange in Regulation of Intracellular pH in Fibroblasts. J. Biol. Chem. 260: 4877.

4.   Olsens S, Tonnessen TI, and Sandvig K. (1986) pH Regulated Anion Transport in Nucleated Mammalian Cells. J. Cell. Biol. 102: 967.

5.   Owen NE, and Prastein, ML. (1985) Sodium Potassium and Chloride Cotransport in Cultured Human Fibroblasts. J. Biol. Chem. 260: 1445.

6.   Lin P and Gruenstein E. (1988) Pathways of Chloride Transport in Human Fibroblasts. Am. J. Physiol. 24: C112.

7.   MacKnight ADC. (1985) The Role of Anions in Cell Volume Regulation. Pfluegers Arch. 405: 12.

8.   Hoffman EK. (1986) Anion Transport System in the Plasma Membrane of Vertebrate Cells. Biochim. Biophys. Acta. 864: 1.

9.   Pato CN, Davis MH, Doughty MJ, Bryant SH, Gruenstein E. (1983) Increased Membrane Permeability to Chloride Duchenne Muscular Dystrophy Fibroblasts and its Relationship to Muscle Function. Proc. Natl. Acad. Sci. USA 80: 4732.

10.   Bryant SH. (1982) In "Disorders of the Motor Unit"; Schotland DL. ed. Wiley, New

York, 381.

11. Newark P. (1985) Testing for Cystic Fibrosis. <u>Nature</u> <u>318</u>: 309.

12. (a) Goodfellow PN. (1987) Cystic Fibrosis: Classical and Reverse Genetics. <u>Nature</u> <u>326</u>: 824. (b) Anderson MP, Gregory RJ, Thompson S, Souza DW, Paul S, Mulligan RC, Smith AE, and Welsh MJ. (1991) Demonstration That CFTR is a Chloride Channel by Alteration of its Anion Selectivity. <u>Science</u> <u>253</u>: 202.

13. Murphy, S.(1987) Cystic Fibrosis in Adults: Diagnosis and Management. <u>Clin. Chest. Med.</u> <u>80</u>: 695.

14. Quinton PM and Bijman I. (1983) Higher Bioelectric Potential Due to Decreased Chloride Absorption in the Sweat Glands of Patients with Cystic Fibrosis. <u>N. Engl. J. Med.</u> <u>308</u>: 1185.

15. Quinton PM. (1983) Chloride Impermeability in Cystic Fibrosis. <u>Nature</u> <u>301</u>: 421.

16. Bijman J and Quinton P. (1987) Permeability Properties of Cell Membranes and Tight Junctions of Normal and Cystic Fibrosis Sweat Ducts. <u>Pflugers Arch</u> <u>408</u>: 505.

17. Sato K and Sato F. (1984) Defective Beta Adrenergic Response of Cystic Fibrosis Sweat Glands in vivo and in vitro. <u>J. Clin. Invest.</u> <u>73</u>: 1763.

18. Knowles M, Gatzy J, and Boucher R. (1981) Increased Bioelectric Potential Difference Across Respiratory Epithelia in Cystic Fibrosis. <u>N. Engl. J. Med.</u> <u>305</u>: 1489.

19. Knowles M, Gatzy J, and Boucher R. (1983) Relative Ion Permeability of Normal and Cystic Fibrosis Nasal Epithelium. <u>J. Clin. Invest</u> <u>71</u>: 1410.

20. Knowles M, Sutts MJ, Spock A, Fischer NL, Gatzy J, and Boucher R. (1983) Abnormal Ion Permeation Through Cystic Fibrosis Respiratory Epithelium. <u>Science</u> <u>221</u>: 1067.

21. Lauger P. (1985) Mechanism of Biological Ion Transport-Carriers, Channels, and Pumps in Artificial Lipid Membranes. Angew. Chem. Int. Ed. Engl. 24: 905.

22. Hilgenferd R and Saenger W. (1982) In "Topics in Current Chemistry"; Boschke FL. ed. Springer Verlag, Berlin, 101: 1.

23. Easwaran KRK. (1985) In "Metal Ions in Biological Systems: Antibiotics and their Complexes"; Sigel H. ed. 19: 109.

24. Pressman BC. (1976) Biological Applications of Ionophores. Ann. Rev. Biochem. 45: 925.

25. Degani H. (1983) Antibiotic Ionophores. In "NMR of Newly Accessible Nuclei"; Laszlo P. ed. Academic Press, New York, 1: 249.

26. Patel DJ. (1973) Carbon Framework of Valinomycin and its Metal Ion Complex in Solution. Biochemistry 12: 496.

27. Haynes DH, Pressman BC, and Kowalsky A. (1971) A Nuclear Magnetic Resonance Study of $^{23}Na^+$ Complexing by Ionophores. Biochemistry 10: 852.

28. Prestegard JH and Chan SI. (1970) Proton Magnetic Resonance Studies of the Cation Binding Properties of Nonactin. II. Comparison of the Sodium Ion, Potassium Ion, and Cesium Ion Complexes. J. Am. Chem. Soc. 92: 4440.

29. Grell E and Funck T. (1973) Carbon-13 Nuclear-Magnetic-Resonance and Infrared-Absorption Spectroscopy of Valinomycin and Its Alkali-Ion Complexes. J. Biochem. 34: 415.

30. (a) Yoshikawa K and Terada H. (1981) Effective Enhancement of Valinomycin-Mediated Potassium Uptake in Organic Phase by Uncouplers of Oxidative Phosphorylation by ^{1}H NMR. J. Am. Chem. Soc 103: 7788. (b) Bennekou B. (1984)

K$^+$-Valinomycin and Chloride Conductance of the Human Red Cell Membrane Biochim. Biophys. Acta 776: 1.

31.   Hladky, SB and Rink TJ. (1976) Potential Difference and the Distribution of Ions Across the Human Red Blood Cell Membrane: A Study of the Mechanism by which the Fluorescent Cation, diS-C$_3$-(5) Reports Membrane Potential. J.Physiol. 263: 287.

32.   Marcus Y. (1985) In " Ion Solvation"; John Wiley and Sons, New York, 184.

33.   Detellier C. (1983) Alkali Metals. In "NMR of Newly Accessible Nuclei". Laszlo P., ed. Academic Press: New York 2: 105.

34.   Berman HA and Stengle TR. (1975) Contact Ion Pairing of the Perchlorate Ion. A Cl-35 Nuclear Magnetic Resonance Study. 1. Solutions in Pure Solvents. J. Phys. Chem. 79: 1001.

35   James DW. (1985) In "Progress in Inorganic Chemistry"; Lippard S. ed. John Wiley and Sons, New York, 33: 353.

36   Boone DJ and Kowalsky A. (1974) Ion Pair of Ionophore Complexes. Nuclear Magnetic Resonance Studies with Paramagnetic Anions. Biochemistry 13: 731.

37.   Illsley NP and Verkman AS. (1987) Membrane Chloride Transport Measured using a Chloride Sensitive Probe. Biochemistry 26: 1215.

38.   Krapf R, and Berry CA, and Verkman AS. (1988) Estimation of Intracellular Cl$^-$ Activity in Isolated Perfused Rabbit Proximal Convoluted Tubules Using a Fluorescent Indicator. Biophys. J. 53: 955.

39.   Amman D. (1986) In "Ion-selective Microelectrodes"; Springer Verlag, Berlin, 1.

40.   Thomas RC. (1977) The Role of Bicarbonate, Chloride, and Sodium Ions in the Regulation of Intracellular pH in Snail Neurons. J. Physiol (London) 273: 317.

41. Zeuthen T. (1980) How to Make and Use Double Barreled Ion-selective Microelectrodes. Curr. Top. Membr. Transp. 13: 31.

42. Thomas RC. (1985) Eccentric Double Micropipette Suitable for both pH_i Microelectrodes and for Intracellular Ionophoresis. J. Physiol. (London) 371: 24.

43. Alvarek-Leefmans FJ, Giraldez F, and Russel, JM. (1990) In "Chloride Channels and Carriers in Nerve, Muscle, and Glial Cells"; Leefmans FJ and Russel JM. ed. Plenum Press, New York, chapter 1, 3.

44. Chen PY and Verkmann AS. (1988) Sodium Dependent Chloride Transport in Basolateral Membrane Vesicles Isolated from Rabbit Proximal Tubules. Biochemistry 27: 655.

45. Chen PY, Illsey NP and Verkman AS. (1988) Renal Brush-border Chloride Transport Mechanisms Characterized using a Fluorescent Indicator. Am. J. Physiol. 254: F114.

46. Chao AC, Dix JA, Sellers MC, and Verkman AS. (1989) Fluorescence Measurements of Cl⁻ Transport in Monolayer Culture Cells: Mechanisms of Chloride Transport in Fibroblasts. Biophys. J. 56: 1071.

47. Gupta RJ and Gupta P (1982) Direct Observation of Resolved Resonances from Intra- and Extracellular Sodium-23 Ions in NMR Studies of Intact Cells and Tissues using Dysprosium (III) Tripolyphosphate as Paramagnetic Shift Reagent. J. Magn. Reson. 47: 344.

48. Pike MM and Springer CS. (1982) Aqueous Shift Reagents for High Resolution Cationic Magnetic Resonance. J. Magn. Reson. 46: 348.

49. Pike MM, Yarmush DM, Balschi JA, Leninski REW, and Springer CS. (1983) Aqueous Shift Reagents for High Resolution Cationic Nuclear Magnetic Resonance.

II. Mg-25, K-39, and Na-23 Resonances shifted by Chelidamate Complexes of Dysprosium (III) and Thulium (III). Inorg. Chem. 22: 2388.

50. Chu SC, Pike MM, Fossel ET, Smith TW, Balschi JA, and Springer JS (1984) Aqueous Shift Reagents for High Resolution Cationic Nuclear Magnetic Resonance. III. Dy(TTHA)$^{3-}$, Tm(TTHA)$^{3-}$, and Tm(PPP)$_2$$^{7-}$. J. Magn. Reson. 56: 33.

51. Sherry AD, Geraldes CFGC (1989) In "Lanthanide Probes in Life, Chemical, and Earth Sciences. Theory and Practice"; Bunzli JCG and Schoppin GR. ed. Elsevier Press, Amsterdam, Netherlands, p.93.

52. Springer CS, Jr. (1987) Transmembrane Ion Pumping: High Resolution Cation NMR Spectroscopy. Ann. N.Y. Acad. Sci. 508: 130.

53. Kirk K. (1990) NMR Methods for Measuring Membrane Transport Rates. NMR Biomed. 3: 1.

54. (a) Espanol MC, Mota de Freitas D. (1987) ^{7}Li NMR Studies of Lithium Transport in Human Erythrocytes. Inorg. Chem. 26: 4356. (b) Ramasamy R, Espanol MC, Long KM, Mota de Freitas D, Geraldes CFGC. (1989) Aqueous Shift Reagents for ^{7}Li$^+$ NMR Transport Studies in Cells. Inorg. Chim. Acta 163: 41.

55. Brophy PJ, Hayer MK, Riddell FG. (1983) Measurement of Intracellular Potassium Ion Concentrations. Biochem. J. 210: 961.

56. (a)Helpern JA, Welch KMA, Halvorson HR. (1989) Rubidium Transport in Human Erythrocyte Suspensions Monitored by ^{87}Rb NMR with Aqueous Shift reagents. NMR Biomed. 2: 47. (b) Allis JL, Dixon RM, Till AM, Radda GK. (1989) ^{87}Rb NMR Studies for Evaluation of K$^+$ Fluxes in Human Erythrocytes J. Magn. Reson. 85: 524.

57. (a) Mota de Freitas D, Espanol MT, Ramasamy R, Labotka RJ. (1990) A Comparison

of Li^+ Transport and Distribution in Human Red Blood Cells in the Presence and Absence of Dysprosium(III) Complexes of Triphosphate and Triethylenetetraminehexaacetate. <u>Inorg. Chem.</u> <u>29</u>: 3972. (b) Ramasamy R, Mota de Freitas D, Jones W, Wezeman F, Labotka RJ, Geraldes CFGC. (1990) Effects of Negatively Charged Shift Reagents on Red Blood Cell Morphology, Li^+ Transport, and Membrane Potential. <u>Inorg. Chem.</u> <u>29</u>: 3979.

58. Seo Y, Murakami M, Suzuki E, Watari H. (1987) A New Method to Discriminate Intracellular and Extracellular K by ^{39}K NMR without Chemical Shift Reagent. <u>J. Magn. Reson.</u> <u>75</u>: 529.

59. Boulanger Y and Vinay AP. (1990) NMR Visibility of ^{39}K and ^{35}Cl in Erythrocytes and Kidney Tubules. <u>Magn. Reson. Med.</u> <u>16</u>: 246.

60. Riddell FG, Argugam S, and Patel A. (1990) Chloride Transport through Model Membranes Studied by ^{35}Cl NMR. <u>J. Chem. Soc. Chem. Commun.</u> 74.

61. Bryden CC, Reilley CN, and Desreux JF. (1981) Multinuclear Magnetic Resonance Study of Three Aqueous Lanthanide Shift Reagents: Complexes with EDTA and Axially Symmetric Macrocycles Polyamino Polyacetate Ligands. <u>Anal. Chem.</u> <u>53</u>: 1418.

62. Shachar-Hil Y and Shulman RG. (1988) Co^{2+} as a Shift Reagent for ^{35}Cl NMR with Vesicles and *in vivo*. XIII International Conference on Magnetic Resonance in Biological Systems. Madison, Wisc. Abstract P6-2.

63. Martinez D and Silvidi AA.(1972) Nuclear Magnetic Resonance of Sodium in Saliva of Patients with Cystic Fibrosis Of Pancrease. <u>Arch. Biochem. Biophys.</u> <u>148</u>: 224.

64. Breg J, Van Halbeek H, Vliegenthart JF, Lamblin G, Houvenaghel MC, and Roussel

P. (1987) Structure of Sialyl-oligosaccharides Isolated form Bronchial Mucus Glycoproteins of Patients (Blood Group O) Suffering from Cystic Fibrosis. Eur. J. Biochem. 168: 57.

65. Lamblin G, Boersma A, Lhermitte M, Roussel P, Mutsaers JHGM, Van Halbeek H and Vliengenthart JFG. (1984) Further Characterization by a Combined High-performance Liquid Chromatography/^{1}H NMR Application, of the Heterogeneity Displayed by the Neutral Carbohydrate Chains of Human Bronchial Mucins. Eur. J. Biochem. 143: 227.

66. Lamblin G, Boersma A, Klein A, Roussel P, Van Halbeek H, and Vliengenthart JF. (1984) Primary Structure Determination of Five Sialylated Oligosaccharides Derived from Bronchial Mucus Glycoproteins of Patients Suffering form Cystic Fibrosis. J. Biol. Chem. 259: 9051.

67. Van Halbeek H, Dordland L, Vliengenthart JF, Hull WE, Lamblin G, Lhermitte M, Boersma A, and Roussel, P. (1982) Primary Structure Determination of Fourteen Neutral Oligosaccharides Derived from Bronchial Mucus Glycoproteins of Patients Suffering form Cystic Fibrosis. Eur. J. Biochem. 127: 7.

68. Gerken TA and Dearborn DG. (1984) ^{13}C NMR Studies of Native and Modified Ovine Submaxillary. Biochemistry 23: 1485.

69. Messiah FS. (1985) In "Metal Ions in Neurology and Psychiatry"; Gabay S, Harris J, Ho BT. ed. Alan R. Liss, Inc., New York, 247.

70. Messiah FS, Krantz JC. (1973) Effect of Cesium on Cerebral Activity of the Mouse. J. Am. Pharm. 145: 17.

71. Messiah FS. (1975) Caesium Ion: Antagonism to Chlorpromazine- and L-Dopa

Produced Behavioral Depression in Mice. <u>J. Pharm. Pharmacol.</u> <u>27</u>: 873.

72.   Browning E. (1969) In "Toxicity of Industrial Metals"; 2nd ed.; Butterworths, London, 114.

73.   Shenkman L, Borkowsky W, Holzman RS, Shopsin B. (1976) Lithium Chloride an Immunologic Adjuvant. <u>Clin. Res.</u> <u>24</u>: 634A.

74.   Messiah FS. (1980) In "Tardive Dyskinesia"; Smith RC, Fann WE, Davis JM, Domino IF. ed. Spectrum, New York, 171.

75.   Messiah FS, Stocco DM. (1983) Effect of Ethanol and Cesium on Hepatoma Growth in Rats. <u>Subst. Alcohol Actions Misuse</u> <u>4</u>: 237.

76.   Davis DG, Murphy E, London, RE. (1988) Uptake of Cesium Ions by Human Erythrocytes and Perfused Rat Heart: A Cesium NMR Study. <u>Biochemistry</u> 27: 3547.

77.   Pfeffer PE, Rolin DB, Brauer D, Tu SI, Kumosinski TF. (1990) In Vivo ^{133}Cs NMR as a Probe for Studying Subcellular Compartmentalization and Ion Uptake in Maize Root Tissue. <u>Biochim. Biophys. Acta</u> <u>1054</u>: 169.

78.   Riddell FG, Arumugam S, Patel A.(1990) Nigericin-Mediated Transport of Caesium Ions Through Phospholipid Bilayers Studied by ^{133}Cs Magnetization Transfer NMR Techniques. <u>Inorg. Chem.</u> <u>29</u>: 2397.

79.   (a) Jameson CJ and Gutowsky HS. (1964) Calculation of Chemical Shifts. I. General Formulation and Z-Dependence. <u>J. Chem. Phys.</u> <u>40</u>: 1714. (b) Popov AI. (1979) NMR Studies of Interionic Interactions in N-Methylformamide. <u>Pure and Appl. Chem.</u> <u>51</u>: 101. (c) Rounaghi G, Popov AI. (1985) ^{133}Cs NMR Study of the Cryptand-222-Cs$^+$-Complex in Binary Solution Mixtures. <u>Polyhedron</u> <u>5</u> : 1935. (d) Shamsipur M, Popov AI. (1988) Study of the Complex Kinetics of Cs$^+$ Ion with Dibenzo-30-Crown-

10 in Some Nonaqueous Solution by ^{133}Cs NMR. J. Phys. Chem. 92: 147. (e) Soong LL, Leroi GE, Popov AI. (1989) NMR Studies of Interionic Interactions in N-Methylformamide. J. Soln. Chem. 18: 561.

80. (a) Einarsson L, Kowalewski J, Nordenskiold L, Rupprecht A. (1989) ^{133}Cs NMR of Orientated CsDNA and Multiple Quantum Spectroscopy of I = 7/2. J. Magn. Reson. 85: 228. (b) Einarsson L, Nordenenskiod L, Rupprecht A, Furo I, and Wong TC. (1991) ^{7}Li and ^{133}Cs Spin Relaxation in Macroscopically Orientated Li-DNA and Cs-DNA Fibers. J. Magn. Reson. 93: 34.

81. (a) Love WD and Burch GE. (1953) A Comparison of Potassium, Rubidium, and Cesium as Tracers of Potassium in the Study of Cation Metabolism of Human Erythrocytes in Vitro. J. Lab. Clin. Med. 41: 351. (b) Beauge, LA and Sjodin RA (1968) Transport of Caesium in Frog Muscle. J. Physiol (London) 194: 105.

82. Kerem B, Rommens JM, Buchanan JA Markiewicz D, Cox TK, Chakravarti A, Buchwald M, and Tsui L. (1989) Identification of the Cystic Fibrosis Gene: Genetic Analysis. Science 245: 1073.

83. Brix O, Thomsen B, Nuutinen, Halkala A, Pudas J, and Giardina B (1990) The Chloride Shift May Facilitate Oxygen Loading and Unloading To/From the Hemoglobin From the Brown Bear (Ursus Artctos L.). Comp. Biochem. Physiol. 95B: 865.

84. Morse PD, Lusczakoski DM, Simpson DA. (1979) Internal Microviscosity of Red Blood Cells and Hemoglobin-Free Resealed Ghosts: A Spin-Label Study. Biochemistry 18: 5021.

85. Dozy AM, Kleihauer EF, Huisman THJ. (1968) Studies on the Heterogeneity of

Hemoglobin J. Chromatography **32**: 723.

86.   Hinckel CC. (1969) Paramagnetic Shifts in Solutions of Cholesterol and the Dipyridine Adduct of Trisdipivalomethanatoeuropium (III). A Shift Reagent. J. Am. Chem. Soc. **91**: 5160.

87.   Geraldes CFGC, Sherry AD, Marques MPM, Alpoim MC, and Cortes, S. (1991) Protonation Sheme for Some Triaza Macrocycles Studied by Potentiometry and NMR Spectroscopy. J. Chem. Soc. Perkin. Trans. **2**: 137.

88.   Desreux JF. (1980) Nuclear Magnetic Resonance Spectroscopy of Lanthanide Complexes with a Tetraacetic Tetraaza Macrocycle.   Unusual Conformation Properties. Inorg. Chem. **19**: 1319.

89.   Sawyer TD, and Roberts JL. (1972) In "Experimental Electrochemistry for Chemists"; John Wiley and Sons, New York.

90.   Perrin DD, Armarego WLF, and Perrin DR. (1987) In "Purification of Laboratory Chemicals"; Pergamon Press, New York.

91.   Steck TL and Kant JA. (1974) Preparations of Impermeable Ghosts and Inside-out Vesicles from Human Erythrocyte Membranes. Methods in Enzymology **31**: 172.

92.   Labotka RJ. (1984) Measurement of Intracellular pH and Deoxyhemoglobin Concentration in Deoxygenated Erythrocytes by ^{31}P NMR. Biochemistry **23**: 5549.

93.   Riddell FG, Arumugam S, Brophy PJ, Cox BG, Payne MCH, and Southon TE. (1988) The Nigericin-Mediated Transport of Sodium and Potassium Ions through Phospholipid Bilayers Studied by ^{23}Na and ^{39}K NMR Spectroscopy. J. Am. Chem. Soc. **110**: 734.

94.   Sparporer M and Civan M. (1974) Effects of Temperature and Field Strength on the NMR Relaxation Times of ^{23}Na in Frog Striated Muscle. Biochim. Biophys. Acta **354**:

291.

95.   London RE and Gabel SA. (1989) Determination of Membrane Potential and Cell Volume by ^{19}F NMR Using Trifluroacetate and Trifluoroacetamide Probes. <u>Biochemistry</u> <u>28</u>: 2378.

96.   (a) Kirk K, Kuchel PW, and Labotka RJ. (1988) Hypophosphite Ion as a ^{31}P Nuclear Magnetic Resonance Probe of Membrane Potential in Erythrocyte Suspensions. <u>Biophys. J.</u> <u>54</u>: 241. (b) Jackson M and Mantsch HH. (1991) Valinomycin and Its Interaction with Ions in Organic Solvents, Detergents, and Lipids Studied by Fourier Transform IR Spectroscopy. <u>Biopolymers</u> <u>31</u>: 1205.

97.   Martell AE and Smith RM. (1974) In "Critical Stability Constants"; Plenum Press, New York, vol 1-3.

98.   (a) Scarpa M, Viglino P, Vianello F, and Rigo A. (1991) ^{19}F NMR Study of the Interactions of Fluoride with Superoxide Dismutase and Hemoglobin in Erythrocytes. <u>Biochem. Biophys. Res. Commun.</u> <u>174</u>: 163. (b) Chapman BE and Kuchel PW. (1990) Fluoride Transmembrane Exchange in Human Erythrocytes Measured with ^{19}F NMR Magnetization Transfer. <u>Eur. Biophys. J.</u> <u>19</u>: 41.

99.   Funder J and Wieth JO. (1966) Chloride and Hydrogen Ion Distribution Between Red Cells and Plasma. <u>Acta Physiol. Scand.</u> <u>68</u>: 234.

100.   (a) Dise CA and Goodman BP. (1985) The Relationship between Valinomycin-Induced Alterations in Membrane Phospholipid Fatty Acid Turnover, Membrane Potential, and Cell Volume in Human Erythrocytes. <u>J. Biol. Chem.</u> <u>260</u>: 2869. (b) Masuda T, Dobson GP, and Veech RL. (1990) The Gibbs-Donnan Near-Equilibrium System of Heart. <u>J. Biol. Chem.</u> <u>265</u>: 20321.

101. Moon RB and Richards JH. (1973) Determination of Intracellular pH by ^{31}P Magnetic Resonance. J. Biol. Chem. 248: 7276.

102. (a) Gupta RJ, Benovic JL, and Rose ZB. (1978) The Determination of the Free Magnesium Level in the Human Red Blood Cell by ^{31}P NMR. J. Biol. Chem. 253: 6172. (b) Raftos JE, Bulliman BT, and Kuchel PW. (1990) Evaluation of an Electrochemical Model of Erythrocyte pH Buffering Using ^{31}P Nuclear Magnetic Resonance Data. J. Gen. Physiol. 95: 1183.

103. Dufilho MD, Montenay-Garestier T, and Devynck MA. (1988) Fluorescence Measurement of Free Ca^{2+} Concentration in Human Erythrocytes Using the Ca^{2+} - indicator fura-2. Cell Calcium 9: 167.

104. Fabry ME and San George RC. (1983) Effect of Magnetic Susceptibility on Nuclear Magnetic Resonance Signals Arising from Red Cells: A Warning. Biochemistry 22: 4119.

105. Dacie JV and Lewis SM. (1975) In "Practical Haematology"; Churchill Livingstone, Edinburgh, 5th edition, 39.

106. Frei, K and Berstein J. (1962) Methods for Determining Magnetic Susceptibility by NMR. J.Chem. Phys. 37: 1891.

107. Xu, ASL, Potts JR, and Kuchel PW. (1991) The Phenomenon of Separate Intra- and Extracellular Resonances of Difluorophosphate in ^{31}P and ^{19}F NMR Spectra of Erythrocytes. Magn. Reson. Med. 18: 193.

108. Gupta RK and Benovic, JL. (1978) Magnetic Resonance Studies of the Interaction of Divalent Metal Cations with 2,3-Bisphosphoglycerate. Biochem. Biophys. Res. Commun. 84: 130.

109. Russ IM, Wu SS, Bupp KA, Ho NT, and Ho C. (1990) ^{1}H and ^{31}P Nuclear Magnetic resonance Investigation of the Interaction Between 2,3-Diphosphoglycerate and Human Normal Adult Hemoglobin. Biochemistry 29: 3785.

110. (a) Modro TA, Yates K, and Janata J. (1975) Operational Scale of Hydronium Ion Activities for Strongly Acidic Media. J. Am. Chem. Soc. 97: 1492. (b) French DC and Crumrine D. (1989) Multinuclear NMR of Arenesulfonates: An Investigation into Concentration, Solvent, Counter Ion, and Temperature Effects. J. Magn. Reson. 84: 548.

111. (a) Marcus Y. (1985) In "Ion Solvation"; J. Wiley and Sons, New York. (b) Amat E, Cox BG, Rzeszotarska J, and Schneider H. (1988) Na$^+$ Exchange Reactions of Monensin in Methanol and Methanol-Water Mixtures: A ^{23}Na NMR Study. J. Am. Chem. Soc. 110: 3368. (c) Grell E and Funck T. (1973) Carbon-13 Nuclear Magnetic Resonance and Infrared Absorption Spectroscopy of Valinomycin and Its Alkali Ion Complexes. Eur. J. Biochem. 34: 415. (d) Patel DJ. (1973) Carbon Framework of Valinomycin and Its Metal Ion Complex in Solution. Biochemistry 12: 496.

112. Chu S C-K, Xu Y, Balschi JA, and Springer CS Jr. (1990) Bulk Magnetic Susceptibility Shifts in NMR Spectra of Compartmentalized Samples. Magn. Reson. Med. 13: 239.

113. Nicholls P and Miller N. (1974) Chloride Diffusion form Liposomes. Biochim. Biophys. Acta. 356:184.

114. Gerencser GA, White JF, Gradmann D, and Bonting SJ. (1986) Is There a Cl$^-$ Pump? International Congress of Physiological Sciences Debates Symposium. Vancouver, Canada.

115. Lassen UV. (1977) In "Membrane Transport in Red Cells"; Ellory, JC and Lew VL. ed. Academic Press, New York, 137.

116. McGivney A, Morita Y, Crews FT, Hirata F, Axelrod J, and Siragarian RP. (1981) Phospholipase Activation in the IgE-Mediated and Ca^{2+} Ionophore A23187-Induced Release of Histamine from Rat Basophilic Leukemia Cells. Arch. Biochem. Biophys. 212: 572.

117. Pressman BC. (1976) Biological Application of Ionophores. Annu. Rev. Biochem. 45: 501.

118. Dise CA. Goodman DBP, and Ramussen H. (1980) Selective Stimulation of Erythrocyte Membrane Phospholipid Fatty Acid Turnover Associated with Decreased Cell Volume. J. Biol. Chem. 255: 5201.

119. Marcey RI, Adorante JS, and Orme FW. (1987) Erythrocyte Membrane Potentials Determined by Hydrogen Ion Distribution. Biochim. Biophys. Acta 512: 284.

120. Cheng K, Haspel HC, Vallano ML, Osotimehin B, and Sonenberg M. (1980) Measurement of Membrane Potentials (Ψ) of Erythrocytes and White Adipocytes by the Accumulation of Triphenylmethylphosphonium Cation. J. Membr. Biol. 56: 191.

121. Vestergaard-Bogind B and Bennekou P. (1982) Calcium-Induced Oscillations in K^+ Conductance and Membrane Potential of Human Erythrocytes Mediated by the Ionophore A23187. Biochim. Biophys. Acta. 688: 37.

122. Freedman JC and Novak TS. (1983) Membrane Potentials Associated with Ca-Induced K Conductance in Human red Blood Cells: Studies with a Fluorescent Oxonol Dye, WW 781. J. Membr. Biol. 72: 59.

123. Knauf PA, Fuhrmann GF, Rothstein S, and Rothstein A. (1977) The Relationship

Between Anion Exchange and Net Anion Flow Across the Human Red Blood Cell Membrane. J. Gen. Physiol. 69: 363.

124. Springer CS. (1987) Measurement of Metal Cation Compartmentalization in Tissue by High-Resolution Metal Cation NMR. Ann. Rev. Biophys. Biophys. Chem. 16: 375.

125. Buster DC, Castro MMCA, Geraldes CFCC, Malloy CR, Sherry AD, and Siemers TC. (1990) Tm(DOTP)$^{5-}$: A ^{23}Na$^+$ Shift Agent for Perfused Rat Heart. Magn. Reson. Med. 15: 25.

126. Wittenkeller L, Mota de Freitas D, Geraldes CFGC, and Tome AJR. (1991) Physical Basis for the Resolution of Intra- and Extracellular ^{133}Cs NMR Resonances in Cs$^+$-Loaded Human Erythrocyte Suspensions in the Presence and Absence of Shift Reagents. Inorg. Chem. in press.

127. Ramasamy R, Mota de Freitas D, Geraldes CFGC, and Peters J. (1991) Multinuclear NMR Study of the Interaction of the Shift Reagent Lanthanide (III) Bis(triphosphate) with Alkali-Metal Ions in Aqueous Solutions and in the Solid State. Inorg. Chem. 30: 3188.

128. Philo JS, Dreyer U, and Schuster TM. (1984) Paramagnetism of Human Apo-, Oxy, and (Carbonmonoxy)hemoglobin. Biochemistry 23: 865.

129. Savicki P, Lang G, and Ikeda-Saito M. (1984) Magnetic Susceptibility Oxy- and Carbonmonoxyhemoglobins. Proc. Natl. Acad. Sci. USA 81: 5417.

130. Cerdonio M, Morante S, Torresani D, Vitale S, DeYoung A, and Noble RW. (1985) Reexamination of the Evidence for Paramagnetism in Oxy- and Carbonmonoxyhemoglobins. Proc. Natl. Acad. Sci. USA 82: 102.

131. Kirk K and Kuchel PW. (1988) The Contribution of Magnetic Susceptibility Effects

to Transmembrane Chemical Shift Differences in the ^{31}P NMR Spectra of Oxygenated Erythrocyte Suspensions. J. Biol. Chem. 263: 130.

132.   Kirk K and Kuchel PW. (1988) Characterization of Transmembrane Chemical Shift Differences in the ^{31}P NMR Spectra of Various Phosphoryl Compounds Added to Erythrocyte Suspensions. Biochemistry 27: 8795.

133.   Kirk K and Kuchel PW. (1988) Physical Basis of the Effect of Hemoglobin on the ^{31}P NMR Chemical Shifts of Various Phosphoryl Compounds. Biochemistry 27: 8803.

134.   (a) Brooks RA, Brunetti A, Alger JR, and Chiro G. (1989) On the Origin of Paramagnetic Inhomogeneity Effects in Blood. Magn. Reson. Med. 12: 241. (b) Matwiyoff NA, Gasparovic C, Mazurchuk R, and Matwiyoff G. (1991) On the Origin of Paramagnetic Inhomogeneity Effects in Whole Blood. Magn. Reson. Med. 20: 144.

135.   Collier HB and Lam A. (1970) Binding of Ca^{2+} and Mg^{2+} by 2,3-Diphosphoglycerate. Biochim. Biophys. Acta 222: 299.

136.   Sovago I, Kiss T, and Martin RB. (1990) 2,3-Diphosphoglycerate Binding of Zn^{2+} and Al^{3+}. Polyhedron 9: 189.

137.   Mendz GL, Kuchel PW, and Wilcox GR. (1988) Interactions of Na^{+} with haemoglobin-Organic Phosphate Complexes. Biophys. Chem. 30: 81.

138.   Petersen A, Kristensen SR, Jacoben JP, and Horder M. (1990) ^{31}P NMR Measurements of ATP, ADP, 2,3-Diphosphoglycerate and Mg^{2+} in Human Erythrocytes. Biochim. Biophys. Acta 1035: 169.

VITA

The author, Lisa Wittenkeller, is the daughter of Gerry and Genevieve Wittenkeller. She was born February 20, 1965, in Oak Park, Illinois.

Her high school education was obtained from Benet Academy in Lisle, Illinois. In August 1983 she entered Saint Mary's College of Notre Dame. She received her Bachelor of Science degree with a major in Chemistry and minors in math and physics in May, 1987.

In August 1987, she joined Loyola University Chicago to pursue graduate studies in Chemistry and was awarded the incoming Chemistry student award. She received a graduate research assistantship from January 1989 to August 1989, funded by a Grant-in-Aid of the American Heart Association of Metropolitan Chicago awarded to Dr. Duarte Mota de Freitas. In September 1990, she was awarded a University Dissertation Fellowship, enabling her to complete the Doctor of Philosophy Degree in 1992, under the supervision of Dr. Duarte Mota de Freitas.

Publications

A) Abstracts:

1. Mota de Freitas D, Espanol M, Ramasamy R, Abraha A, and Wittenkeller L. (1989) ^{7}Li NMR Relaxation Studies of Li$^+$ Storage and Transport in RBCs. <u>J. Inorg. Biochem.</u> <u>36</u> : 187.

2. Wittenkeller L and Mota de Freitas D. (1991) Physical Basis for the Resolution of Intra- and Extracellular ^{133}Cs NMR Resonances. 9th <u>Magn. Reson. Med.</u> works in progress, New York.

3. Mota de Freitas D, Abraha A, Rong Q, Mo S, and Wittenkeller L. (1991) Elucidation of Transport Mechanisms for Alkali Cations in Human RBC by Metal NMR. <u>J. Inorg. Biochem.</u> <u>43</u>: 386.

B) Manuscripts:

1. Wittenkeller L, Abraha A, Ramasamy R, Mota de Freitas D, Crans D, and Theisen L. (1991) Vanadate Interactions with Bovine Copper,Zinc-Superoxide Dismutase as Probed by ^{51}V NMR Spectroscopy. <u>J. Am. Chem. Soc.</u> <u>113</u>: 7872-7881.

2. Wittenkeller L, Mota de Freitas D, Geraldes, CFGC, and Tome, AJR. (1992) Physical Basis for the Resolution of Intra- and Extracellular ^{133}Cs NMR Resonances. <u>Inorg. Chem.</u> in press.

3. Wittenkeller L, Mota de Freitas D, and Ramasamy R. (1992) Ionophore-Induced Cl$^-$ Transport in Human Erythrocyte Suspensions. A Multinuclear Magnetic Resonance Study. <u>FEBS Lett.</u> submitted for publication.

APPROVAL SHEET

The dissertation submitted by **Lisa Wittenkeller** has been read and approved by the following committee:

Dr. Duarte Mota de Freitas, Director
Associate Professor of Chemistry, Loyola

Dr. Patrick M. Henry
Professor of Chemistry, Loyola

Dr. Bruno Jaselskis
Professor of Chemistry, Loyola

Dr. Kenneth W. Olsen
Professor of Chemistry, Loyola

Dr. Richard J. Labotka, MD
Head, Division of Hematology/Oncology
Department of Pediatrics
University of Illinois at Chicago

The final copies have been examined by the director of the dissertation and the signature which appears below verifies the fact that any necessary changes have been incorporated and that the dissertation is now given final approval by the committee with reference to content and form.

The dissertation is therefore accepted in partial fulfillment of the requirements for the degree of **Doctor of Philosophy**.

2/2×/92
Date

Director's Signature